

Adaptive Controller Design for Refrigeration Cycle Using the Natural Refrigerant CO₂

Masterarbeit

Autor: Julius Martensen
Betreuer: Dipl. Ing. Michael Nöding
Prüfer: Prof. Dr.-Ing. Jürgen Köhler
October 16, 2017



Institut für Thermodynamik

Prof. Dr.-Ing. Jürgen Köhler
Hans-Sommer-Str. 5
D-38106 Braunschweig
Tel.: +49 (531) 391-2627
Fax: +49 (053) 391-7814
E-Mail: J.Koehler@tu-bs.de
Braunschweig, 29.09.2014

Vorlesungsankündigung

Im Wintersemester 14/15 werden die folgenden Lehrveranstaltungen abgehalten:

Thermodynamik

Prof. Dr. J. Köhler/Dipl.-Ing. M. Buchholz

Die allererste Vorlesung ist am Donnerstag, 23.10.2014 von 15.00 bis 16.30 Uhr im AM					
2V	Vorlesung	MI	15:00 - 16:30	AM	29.10.2014
1V	Vorlesung	DO	14:55 - 15:40	AM	23.10.2014
2519029	1Ü	Übung	DO 15:50 - 16:55	AM	23.10.2014
2519004	2S	Seminargruppe	FR 08:15 - 11:15	ZI 24.1 - ZI 24.3	31.10.2014

Thermodynamik der Gemische

Prof. Dr. J. Köhler/Dr. G. Raabe

2519038	2V	Vorlesung	FR	11:30 - 13:00	PK 4.1	24.10.2014
2519039	1Ü	Übung	FR	13:10 - 13:55	PK 4.1	24.10.2014

Modellierung thermischer Systeme in Modelica

Prof. Dr. J. Köhler/Dr. W. Tegethoff

2519006	2V	Vorlesung	nach Absprache	HS 5.1	Beginn: siehe gesonderter Aushang
2519008	1Ü	Übung	nach Absprache	HS 5.1	Beginn: siehe gesonderter Aushang

Objektorientierte Simulationsmethoden in der Thermo- und Fluideodynamik

Prof. Dr. J. Köhler/Dr. W. Tegethoff

2519011	2V	Vorlesung	nach Absprache	HS 5.1	Beginn: siehe gesonderter Aushang
2519012	1Ü	Übung	nach Absprache	HS 5.1	Beginn: siehe gesonderter Aushang

Seminar für Thermodynamik

Prof. Dr. J. Köhler/Wiss. Mitarbeiter N.N.

2519024	2S	Seminar	MO 13:15-14:45	HS 5.1	
---------	----	---------	----------------	--------	--

Fahrzeugklimatisierung

Prof. Dr. J. Köhler/Dr. N. Lemke

2519003	2V	Vorlesung	DI 16:45 - 18:15	HS 5.1	Beginn: siehe gesonderter Aushang
2519034	1Ü	Übung	siehe gesonderter Aushang		Beginn: siehe gesonderter Aushang

Prof. Dr.-Ing. Jürgen Köhler

Eidesstattliche Erklärung

Hiermit erkläre ich eidesstattlich, dass ich diese Arbeit eigenständig angefertigt und keine anderen als die angegebenen Hilfsmittel verwendet habe.

Braunschweig den October 16, 2017

Contents

1	Introduction	2
1.1	Motivation	2
1.2	Literature Review	2
2	Control Theoretic Model and Problem Statement	3
2.1	Basics of Control Theory	3
2.2	Feedback Control in Presence of Uncertain Signals	4
2.3	Stability and Robustness of Feedback Control Systems	5
2.4	Gain Scheduling	9
3	Process Models and System Identification	10
3.1	First Order Time Delay Model	11
3.2	Integral Fitting Approach	15
3.3	Asymmetric Relay Experiment	18
3.4	Review	20
4	Multivariable PI/PID Controller Design	21
4.1	AMIGO Tuning Rules	21
4.2	Interaction Measures of Multivariable Processes	23
4.3	Decoupling of Multivariable Processes	26
4.3.1	Decoupling Control proposed by Åström et.al.	26
4.3.2	A Modified Controller Design Based on Åström et.al. - Robust Relative Dynamic Decoupling	31
4.4	Review of the Methods	39
5	Control of Simple Multivariable Processes	40
5.1	Analytic Decoupling	40
5.1.1	Controller Design via Relative Gain Array Analysis	40
5.1.2	Controller Design via Åström et. al.	41
5.2	Rosenbrocks Function	46
5.2.1	Decentralized Controller	46
5.2.2	Decoupled Controller based on Åström	47
5.2.3	Decoupled Controller based on Robust Relative Dynamic Detuning	48
5.2.4	Results	49
5.3	Wood-Berry's Binary Distillation Column	56
5.4	McAvoy et. al.	62
5.5	66

5.6 Performance Review	67
6 Robustness Study Using Monte Carlo Methods	68
6.1 Definition of Parameter Boundaries and Evaluation Methods	69
6.2 Robustness of SISO Systems	72
6.2.1 Constant Sum Time	72
6.2.2 Pole Multiplicity	75
6.2.3 Random Time Constants	77
6.3 Robustness of Multivariable Systems	80
6.3.1 Constant Sum Time	80
6.3.2 Random Pole Multiplicity	85
6.4 Review	89
7 Application to Physical Process Models	91
7.1 Process Description and Problem Statement	91
7.2 Identification of the FOTD model	94
7.3 Closed Loop Results	100
7.4 Review	105
8 Conclusion and Outlook	107
Bibliography	108
Anhang	111
A.1 Erster Anhang	111
A.2 Zweiter Anhang	111

List of Figures

2.1	Two Degree of Freedom Feedback Control	5
2.2	Illustration of the Connection between the maximum sensitivity, the open loop gain and the Nyquist Criterion	7
2.3	Illustration of the singular value decomposition	8
2.4	Example for the maximum singular value as an upper limit to the gain	9
3.1	Gain of a high order transfer function and corresponding FOTD model	13
3.2	Nyquist diagram of high order transfer function and corresponding FOTD model . .	14
3.3	Phase of High Order Transfer Function and Corresponding FOTD model	15
3.4	Interpretation of the Integral Fitting Approach using Areas given by a unit step response	17
3.5	Identification of the Systems Gain using the Supremum of the Step Response	18
4.1	Coupling in P-canonic structure	26
4.2	Coupling in V-canonic structure	26
4.3	Block diagram of the decoupled system	27
4.4	Interpretation of the splitter within the disturbance rejection framework	35
4.5	Interpretation of the splitter within the feed forward compensation framework	35
4.6	Compensator implementation of the splitter in a two input two output system	35
5.1	Simulation of Rosenbrock's System without detuning	50
5.2	Singular values of the sensitivity (red) and complementary sensitivity (green) function of Rosenbrock's system without detuning	52
5.3	Simulation of Rosenbrock's System with detuning	54
5.4	Singular values of the sensitivity (red) and complementary sensitivity (green) function of Rosenbrock's system with detuning	55
5.5	Simulation of Wood-Berry's binary distillation column without detuning	57
5.6	Singular values of the sensitivity (red) and complementary sensitivity (green) function of Wood-Berry's binary distillation column without detuning	59
5.7	Simulation of Wood-Berry's binary distillation column with detuning	60
5.8	Singular values of the sensitivity (red) and complementary sensitivity (green) function of Wood-Berry's binary distillation column with detuning	61
5.9	Simulation of McAvoy's system without detuning	63
5.10	Singular values of the sensitivity (red) and complementary sensitivity (green) function of McAvoy's system without detuning	64
5.11	Simulation of McAvoy's system with detuning	65

5.12	Singular values of the sensitivity (red) and complementary sensitivity (green) function of McAvoy's system with detuning	66
5.13	Step of the MIMO	67
6.1	Example of a system with pole multiplicity	72
6.2	Results of the robustness study, maximum Sensitivity of the real System and the identified system	73
6.3	Results of the robustness study, maximum sensitivity of the real System over normalized time delay	74
6.4	Results of the robustness study, model delay and lag over the process parameter . . .	74
6.5	Results of the robustness study, normalized time delay of the real system and the FOTD model	75
6.6	Results of the robustness study, maximum sensitivity of the model system over the maximum sensitivity of the real system	76
6.7	Results of the robustness study, model delay and lag over the process parameter . .	77
6.8	Results of the robustness study, maximum sensitivity of the real system and the identified system	78
6.9	Results of the robustness study, cumulative density plot of the maximum sensitivity of the real system	79
6.10	Results of the robustness study, model delay and lag over the process parameter . .	79
6.11	Results of the robustness study, maximum singular values and corresponding frequency for decentralized control	80
6.12	Results of the robustness study, maximum singular values and corresponding frequency for static decoupled control, $h_{ij,Max} \leq 0.5$	81
6.13	Results of the robustness study, maximum singular values and corresponding frequency for R2D2 control, $h_{ij,Max} \leq 0.5$	81
6.14	Results of the robustness study, maximum singular values cumulative densities of all methods, $h_{ij,Max} \leq 0.5$	82
6.15	Results of the robustness study, maximum singular values and corresponding frequency for static decoupled control, $h_{ij,Max} \leq 0.1$	83
6.16	Results of the robustness study, maximum singular values cumulative densities of all methods, $h_{ij,Max} \leq 0.1$	84
6.17	Results of the robustness study, maximum singular values and corresponding frequency for decentralized control, $h_{ij,Max} \leq 0.5$	85
6.18	Results of the robustness study, maximum singular values and corresponding frequency for static decoupled control, $h_{ij,Max} \leq 0.5$	85
6.19	Results of the robustness study, maximum singular values and corresponding frequency for simple decoupled control, $h_{ij,Max} \leq 0.5$	86
6.20	Results of the robustness study, maximum singular values cumulative densities of all methods, $h_{ij,Max} \leq 0.5$	87
6.21	Results of the robustness study, maximum singular values and corresponding frequency for static decoupled control, $h_{ij,Max} \leq 0.1$	88

6.22	Results of the robustness study,maximum singular values and corresponding frequency for simple decoupled control, $h_{ij,Max} \leq 0.1$	88
6.23	Results of the robustness study,maximum singular values cumulative densities of all methods, $h_{ij,Max} \leq 0.1$	89
7.1	Pressure over specific enthalpy diagram of the refrigeration cycle, Effects of an increase in A_{eff} (blue) and n (green)	95
7.2	Example of the influence of scaled input steps within the simulation model	96
7.3	Variation of the FOTD model parameter due to simulation parameter and operating conditions	97
7.4	Error within the model use of the main diagonal within R2D2, steady state of the system	98
7.5	Relative magnitude within the model for decentralized control (full) and simple decoupling (dashed), steady state of the system	99
7.6	Disturbance rejection of the closed loop simulated by a step acting on the systems input, Example 1	100
7.7	Tracking behavior of the closed loop simulated by a step acting on the systems set point, Example 1	101
7.8	Disturbance rejection of the closed loop simulated by a step acting on the systems input, Example 2	102
7.9	Tracking behavior of the closed loop simulated by a step acting on the systems set point, Example 2	103
7.10	Disturbance rejection of the closed loop simulated by a step acting on the systems input, Example 3	104
7.11	Tracking behavior of the closed loop simulated by a step acting on the systems set point, Example 3	105

1 Introduction

1.1 Motivation

The great motivational Speak follows in this section.

Hier schon folgende Quellen erwähnen:

[6]

1.2 Literature Review

The great literature review follows in this section.

2 Control Theoretic Model and Problem Statement

The following chapter gives a brief introduction to the concepts of control theory used in this work. Further information can be found in the literature. A standard, comprehensive introduction is given in the works [20],[19] and [3]. The basics concepts are explained and investigated in great detail. The control of multivariable systems is explained in [21] and [14]. Standards about the design of robust control are [26], [27] and [12]. The concepts of nonlinear control are covered extensively in [1].

Sec. 2.1 starts by explaining several notations of dynamical systems in the context of control.

Afterwards, the concept of feedback control is elucidated in Sec. 2.2. The influence of disturbances and measurement noise is captured in form of mathematical matrix notations.

The essentials of robustness and stability of the introduced system is investigated further in Sec.2.3. Here the general concepts of a single input single output system is extended to multiple input multiple output systems.

The chapter concludes in Sec.2.4 with a short introduction to gain scheduling in the context of linearized control.

2.1 Basics of Control Theory

A general nonlinear, dynamical system can be described with Eq. 2.1 [1]

$$\begin{aligned}\dot{x} &= f(x, u, t) \\ y &= h(x, u, t)\end{aligned}\tag{2.1}$$

Where $t \in \mathbb{R}^+$ is the time, $x \in \mathbb{R}^{n_x}$ is called the state vector, or states, and $u \in \mathbb{R}^{n_u}$ the input vector, or inputs, of the system. The output $y \in \mathbb{R}^{n_y}$ of the system is described by the functions $h : \mathbb{R}^{n_x}, \mathbb{R}^{n_u}, \mathbb{R}^+ \mapsto \mathbb{R}^{n_y}$ and the evolution of the system over time is given by $f : \mathbb{R}^{n_x}, \mathbb{R}^{n_u}, \mathbb{R}^+ \mapsto \mathbb{R}^{n_x}$.

The system given by Eq. 2.1 can be used to describe almost every natural or technical system. Due to several reasons, e.g. controller design, measurements, modelling issues and errors, in most technical applications the model is simplified by assuming linear, time invariant (LTI) behavior. The LTI system is represented by a set of first-order differential equations [19] called state space representation:

$$\begin{aligned}\dot{\mathbf{x}} &= \mathbf{A} \mathbf{x} + \mathbf{B} \mathbf{u} \\ \mathbf{y} &= \mathbf{C} \mathbf{x} + \mathbf{D} \mathbf{u}\end{aligned}\tag{2.2}$$

The state matrix $\mathbf{A} \in \mathbb{R}^{n_x \times n_x}$ describes the influence of the current states, the input matrix $\mathbf{B} \in \mathbb{R}^{n_x \times n_u}$ the influence of the current input on the future states and output. The output is given by the output matrix $\mathbf{C} \in \mathbb{R}^{n_y \times n_x}$ and the feedthrough matrix $\mathbf{D} \in \mathbb{R}^{n_y \times n_u}$.

Both Eq. 2.1 and Eq. 2.2 are can be used as a base for a variety of different controllers, see e.g. [1], [19], [20]. The ability to design controller via state space methods is connected to a high information content about (physical) parameters and equations or in form of measurement data.

Hence a more compressed form is commonly used to design controller for most technical and industrial applications. The transfer function matrix [19, p.20] $\mathbf{G} \in \mathbb{C}^{n_y \times n_u}$ can be derived via the Laplace transform of Eq.2.2:

$$\mathbf{G} = \mathbf{C} (s\mathbf{I} - \mathbf{A})^{-1} \mathbf{B} + \mathbf{D} \tag{2.3}$$

The transfer function matrix consist of single transfer functions $g_{ij}(s)$, $i \leq n_y, j \leq n_u$ and maps the transformed input of a system directly to its transformed output. It describes the relationship between input and output directly and is hence a compact form of describing the behavior of LTI systems. To control a system with two outputs in every wanted direction a necessary condition is given by $n_y \leq n_u$. It is assumed that all following systems suffice $\dim \mathbf{G} = n_y \times n_y$.

2.2 Feedback Control in Presence of Uncertain Signals

The aim of control theory is to manipulate a systems trajectory via its inputs in such a way, that a desired output is reached and maintained. To do this, several techniques can be used. Most commonly the systems desired output, the set-point y_r , is compared to the actual output of the system \mathbf{y} via a feedback loop. The result of this comparison is called the error $e \in \mathbb{R}^{n_y}$. This signal is fed into the controller $\mathbf{K} \in \mathbb{C}^{n_y \times n_y}$ and the result is used as an input for the system. This approach is called feedback control, see e.g. [3], with a single degree of freedom controller.

A variation of this approach is to use a weighted set-point and output signal to generate the input. The pair of weighting matrices \mathbf{K}_r for the setpoint and \mathbf{K}_y for the output is called a two degree of freedom controller. The structure of such a controller design is shown in Fig. 2.1.

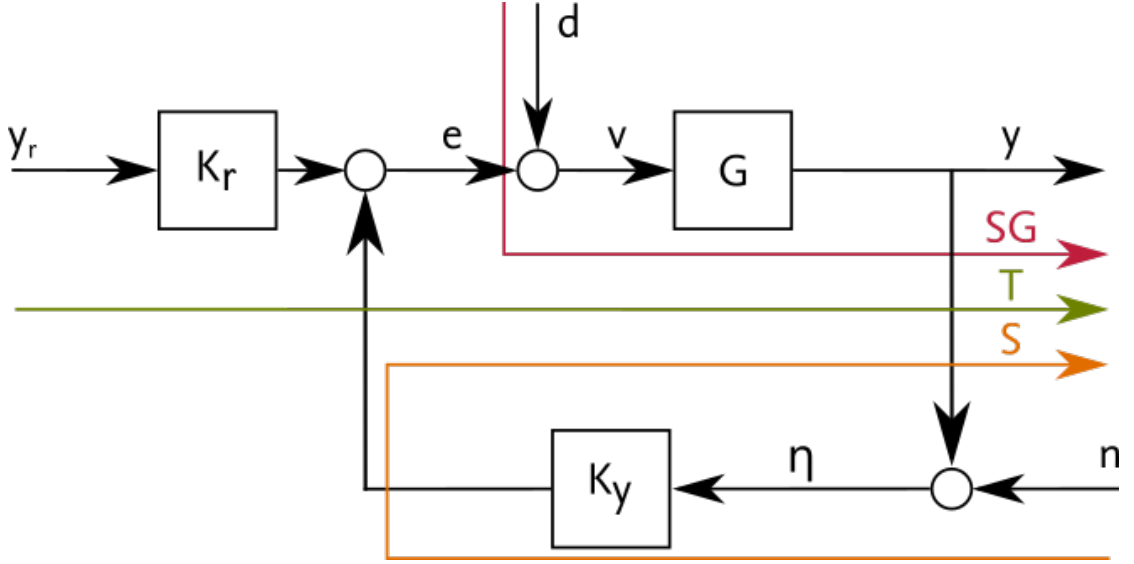


Figure 2.1: Two Degree of Freedom Feedback Control

In Fig. 2.1 further signals are added. The disturbances $d \in \mathbb{R}^{n_y}$ are acting on the systems input, the signal $v \in \mathbb{R}^{n_y}$ is the disturbed input of the plant. $y \in \mathbb{R}^{n_y}$ is the plants output without measurement noise which will be referred to as real output. The measurement noise is given by $n \in \mathbb{R}^{n_y}$. The superposition of noise and real output is η which will be referred to simply as output. The closed loop transfer function is given by:

$$y = [I - GK_y]^{-1} [GK_r y_r + n + Gd] \quad (2.4)$$

Eq. 2.4 relates the output of a system to the influences of set point, disturbances and measurement noise. Rewriting the equation as:

$$y = Ty_r + S[n + Gd] \quad (2.5)$$

defines the Sensitivity Function $S = [I - GK_y]^{-1} \in \mathbb{C}^{n_y \times n_y}$ which relates the influences of measurement noise and load disturbance to the systems outputs. The Complementary Sensitivity Function $T = [I - GK_y]^{-1} GK_r \in \mathbb{C}^{n_y \times n_y}$ describes the response to the reference signal. Both Functions play an important role in the investigation of the systems Robustness and are connected to each other via $T = SGK_r$.

2.3 Stability and Robustness of Feedback Control Systems

The stability of dynamical systems is a key concept of control theory. In general, a system is said to be stable if all trajectories starting near a final state end in or near this state [1, p.10]. Several measurements, e.g. Lyapunov based methods, exist to proof a system is stable, see [20],[19] or [1]. A necessary condition for a stable state $x_S \in \mathbb{R}^{n_y}$ can be formulated for the system given in Eq. 2.1 as:

$$\mathbf{x}_S = \{\mathbf{x} \in \mathbb{R}^{n_y} \mid f(\mathbf{x}) = \mathbf{0}\} \quad (2.6)$$

Robustness refers in general to the stability of the system in presence of uncertainties and has been studied extensively, see e.g. [26],[27], [12]. To give a better understanding of the relevant points of the subject both SISO and MIMO cases are presented.

For any given SISO system with a transfer function $g : \mathbb{R} \mapsto \mathbb{C}$ we see from Eq. 2.4 that the behaviour of the output with respect to measurement noise and disturbances is strongly dependent on the sensitivity function. A necessary condition for the system to reach the reference is that disturbance and noise are attenuated near the steady state. Furthermore the destabilizing effect due to uncertain signals can be quantified via the maximum of the sensitivity function. Therefore the Maximum Sensitivity is defined as:

$$\begin{aligned} M_S &= \max_{\omega} |S| \\ &\geq \left| \frac{1}{1 - g k_y} \right| \end{aligned} \quad (2.7)$$

With Eq. 2.7 an upper boundary on the gain can be found and be used as a measure of robustness of the closed loop [3, p.323 ff.]. The maximum sensitivity is also connected to the nyquist stability and the stability margin of a system via:

$$\begin{aligned} M_S &= \frac{1}{s_M} \\ &= \frac{1}{1 - \max_{\omega} |g k_y|} \end{aligned} \quad (2.8)$$

Or rearranged to be:

$$\max_{\omega} |g k_y| = 1 - s_M \quad (2.9)$$

Due to Eq. 2.8 the maximum gain of the open loop is limited by the maximum sensitivity. Hence, the critical point is only encircled iff the maximum sensitivity is zero. Hence the system is only stable in the sense of the Nyquist Criterion if the maximum sensitivity is sufficiently small.

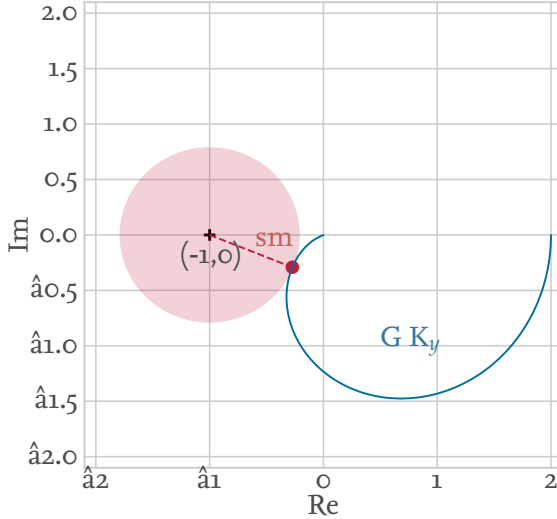


Figure 2.2: Illustration of the Connection between the maximum sensitivity, the open loop gain and the Nyquist Criterion

While the maximum sensitivity is well defined for SISO systems, a MIMO system requires a more general approach due to the interconnection of the systems out- and inputs. A general condition is given by the Small Gain Theorem [21, p.150 ff]. The theorem states, that a given feedback system is stable iff the open loop transfer function matrix is stable and its sufficient conditioned matrix norm is less than 1 over all frequencies.

$$\|GK_y\| < 1 \quad \forall \omega \quad (2.10)$$

Eq. 2.10 can be used with several matrix norms and can be viewed as an MIMO Interpretation of the Nyquist Criterion.

For further robustness analysis, the concept of singular values has to be investigated. The singular value decomposition, see e.g. [25, p.144 f.], states that any matrix $G \in \mathbb{C}^{n_a \times n_b}$ can be factorized such that

$$G = U\sigma V^* \quad (2.11)$$

Where $U \in \mathbb{C}^{n_a \times n_a}$ and $V \in \mathbb{C}^{n_b \times n_b}$ are unitary matrices representing the left and right eigenvectors of the transfer function matrix. The matrix $\sigma \in \mathbb{C}^{n_a \times n_b}$ is a quadratic, diagonal matrix consisting of the singular values $\sigma \in \mathbb{C}$ of G . A practical point of view suggest a rotation of any given input vector via V^* , distributing the magnitude of the input over the columns of σ , where they are scaled according to the magnitude of the corresponding singular value. Then the scaled and rotated vector is once again rotated by U and distributed over the output vector.

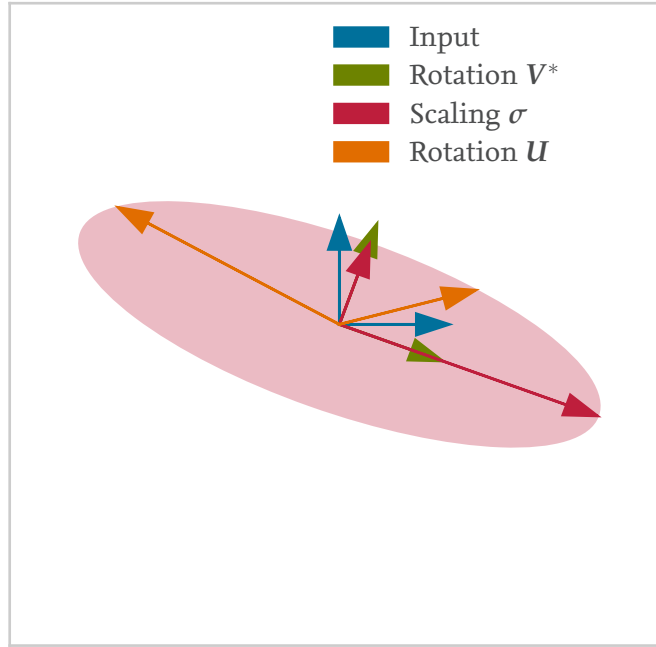


Figure 2.3: Illustration of the singular value decomposition

An example of this process is illustrated in Fig. 2.4 for a system with two inputs u_1, u_2 and two outputs y_1, y_2 . The output is bounded by the ellipsoid described by the maximum singular value $\bar{\sigma}$ and the minimum singular value $\underline{\sigma}$. The orientation and the magnitude of the outputs change depending on the frequency but will never exceed these limits. The singular values of a matrix are hence representing the highest possible gain for any given input if $U = V^* = I$.

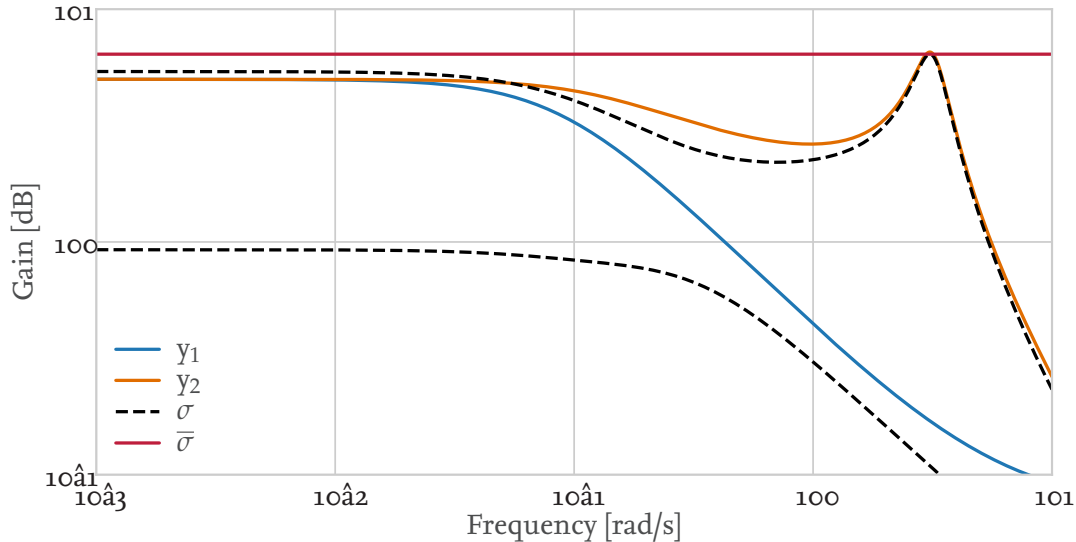


Figure 2.4: Example for the maximum singular value as an upper limit to the gain

With that, the induced 2-Norm for a matrix can be defined as:

$$\begin{aligned}
 \|G\|_2 &= \frac{\|Gu\|_2}{\|u\|_2} \\
 &= \max \sqrt{\lambda(G^*G)} \\
 &= \bar{\sigma}
 \end{aligned} \tag{2.12}$$

The induced 2-Norm is used to establish an upper bound on the gain of the transfer function matrix G . $\lambda(G^*G) \in \mathbb{C}$ are the eigenvalues of the product of the complex conjugate of the transfer function matrix and the transfer function matrix.

2.4 Gain Scheduling

3 Process Models and System Identification

The following chapter serves as an introduction to the modeling of energy and process plants with analogous models. Its secondary aim is to provide a short introduction to the field of system identification in general while giving an in-depth view of two simple but nonetheless very useful methods.

In Sec. 3.1 the first order time delay model is introduced. The parameters and key properties are introduced. Furthermore, an interpretation of the model error with respect to the dynamic behavior of the system is given.

Afterwards the first parameter estimation method is presented in Sec. 3.2. The basic concept is explained and visualized. An algorithm in pseudo-code is provided to clarify the approach.

The second model based fitting process is explained in Sec. 3.3. Like earlier, important relations between the measured data are given to provide the necessary steps of estimating the parameters.

A critical review of both algorithms finishes the chapter in Sec. 3.4. Drawbacks of both methodology are enlisted. It closes with recommending a procedure.

Since this chapter deals with system identification, a brief introduction to the subject is given in advance. To design a controller for a given process either a theoretical model based on physical laws or first principles, e.g. energy conservation, Newton's laws or the laws of thermodynamics, or an analogous model based on the measured relation between input and output is required. Since not all processes are well-fitted to be physically modeled, the field of system identification provides a vast toolbox for deriving the needed mathematical description. A good, practical approach towards the principles is given in [17], while [15] and [16] covers most of the techniques used today. An overview from a more philosophical and methodological perspective is [18].

An important aspect of current techniques is the statistical evaluation of the signals measured. Many simplifications to these data processing procedures require the input to be statistical independent from itself and the output. While in theory possible, in reality a signal called pseudo random binary sequence (PRBS) is used.

The most important and common used algorithm is called Least squares (LS), e.g. [17, p.62 ff]. Here the estimation process is viewed as a regression problem. LS is a parameter based estimation

approach, and able to estimate models up to nearly infinite order. Several enhancements have been provided so that the algorithm is both fast and effective while being able to handle even nonlinear models. Despite its many advantages, the need for a high order model is neither desirable nor effective. Dealing with PI/PID control requires a robust set of few parameter.

3.1 First Order Time Delay Model

As discussed earlier system identification enables the user to use various methods to process information to derive a suitable dynamical model. To ensure a deterministic, robust and simple controller, an identification based on a process model with simple dynamics is chosen. The reasons for this approach are based on the variety of the process itself as well as the algorithms used for determination of the controller parameters, see [2], [4].

The model structure used in the scope of the work is given by the transfer function

$$\hat{G} = \frac{\hat{K}}{\hat{T}s + 1} e^{-\hat{L}s} \quad (3.1)$$

Eq. 3.1 describes the function $\hat{G} : \mathbb{C} \mapsto \mathbb{C}$ in the s-plane and is called a first order time delay (FOTD) or first order plus deadtime (FOPDT) model, [2, p.16], [4, p.20, p.26], [13], [10]. The model gain $\hat{K} \in \mathbb{R}$ is the steady state gain of the system, a model time constant $\hat{T} \in \mathbb{R}^+$ and a model time delay $\hat{L} \in \mathbb{R}^+$ describe the dynamic gain and phase. Its representation as a differential equation is given to be

$$\hat{T} \frac{dy}{dt} + y = \hat{K} \sigma(t - \hat{L}) u \quad (3.2)$$

The general solution for a step response acting on Eq.3.2 is

$$y = \hat{K} \left(1 - e^{-\frac{t-\hat{L}}{\hat{T}}} \right) \sigma(t - \hat{L}) u \quad (3.3)$$

The Heavyside step function $\sigma(t) : \mathbb{R} \mapsto \mathbb{R}$ is defined as

$$\sigma(t) = \begin{cases} 0, & t < 0 \\ 1, & t \geq 0 \end{cases} \quad (3.4)$$

and hence models the delay acting on the connection between the output and the input. It is worth noting that in the special case of a SISO system a delay acting on the systems input or output is mathematical equivalent. However, for a given MIMO system model it can be of importance to model correctly where the delay intervenes.

An important characteristic with respect to the time behavior of the process is given by the normalized time $\tau, [0 \leq \tau \leq 1]$ [2, p.16]

$$\tau = \frac{\hat{L}}{\hat{L} + \hat{T}} \quad (3.5)$$

Eq. 3.5 gives the ratio of the delay and the sum of delay and time constant, called average residence time. It can be used as a rating regarding the difficulty of controlling the process, since a high normalized time indicates a delay dominance and hence a very difficult process to control. It can also be connected to the gain ratio [4, p.27].

Since the process model is of utmost interest for the overall process, a detailed investigation of its properties is conducted. This detailed description is started by investigating the model gain over the frequency. It is conventional to substitute the complex variable s with the complex frequency $s = j\omega$. The gain of the process model is hence given by:

$$\begin{aligned} |\hat{G}| &= \left| \frac{\hat{K}}{\hat{T}j\omega + 1} e^{-\hat{L}j\omega} \right| \\ &= \left| \frac{\hat{K}}{\hat{T}j\omega + 1} \right| \underbrace{\left| e^{-\hat{L}j\omega} \right|}_{|\cos(\hat{L}\omega) + j\sin(\hat{L}\omega)|=1} \\ &= \left| \frac{\hat{K}}{\hat{T}j\omega + 1} \right| \end{aligned} \quad (3.6)$$

Eq.3.6 shows that the gain over the frequency of a FOTD model is equal to the gain of a first order system with the same time constant. The effect of the time delay is canceled due to the use of Euler's identity, which can be interpreted as an orthonormal rotation in the complex plane by an angle $\hat{L}\omega \in \mathbb{R}^+$ around the origin.

The systems phase can be described as

$$\begin{aligned} \hat{\phi} &= \arg(\hat{G}) \\ &= \arg\left(\frac{\hat{K}}{\hat{T}j\omega + 1} e^{-\hat{L}j\omega}\right) \\ &= \arg\left(\frac{\hat{K}}{\hat{T}j\omega + 1}\right) + \arg(e^{-\hat{L}j\omega}) \\ &= \arg\left(\frac{\hat{K}}{\hat{T}j\omega + 1}\right) - \hat{L}\omega \end{aligned} \quad (3.7)$$

From Eq.3.7 the effect of the time delay follows directly. It imposes a negative shift in phase proportional to the frequency on the system.

Defining an error between the real, unknown system and the FOTD model requires the following identities of a general transfer function:

$$\begin{aligned}
G &= \frac{\sum_{i=0}^n a_i s^i}{\sum_{k=0}^m b_k s^k} \\
&= \frac{\prod_{i=0}^n (s^i - z_i)}{\prod_{k=0}^m (s^k - p_k)}
\end{aligned} \tag{3.8}$$

Eq.3.8 shows the identities of a transfer function given as a polynomial in s and its equivalent representation as a product of linear factor, see [20, p.269 ff]. The linear factorization consists of its zeros $z_i \in \mathbb{C}$ and poles $p_k \in \mathbb{C}$. Both identities will be useful due to the different properties of the gain and phase. Additionally it is assumed that the first order dynamics have been ideally identified. Hence, the error depends only on dynamics of higher order.

The relative error in Gain $\Delta_K \in \mathbb{C}$ can therefore be described as

$$\begin{aligned}
\Delta_K &= \left| \frac{\hat{G}}{G} \right| \\
&= \underbrace{\left| \frac{\hat{K}}{\hat{T} j\omega + 1} \frac{(1-p_0)(s-p_1)}{1-z_0} \right|}_{\approx 1} \left| \frac{\prod_{k=2}^m (s^k - p_k)}{\prod_{i=1}^n (s^i - z_i)} \right| \\
&\approx \left| \frac{\prod_{k=2}^m (s^k - p_k)}{\prod_{i=1}^n (s^i - z_i)} \right|
\end{aligned} \tag{3.9}$$

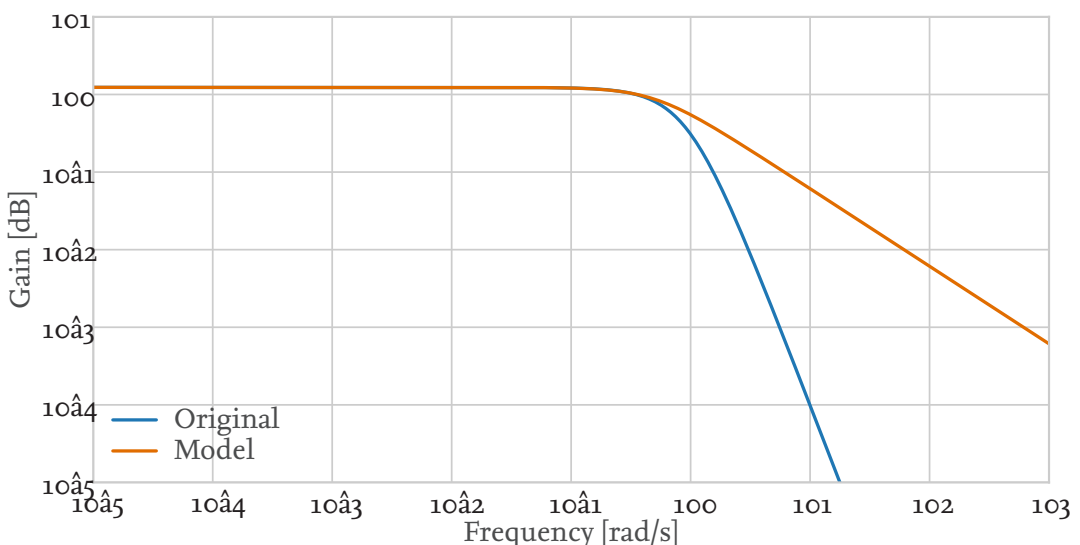


Figure 3.1: Gain of a high order transfer function and corresponding FOTD model

From Eq.3.9 two important conclusions can be conducted. First, the error is small near the steady state iff the first order dynamics are estimated correctly. The steady state model is even error free,

iff the true gain can be identified. Secondly, the error will increase dramatically for higher order dynamics since the model is not able to project these frequencies in an adequate manner. Another source of error can be found in low order zeros of the system, which will result in an infinite error of the gain. The gain error is visualized in Fig.3.2. Here a high order system with a dominant first order dynamics is approximated by a FOTD process model. The gain is nearly identical until the point $\{[2, -j6]\}$. Here the system models time delay rotate the real and imaginary part and hence transforms the position of the trajectory.

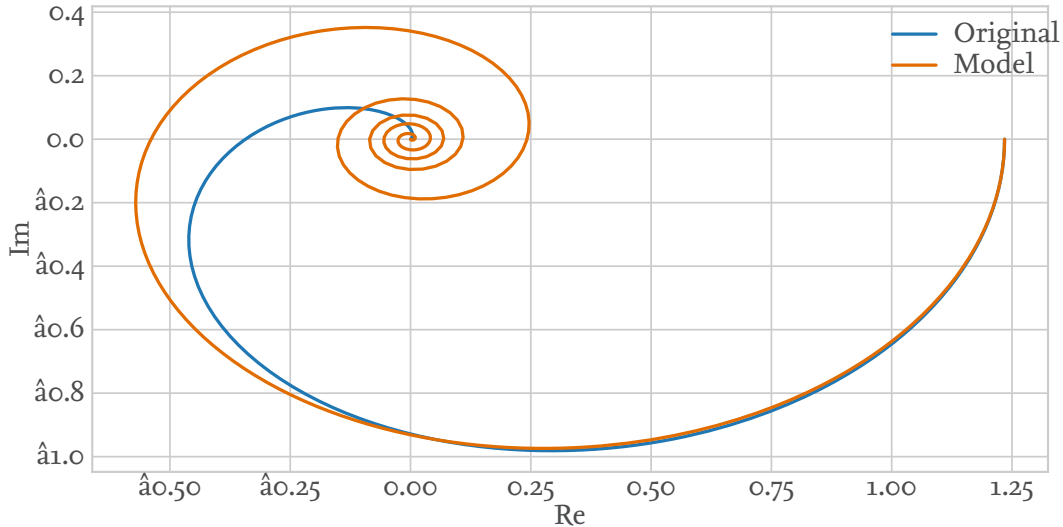


Figure 3.2: Nyquist diagram of high order transfer function and corresponding FOTD model

Likewise, the relative error in phase $\Delta_\varphi \in \mathbb{C}$ is given as:

$$\begin{aligned}
 \Delta_\varphi &= \arg \left(\frac{\hat{G}}{G} \right) \\
 &= \arg \left(\underbrace{\frac{\hat{K}}{\hat{T} j\omega + 1} \frac{(1-p_0)(s-p_1)}{1-z_0}}_{\approx 1} \frac{\prod_{k=2}^m (s^k - p_k)}{\prod_{i=1}^n (s^i - z_i)} e^{-\hat{L} s} \right) \\
 &= -L \omega + \arg \left(\frac{\prod_{k=2}^m (s^k - p_k)}{\prod_{i=1}^n (s^i - z_i)} \right)
 \end{aligned} \tag{3.10}$$

Eq. 3.10 gives an important insight to the function of the time delay. It compensates for the higher order dynamics in phase, effectively reducing the error in phase. An example is given in Fig.3.3. In Fig. 3.10 shows the ability of the approximation to mimic the phase of the real process. Until $\omega \approx 0.13 \frac{rad}{s}$ the phase of the system model is nearly equivalent to the original system. After crossing this frequency, the model approximates a phase less than that of the original system, which is identical with a conservative estimate of the dynamic behavior.

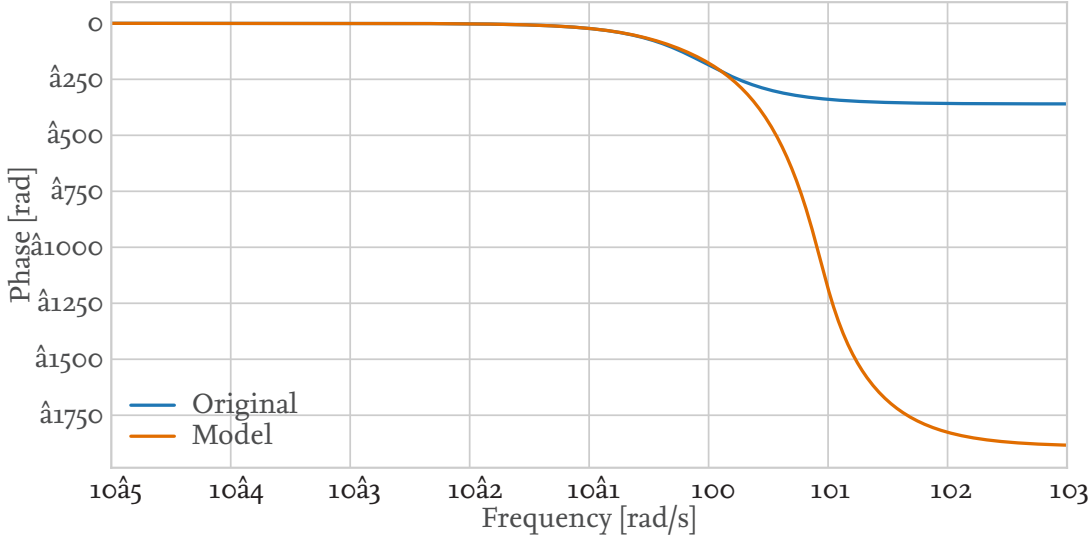


Figure 3.3: Phase of High Order Transfer Function and Corresponding FOTD model

3.2 Integral Fitting Approach

The first algorithm to estimate the parameter of the model is based on inherent knowledge of the time behavior of the model. These properties described in the section can be found in e.g. in [10], [13] and are part of mostly any undergraduate course in control theory. The experiment providing the needed data is a step response around the working point. The algorithm depends on the collected data of the input, the output and the time. It processes the data by evaluating several numerical integrals and connects the outcomes to the process parameters.

At first, the difference between the settling value of the output, $y(\infty)$, and the current value, $y(t)$, is computed over time

$$\begin{aligned}
 \int_0^\infty [y(\infty) - y(t)] dt &= \int_0^\infty \left[y(\infty) - \hat{K} \left(1 - e^{-\frac{t-\hat{L}}{\hat{T}}} \right) \sigma(t - \hat{L}) \right] dt \\
 &= \hat{K} \int_0^{\hat{L}} \sigma(t) dt + \hat{K} \int_0^\infty e^{-\frac{t}{\hat{T}}} dt \\
 &= \hat{K} \hat{L} + \hat{K} \left(-\hat{T} e^{-\frac{\hat{L}}{\hat{T}}} \right) \Big|_0^\infty \\
 &= \hat{K} (\hat{T} + \hat{L}) \\
 &= \hat{K} \hat{T}_{ar}
 \end{aligned} \tag{3.11}$$

In Eq.3.11 the average residence time $\hat{T}_{ar} \in \mathbb{R}^+$ is calculated from the integral. To simplify the equation above the linearity of the integral has been employed. Additionally the properties of the Heavyside function enabled a change in the lower boundary, hence the simplification.

Further exploitation of Eq. 3.3 leads to the following integral

$$\begin{aligned}
 \int_0^{\hat{T}_{ar}} y(t) dt &= \int_0^{\hat{T}_{ar}} \left[\hat{K} \left(1 - e^{-\frac{t-\hat{L}}{\hat{T}}} \right) \sigma(t - \hat{L}) \right] dt \\
 &= \int_{\hat{L}}^{\hat{T}_{ar}} \left[\hat{K} \left(1 - e^{-\frac{t}{\hat{T}}} \right) \right] dt \\
 &= \hat{K} \left(t + \hat{T} e^{-\frac{t}{\hat{T}}} \right) \Big|_{\hat{L}}^{\hat{T}_{ar}} \\
 &= \frac{\hat{K}}{e} \hat{T}
 \end{aligned} \tag{3.12}$$

At last, the gain \hat{K} has to be computed. With the common definition, e.g. given in [20, p.213], the parameter can be computed using

$$\hat{K} = \lim_{t \rightarrow \infty} \frac{y(t) - y(0)}{u(t) - u(0)} \tag{3.13}$$

This interpretation is rooting in the final value theorem. Using Eq. 3.13 in combination with the other two relations one is able to compute all needed parameters.

Assuming a disturbed output η as described earlier, where measurement noise is added to the real output, one can see the benefits of using Eq. 3.11 and 3.12. Since the expected value / mean of the noise is given by

$$\begin{aligned}
 \int_{-\infty}^{\infty} \eta(t) dt &= \int_{-\infty}^{\infty} [y(t) + n(t)] dt \\
 &= \int_0^{\infty} y(t) dt + \underbrace{\int_0^{\infty} n(t) dt}_{=0} \\
 &= \int_0^{\infty} y(t) dt
 \end{aligned} \tag{3.14}$$

From Eq. 3.14 follows that measurement noise has no effect on the average residence time and the time constant. Hence, both model parameter can robustly be estimated. In contrast, Eq. 3.13 is strongly reliant on the signal to noise ratio. If the system is strictly monotone, meaning its outputs is only increasing over time, one can use an average over a measured time interval $\Delta T \in \mathbb{R}^+$. The model gain can be estimated with

$$\hat{K} = \lim_{\Delta T \rightarrow \infty} \frac{1}{\Delta T} \frac{\int_0^{\Delta T} [y(t) - y(0)] dt}{u(t) - u(0)} \tag{3.15}$$

The system of equations as described above are called area-based methods, [13], with regards to its visualization displayed in Fig. 3.4, where the response to a unit step of a FOTD system is shown.

Another, likewise valid understanding is given as the minimization of the integral of the error between the real system and the model over time.

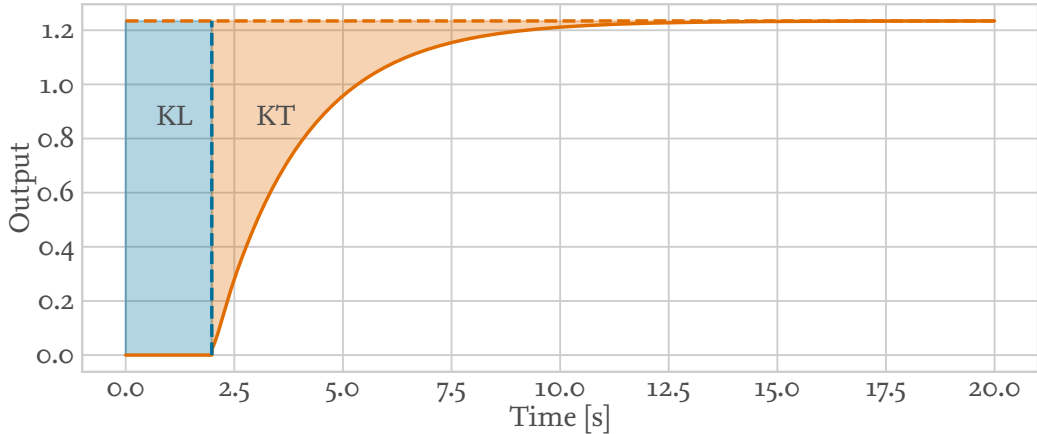


Figure 3.4: Interpretation of the Integral Fitting Approach using Areas given by a unit step response

However, the algorithm described above is not robust. It only converges iff the systems gain is equivalent with the infinity norm of the output. This resembles a dominant steady state gain. In other words, the integral Eq. 3.11 must be positive definite, meaning the time response of the process is monotonic increasing. To ensure this, several options are available.

Since a conservative estimation of the system will result in a robust controller, the gain is preferred to be calculated to big. Likewise a smaller phase increases the immunity to disturbance. Hence, a conservative bound is established with truncating the data so that the maximum output is corresponding to the end of measurement. The systems gain will be computed as

$$\hat{K} = \lim_{t \rightarrow t^*} \frac{y(t^*) - y(0)}{u(\infty) - u(0)}, \quad y(t^*) = \sup_{0 \leq t \leq \infty} y(t) \quad (3.16)$$

Eq. 3.16 defines the gain as the ratio between the supremum of the measurement data and the change in input. This results in a positive semidefinite value of the integral given by Eq.3.11. Furthermore, the results in two extreme cases. The algorithm can provide the real system, iff the output data is monotonically increasing. With that, the supremum of the collected data is equal to the final value and Eq.3.16 converges to Eq. 3.13. On the other hand the system is identified as a (scaled) step response or a strictly proportional element, iff the supremum is equal to the first collected data point. An illustration of the former reasoning is given in Fig.3.5, where some responses of a not monotonic behavior are identified using the supremum gain.

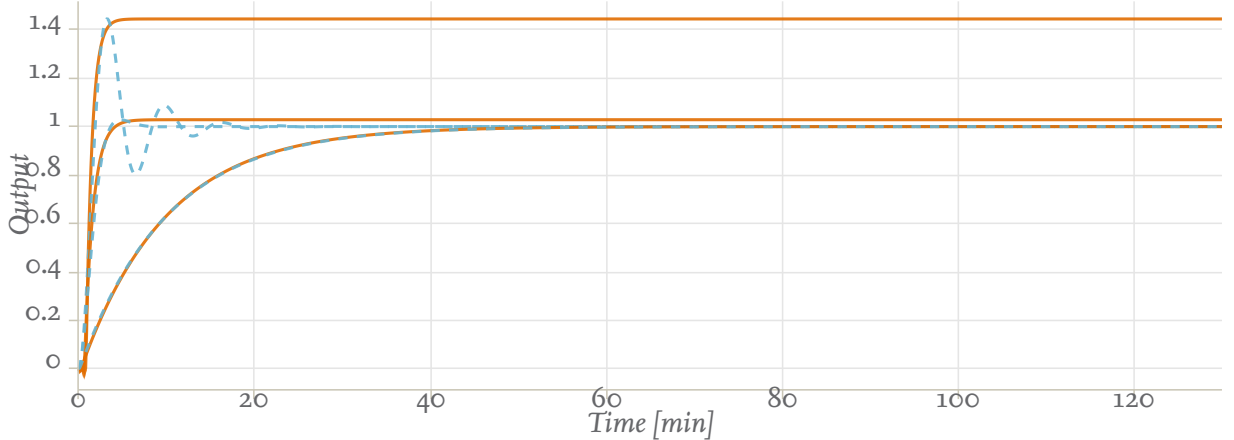


Figure 3.5: Identification of the Systems Gain using the Supremum of the Step Response

3.3 Asymmetric Relay Experiment

Another class of experimental methods based on a priori model structure is called relay experiments. These methods have been introduced in the early 1980's, ZITIEREN, and have since then been investigated, developed and used in an industrial context, see . The following section is mainly based on the recent works [9], [7] and [8].

The key concept to estimate the needed parameters is based on the systems response to an (asymmetric) relay input, forcing a semi-stationary limit cycle. This behavior is illustrated in FIG. .

HIER FIGURE

The block diagram used to generate the output is shown in FIG.

HIER FIGURE

The relay generating the input signal of the process can be described as follows:

$$u(t) = \begin{cases} u_H & e(t) > h, \dot{e}(t) > 0 \\ u_H & e(t) < h, \dot{e}(t) < 0 \\ u_L & e(t) > -h, \dot{e}(t) > 0 \\ u_L & e(t) < -h, \dot{e}(t) < 0 \end{cases} \quad (3.17)$$

In Eq. 3.17 the output switches between an upper and lower limit, $u_H, u_L \in \mathbb{R}$, $u_H \geq u_L$ depending on the hysteresis $h \in \mathbb{R}^+$, the error of the signal and its time derivative. Iff the relation $|u_H| = |u_L|$ holds true, the relay is called symmetric, if not it is an asymmetric relay, with $|u_H| > |u_L|$. Note that the system of equations above can be formulated with respect to the former value of itself. Since the process is defined around a set point $y_R \in \mathbb{R}$ it is useful to define the corresponding input

$u_R \in \mathbb{R} | y = y_R$. Hence, the difference in input is given by $\delta u_H = |u_H - u_R|$ and $\delta u_L = |u_L - u_R|$.

From FIG a difference the period $t_P = t_{on} + t_{off} \in \mathbb{R}^+$ consisting of the sum of the half-periods $t_{on} \in \mathbb{R}^+ | u = u_H$ and $t_{off} \in \mathbb{R}^+ | u = u_L$.

To estimate the parameter set of a FOTD model, the normalized time delay is approximated according to [7, p.26 f.]:

$$\begin{aligned}\tau &= \frac{\hat{L}}{\hat{T} + \hat{L}} \\ &= \frac{\gamma - \rho}{(\gamma - 1)(0.35\rho + 0.65)}\end{aligned}\tag{3.18}$$

With the half-period ratio $\rho = \frac{\max(t_{on}, t_{off})}{\min(t_{on}, t_{off})} \in \mathbb{R}^+$ and $\gamma = \frac{\max(\delta u_H, \delta u_L)}{\min(\delta u_H, \delta u_L)}$ being the asymmetry level of the relay. Notice the impact of an symmetry in the relay, since it immediately follows that Eq. 3.18 is singular if the amplitudes are symmetric. Furthermore, the delay is zero estimated to zero iff the half-period ratio is equal to the asymmetry level.

To compute the gain the following relationship can be utilized:

$$\begin{aligned}\hat{K} &= \frac{\int_{t_p} y(t) - y_R dt}{\int_{t_p} u(t) - u_R dt} \\ &= \frac{\int_{t_p} y(t) - y_R dt}{(u_H - u_R) t_{on} - (u_L - u_R) t_{off}}\end{aligned}\tag{3.19}$$

Eq. 3.19 calculates the gain as a ratio between the quasi stationary limit cycles. The importance of the asymmetry is again visible by investigating the denominator. Singularities of Eq. 3.19 are given iff the quantities of turn-on and turn-off phase are either equal, which resembles a symmetric relay, or in a suitable ratio to each other.

The time constant of the model can be calculated using one of the following equations:

$$\begin{aligned}t_{on} &= \hat{T} \log \left(\frac{h/\hat{K} - \delta u_L + e^{\frac{\hat{L}}{\hat{T}}} (\delta u_H + \delta u_L)}{\delta u_H - h/\hat{K}} \right) \\ t_{off} &= \hat{T} \log \left(\frac{h/\hat{K} - \delta u_H + e^{\frac{\hat{L}}{\hat{T}}} (\delta u_H + \delta u_L)}{\delta u_L - h/\hat{K}} \right)\end{aligned}\tag{3.20}$$

Eq. 3.20 can be exploited by using the Eq. 3.18 by solving it for the ratio between time delay and time constant. Hence, the system can be used to computed \hat{T} and thus \hat{L} .

While computing the gain is robust to measurement noise, see Eq. 3.14, an immediate disadvantage can be seen from the computation of the systems delay and time constant. If the delay of a

real process is small, the experiment does give parameter in adequate error limit [9] and different process models need to be used, eventually requiring numerical parameter fitting [7, p. 31 ff.]. Furthermore the needed experimental parameter, such as asymmetry and hysteresis, take influence on the result of the estimation [9] and have to be chosen according to the process itself. Hence, several experiments are needed to fully identify the systems parameter. At last, the

3.4 Review

Above two important and well known fitting techniques based on structural knowledge of a FOTD and hence mathematical formulations of the model have been introduced. Even though both methods are used throughout industry, there are certain drawbacks to each method which should be considered.

While the asymmetric relay process introduced in Sec. 3.3 is especially useful in determining the model parameter with a quasi stationary limit cycle it requires several in depth adjustments and process knowledge. Adjusting the asymmetry and the hysteresis in a proper way has an notable impact on the result [9]. The noise level, process gain and sampling times influences the algorithm. Hence, prior experiments have to be made. Additionally, not every process is suited to be estimated in the described way [9],[7]. Depending on the normalized time delay several changes in model structure or additional experiments must be performed. Depending on the process time scale and the requirement of a quasi stationary cycle the experiment can require several hours.

Apparently, the parameter estimation based on area methods as given in Sec.3.2 has the disadvantage of both requiring a steady process output. Hence, the parameter can not fully be estimated. Another drawback is given by the assumption of a dominant static gain. The error in gain and phase get higher by using Eq.3.16.

However, both methods are - up to a certain degree - independent from measurement noise and well established. Due to the simplicity and robustness of the area based identification it is commendable to use this algorithm.

4 Multivariable PI/PID Controller Design

Chapter 4 gives an overview about basic concepts used in the context of this work. The fundamentals can be found in the literature already mentioned in Ch.2. Additional information on process control and especially PID control is given in [2] and [4]. The concepts of decoupling control are explained in great detail in [23].

The chapter starts in Sec. 4.1 with a brief explanation of the tuning rules used to derive the parameter set of the controller.

Afterwards a method to evaluate the input output coupling in multivariable process models is explained in Sec.4.2. Some interesting properties are explained in detail.

In Sec.4.3 the key concept of this work is explained. Starting by introducing a method presented in [5] and developing it to an equivalent, but more useful representation, the design of decoupled control loops is given.

4.1 AMIGO Tuning Rules

Many rules to design proportional-integral-derivative controller exist [4, p.158 ff.]. The most famous set of rules has been developed by Ziegler and Nichols. Other rules, such as Cohen-Coon, can be named as well. The simple set of rules, derived by experimental procedures, have since then been reused for several tuning approaches [4, p.169]. Other, analytical methods e.g. Pole Placement or Haalman's Method exists as well, but require a detailed model of the process. In [4, p.206 ff.] a robust loop shaping based on optimization has been introduced. A key concept is illustrated by the robustness region of a given process, depending on the controllers parameter set and the constrain in form of a maximum sensitivity. These optimization process lead to the M constrained Integral Gain Optimization (MIGO) method [4, p.217], an iterative algorithm calculating the needed parameter values. The Approximate MIGO (AMIGO) tuning rules have been introduced in [4, p.225 ff.]. They are derived by applying the MIGO algorithm to a test batch while demanding $M_S = 1.4$. All processes of the test batch are approximated by a sufficiently analogous model, namely a integrating process with delay, a FOTD model , as described in Sec.3.1 and a second order model.

The investigation of the optimization results can be condensed into the following set of equations for a simple proportional-integral controller based on a FOTD model approximation:

$$\begin{aligned} K_P &= \frac{0.15}{\hat{K}} + \left(0.35 - \frac{\hat{L} \hat{T}}{(\hat{L} + \hat{T})^2} \right) \frac{\hat{T}}{\hat{K} \hat{L}} \\ T_I &= 0.35 \hat{L} + \frac{13 \hat{L} \hat{T}^2}{\hat{T}^2 + 12 \hat{L} \hat{T} + 7 \hat{L}^2} \end{aligned} \quad (4.1)$$

Eq.4.1 defines the proportional gain of the controller $K_P \in \mathbb{R}$ and the integral time $T_I \in \mathbb{R}$.

Additionally, the optimal calculated parameter of a proportional-integral-derivative controller are formulated as

$$\begin{aligned} K_P &= \frac{1}{\hat{K}} \left(0.2 + 0.45 \frac{\hat{T}}{\hat{L}} \right) \\ T_I &= \frac{0.4 \hat{L} + 0.8 \hat{T}}{\hat{L} + 0.1 \hat{T}} \hat{L} \\ T_D &= \frac{0.5 \hat{L} \hat{T}}{0.3 \hat{L} + \hat{T}} \end{aligned} \quad (4.2)$$

Eq.4.2 introducing the derivative Time $T_D \in \mathbb{R}$.

The AMIGO rules presented above hold several properties described in [4, p.229 ff]. Important advice in the context of this work is given in form of a recommendation for set-point weighting [4, p.229 f, p.235 ff] and a drawback with respect to lag dominance [4, p.231 ff].

In [4, p.253 ff.] the detuning process is described. Since detuning is an essential element of the overall design procedure, as shown later, the method will be explained here. It is used if the controller is acting too fast and hence producing unwanted overshoot. To reduce this effect, the controller parameter need to be scaled to smaller values while ensuring the stability. Therefore an algorithm describing the adjustment of the gains with respect to each other is needed.

Based on the maximum sensitivity the following dimensionless factors are defined

$$\begin{aligned} \alpha_D &= \frac{M_S - 1}{M_S} \\ \beta_D &= M_S \frac{M_S + \sqrt{M_S^2 - 1}}{2} \end{aligned} \quad (4.3)$$

Eq. 4.3 defines the factors needed for calculating the new value of the integral gain $K_I = \frac{K_P}{T_I}$ according to

$$K_I^{i+1} = \begin{cases} K_I^i \frac{\alpha_D + K_P^{i+1} \hat{K}}{\alpha_D + K_P^i \hat{K}}, & K_P^{i+1} \hat{K} \geq \frac{K_I^i \hat{K} (\hat{L} + \hat{T})}{\beta_D (\alpha_D + K_P^{i+1} \hat{K})} - \alpha_D \\ \beta_D \frac{(\alpha_D + K_P^{i+1} \hat{K})^2}{\hat{K} (\hat{L} + \hat{T})}, & K_P^{i+1} \hat{K} < \frac{K_I^i \hat{K} (\hat{L} + \hat{T})}{\beta_D (\alpha_D + K_P^{i+1} \hat{K})} - \alpha_D \end{cases} \quad (4.4)$$

Eq.4.4 is derived by investigating the robustness of a FOTD system in dependence of the parameter of the controller and approximation of the same.

4.2 Interaction Measures of Multivariable Processes

Current controller design in the problem set of this work is mostly relying on the assumption that the system is behaving like an assembly of single input single output processes. It is based not on holistic approaches but on calculating the parameter solely with regards to the current loop. To choose the right pairing of in- and outputs resembling with a maximal dominance over the output the relative gain array (RGA) has been introduced by [11]. Other measurements and indicators, like the Hankel Singular Values, Hankel Interaction Indexes or the Participation Matrix, have been developed as well, see e.g. QUELLEN. The RGA however is used intensively in industry and described in literature [21, p. 88 ff], [14, p.219 ff]. The RGA is defined as

$$\Lambda(\mathbf{G}) = \mathbf{G} \circ \mathbf{G}^{-T} \quad (4.5)$$

The RGA $\Lambda : \mathbb{C}^{n_y \times n_y}, \mathbb{C}^{n_y \times n_y} \mapsto \mathbb{C}^{n_y \times n_y}$ as defined in Eq.4.5 is given by the hadamard product of the transfer function matrix and its transposed inverse. It can be interpreted as a ratio between open loop control and closed loop control [14, p.221]. Most commonly, the RGA is computed in the steady state of the system, but the elements near the crossover frequency give likewise useful information. To illustrate this, consider a simple system with a steady state gain and its inverse given by

$$\begin{aligned} |\mathbf{G}|_{s=0} &= \begin{bmatrix} 2 & -1 \\ 5 & 10 \end{bmatrix} \\ |\mathbf{G}|_{s=0}^{-1} &= \frac{1}{25} \begin{bmatrix} 10 & 1 \\ -5 & 2 \end{bmatrix} \end{aligned} \quad (4.6)$$

The corresponding RGA is given by:

$$\begin{aligned} \Lambda(\mathbf{G}) &= \begin{bmatrix} 2 & -1 \\ 5 & 10 \end{bmatrix} \frac{1}{25} \begin{bmatrix} 10 & 1 \\ -5 & 2 \end{bmatrix}^T \\ &= \frac{1}{25} \begin{bmatrix} 2 & -1 \\ 5 & 10 \end{bmatrix} \begin{bmatrix} 10 & -5 \\ 1 & 2 \end{bmatrix} \\ &= \frac{1}{25} \begin{bmatrix} 20 & 5 \\ 5 & 20 \end{bmatrix} \\ &= \begin{bmatrix} 0.8 & 0.2 \\ 0.2 & 0.8 \end{bmatrix} \end{aligned} \quad (4.7)$$

Which indicates a pairing of the main diagonals, since the matrix is diagonal dominant. In other terms, the system in closed loop control will behave nearly like the open loop control system. To discuss the RGA at crossover frequency, assume the system is in reality described by:

$$G(s) = \begin{bmatrix} \frac{2}{s+1} & \frac{5s-1}{s+1} \\ \frac{5}{s+1} & \frac{10}{s+1} \end{bmatrix} \quad (4.8)$$

The gain crossover frequency of MIMO systems is defined as the first frequency at which any of the transfer functions crosses the unit gain, or equivalently zero dB, from above [21, p.37]. Assuming normalized gains $k_{ij} = 1$ holds that $\omega_C = \min(\frac{1}{T_{ij}})$ for any pure lag systems. Hence, the estimated crossover frequency of above system is $\omega_C \approx 1$. The systems gain and its inverse is given by the complex matrices:

$$\begin{aligned} |G|_{s=j} &= \frac{1}{j+1} \begin{bmatrix} 2 & 5j-1 \\ 5 & 10 \end{bmatrix} \\ |G|_{s=j}^{-1} &\approx \begin{bmatrix} 0.000 & 0.200 \\ 0.000 & 0.000 \end{bmatrix} + j \begin{bmatrix} 0.400 & 0.040 \\ 0.200 & 0.080 \end{bmatrix} \end{aligned} \quad (4.9)$$

The complex valued RGA of the system at the given frequency computes to be:

$$\Lambda(G|_{s=j}) = \begin{bmatrix} 0.400 & 0.600 \\ 0.600 & 0.400 \end{bmatrix} + j \begin{bmatrix} 0.400 & -0.400 \\ -0.400 & 0.400 \end{bmatrix} \quad (4.10)$$

Which indicates a cross pairing over the minor diagonal of the system, since the real parts of the matrix are dominant.

Interesting properties of the RGA can be found in literature, eg. [21], [2], [4]. However, the connection between the condition number $\kappa_C : \mathbb{R}, \mathbb{R} \mapsto \mathbb{R}$ and the RGA explained in [21, p.88 f.] is worth noticing. The condition number is given as

$$\begin{aligned} \kappa_C &= \frac{\bar{\sigma}(G)}{\underline{\sigma}(G)} \\ &= \bar{\sigma}(G)\bar{\sigma}(G^{-1}) \end{aligned} \quad (4.11)$$

with the $\underline{\sigma} = \min(\sigma)$ being the lower bound of the singular values of a transfer function matrix. Eq.4.11 can be interpreted as an index for the balance, meaning the ratio of the biggest and smallest possible gain, of a process. Furthermore, it can be interpreted as a measure of equivalence between the input-output relationship represented by the transfer function matrix. Hence, very large or very small condition numbers are not desirable and indicate a very poor performance. It can be minimized using scaling matrices best to be chosen by physical meaningful interpretations [21, p.87]. The sum norm of the RGA, meaning the sum over all elements of $\Lambda(G)$, is close to this minimal realizable value. Hence, large elements of the RGA indicate an ill-conditioned process.

Investigating the RGA leads to several conclusions about the optimal pairing of inputs and outputs. A selection with respect to this work is presented in the following.

If the elements of the RGA are large around the crossover frequency, a decoupler or inverse based controller should not be used [21, p. 89], where large is corresponding to values ≥ 10 . Here the robustness to the uncertainty of inputs is not given [21, p.243]. If an element of the RGA calculated around steady state is negative, the decentralized controller tend towards instability [21, p.90, p.447].

4.3 Decoupling of Multivariable Processes

Designing controller for multivariable processes has inevitable challenges. Since a general MIMO plant consists of a main coupling, represented in the main diagonal of the transfer function matrix, and cross coupling given by the minor elements of the transfer function function matrix. An illustration of this problem is given in FIG. where both forward and backward coupling is pictured in a block diagram.

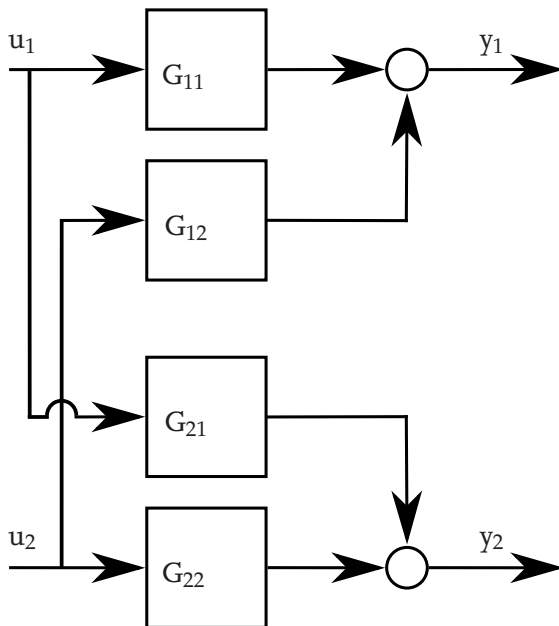


Figure 4.1: Coupling in P-canonic structure

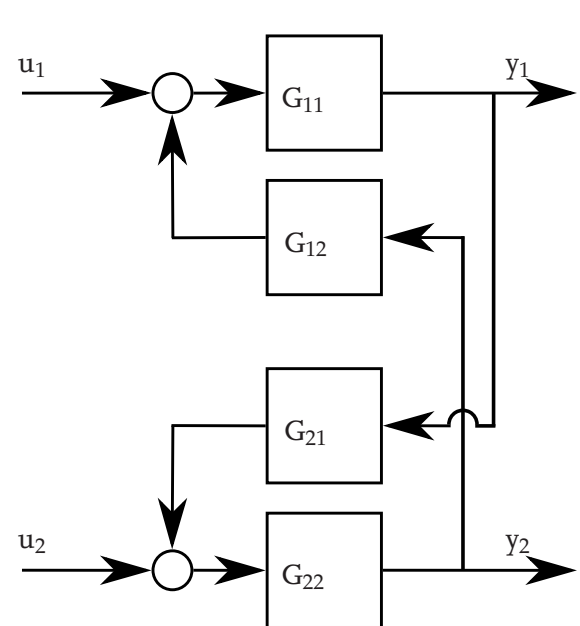


Figure 4.2: Coupling in V-canonic structure

By closing a feedback loop a connection between these two elements is made out of necessity. Hence, the overall performance and robustness of a closed loop is influenced by the cross couplings between the inputs and outputs. To achieve better results regarding these two major aspects of the control paradigm, several techniques can be used solely or in combination to reduce the influence of the minor diagonal entries.

4.3.1 Decoupling Control proposed by Åström et.al.

A method for the design of decoupling controllers is proposed in [5] and [4]. A diagonal controller K^* which limits the interaction near the steady state of the plant within certain limitations is designed. To achieve this behavior a decoupler $D \in \mathbb{R}^{n_y \times n_y}$ is introduced. A static decoupling is proposed such that $D = G^{-1}|_{s=0}$ that transforms the system with the mapping $GD = G^* \in \mathbb{R}^{n_y \times n_y}$. Since the decoupler is defined to be the inverse of the steady state gain, the steady state of the transformed system is given by the identity matrix $I \in \mathbb{R}^{n_y \times n_y}$. The block diagram of the decoupled system is given in Fig.4.3.

The resulting closed loop of the transformed system with a setpoint controller K_r and a feedback controller K_y is given by:

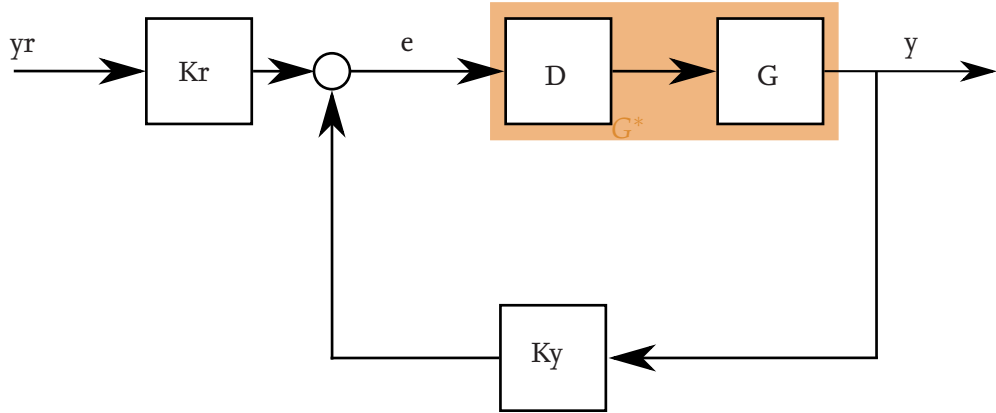


Figure 4.3: Block diagram of the decoupled system

$$\begin{aligned}
 H &= [I - GK_y]^{-1} GK_r \\
 &= [I - GDK_y^*]^{-1} GDK_r^* \\
 &= [I - G^*K_y^*]^{-1} G^*K_r^*
 \end{aligned} \tag{4.12}$$

Eq. 4.12 gives various important transformations between the controller and system of the original identified system and the new transformed system. The diagonal controller K^* , designed based on the decoupled system G^* is connected to the controller of the original system via $K^* = DK$.

A Taylor series around the steady state of the transformed system is given by:

$$\begin{aligned}
 G^* &= \sum_{i=0}^{\infty} \frac{d^i}{ds^i} G^*|_{s=0} \frac{s}{i!} \\
 &= I + s\Gamma^* + \mathcal{O}(s^2) \\
 &\approx I + \Gamma^*s \\
 &\approx I + (\Gamma_D^* + \Gamma_A^*)s
 \end{aligned} \tag{4.13}$$

In Eq.4.13 the coupling for small frequencies can be described via the coupling matrix $\Gamma^* = (\gamma_{ij}^*) \in \mathbb{R}^{n_y \times n_y}$. The matrix consists both of diagonal and anti diagonal entries $\Gamma^* = \Gamma_D^* + \Gamma_A^*$ which describes the small signal behavior of the system, represented by the first order of the series sufficiently.

Substitute Eq.4.13 in the numerator of Eq. 4.12 holds:

$$\begin{aligned}
 H &\approx [I - G^*K_y^*]^{-1} [I + \Gamma^*s] K_r^* \\
 &\approx [I - G^*K_y^*]^{-1} [I + (\Gamma_D^* + \Gamma_A^*)s] K_r^*
 \end{aligned} \tag{4.14}$$

The anti diagonal entries are given by

$$\mathbf{H}_A \approx \left[\mathbf{I} - \mathbf{G}^* \mathbf{K}_y^* \right]^{-1} [\boldsymbol{\Gamma}_A^* s] \mathbf{K}_r^* \quad (4.15)$$

According to [5], every entry of the matrix $\mathbf{H}_A = (h_{ij}) \forall i \neq j \in \mathbb{R}^{n_y \times n_y}$ simplifies to:

$$|h_{ij}| = \left| \left(\prod_{k=1}^{n_y} S_k^* \right) \gamma_{ij}^* s k_{r,jj}^* \right| \quad (4.16)$$

Where $k_{r,jj}^*$ is the j-th entry of the diagonal controller used for the reference signal \mathbf{K}_r^* , weighted by the product of the sensitivities S_k^* of all control loops. Eq. 4.16 can be used to describe the interconnections of the system and therefore the influence of each controller due to the couplings.

Next, an upper limit $h_{ij,Max}^* \geq |h_{ij}^*| \in \mathbb{R}^+$ which describes the maximal allowed or desired interaction between the j-th input and the i-th output is introduced. Typical values for the upper bound are in the range [0.1, 0.5]. Since the steady state of the transformed system is given by the identity matrix, $h_{ij,Max}$ can be interpreted as a relative error in output caused by the cross coupling, i.e. the anti diagonal entries of the system.

For the special case where $k_{r,jj}^*$ is a pure integrator $k_{r,jj}^* = \frac{k_{I,jj}^*}{s}$ Eq. 4.16 becomes:

$$\begin{aligned} |h_{ij}| &= \left| \left(\prod_{k=1}^{n_y} S_k^* \right) \gamma_{ij}^* k_{I,jj}^* \right| \\ &\leq \left| \left(\prod_{k=1}^{n_y} M_{S,k}^* \right) \gamma_{ij}^* k_{I,jj}^* \right| \\ &\leq |h_{ij,max}| \end{aligned} \quad (4.17)$$

The relation given by Eq. 4.17 gives a condition for detuning a purely integral controller. Since not every controller is given in this form, the structure is extended to PI control with set-point-weight by:

$$\begin{aligned} |h_{ij}| &\leq \left| \left(\prod_k M_{S,k} \right) \gamma_{ij}^* s \left(b k_{P,jj}^* + k_{I,jj}^* \frac{1}{s} \right) \right| \\ &\leq \left| \left(\prod_k M_{S,k} \right) \gamma_{ij}^* \right| \left| \left(b k_{P,jj}^* s + k_{I,jj}^* \right) \right| \\ &\leq \left| \left(\prod_k M_{S,k} \right) \gamma_{ij}^* \right| \left| \left(b k_{P,jj}^* j\omega + k_{I,jj}^* \right) \right| \\ &\leq \left| \left(\prod_k M_{S,k} \right) \gamma_{ij}^* \right| \sqrt{\left(b k_{P,jj}^* \omega \right)^2 + \left(k_{I,jj}^* \right)^2} \end{aligned} \quad (4.18)$$

While Eq.4.17 describes a relation for a pure integrator transferring the set-point signal into the systems input, this is not a general notion. In Eq.4.18 the influence of the proportional controller is increasing with the frequency and thus the interaction. Adding a derivative term to the equation leads to further frequency related increases of the interaction. Since [5] focuses purely on the special case $b = 0$, a practical solution for the frequency dependence is proposed.

To detune the controller sufficiently, an adequate frequency must be chosen. In [21, p.172 f.] the crossover frequency of a pure time delay transfer function is limited by an upper bound

$$\omega_c \leq \frac{1}{L} \quad (4.19)$$

Eq. 4.19 states that the crossover frequency is inversely proportional to the delay of a system. From a practical point of view, systems with a high delay have a very limited bandwidth and can only be controlled properly near the steady state. For a more general system, it is not practical to rely only on the delay for determination of the upper boundary of the frequency. Imagine a process with a small normalized time delay and an induced high first order dynamics. The crossover frequency is dominated by the time constant T , meaning $\omega_c \approx \frac{1}{T} \ll \frac{1}{L}$. This assumption relies on the behavior of the gain of a lag dominant n-th order model which is monotonic decreasing with $-3\frac{dB}{dec}$ for frequency $\omega \geq \frac{1}{T}$. To ensure a robust detuning, another bound needs to be established.

Since the detuning process relies on the first order approximation of the process via a Taylor series around $s = 0$, a bound can be found by ensuring the frequency dependent dominance of the expression. This is given as long as the second order terms are small in relation to the first order:

$$\begin{aligned} |(T + L) s| &\geq \left| [(T^2 + L^2) + T^2] \frac{s^2}{2} \right| \\ |s| &\leq 2 \left| \frac{T + L}{(T^2 + L^2) + T^2} \right| \\ \omega_c &\leq 2 \left| \frac{T + L}{(T^2 + L^2) + T^2} \right| \end{aligned} \quad (4.20)$$

The statement given by Eq. 4.20 relates the crossover frequency to the both delay and time constant of the system. If the delay of a system is small, $L \rightarrow 0$ than the corresponding crossover frequency corresponds to $\omega_c \rightarrow \frac{1}{T}$, which is identical to a simple first order process. To ensure a robust detuning, the frequency used is multiplied by a safety factor $R \in [1, 2]$, since the RHS of Eq. 4.18 is monotonically increasing in ω . A graphical interpretation of the reasoning above is given in FIG

HIER FIG

Likewise to Eq.4.18 the interaction for a PID controller with set-point-weight can be estimated with:

$$\begin{aligned}
|h_{ij}| &\leq \left| \left(\prod_k M_{S,k} \right) \gamma_{ij}^* s \left(b k_{P,jj}^* + k_{I,jj}^* \frac{1}{s} + b_D k_{D,jj}^* s \right) \right| \\
&\leq \left| \left(\prod_k M_{S,k} \right) \gamma_{ij}^* \right| \left| \left(b k_{P,jj}^* s + k_{I,jj}^* + b_D k_{D,jj}^* s^2 \right) \right| \\
&\leq \left| \left(\prod_k M_{S,k} \right) \gamma_{ij}^* \right| \left| \left(b k_{P,jj}^* j\omega + k_{I,jj}^* + b_D k_{D,jj}^* (j\omega)^2 \right) \right| \\
&\leq \left| \left(\prod_k M_{S,k} \right) \gamma_{ij}^* \right| \sqrt{\left(b k_{P,jj}^* \omega \right)^2 + \left(k_{I,jj}^* - b_D k_{D,jj}^* \omega^2 \right)^2}
\end{aligned} \tag{4.21}$$

From Eq. 4.21, where $b_D \in 0, 1$ denotes the set-point-weight of the derivative gain of the controller, it is obvious that the derivative gain reduces the impact of the integral gain with respect to the frequency. Hence, for larger ω the effect of the derivative gain is of much more importance.

Eq. 4.17, 4.18 and 4.21 can be rewritten in matrix form $H_{Max} = (h_{ij,Max}) \in \mathbb{R}^{n_y \times n_y}$ and the matrix of the maximum sensitivities of the diagonal transfer functions $M_S^* = (M_{S,i}^*) \in \mathbb{R}^{n_y \times n_y}$. Using the definition of the maximum sensitivity matrix as diagonal, one can rewrite $\prod_k M_{S,k}^* = \det(M_S)$. Once again dividing into a diagonal and anti diagonal matrix holds:

$$H_{A,Max} \geq \det(M_S^*) \Gamma_A^* s K_{r,Max}^* \tag{4.22}$$

Eq. 4.22 can be used to detune with the given interaction. In [4, p.357] a more progressive approach is given. Following the assumption of a sufficiently decoupled process, the matrix of sensitivity functions is nearly diagonal. Hence, the 4.16 can be rewritten to:

$$|h_{ij}| = S_i^* \gamma_{ij}^* s k_{r,jj}^* \tag{4.23}$$

Which induces Eq.4.22 to change to be

$$H_{A,Max} \geq M_S^* \Gamma_A^* s K_{r,Max}^* \tag{4.24}$$

Good results on classic theoretical examples, e.g. Rosenbrocks System, can be produced and are shown in Ch.5. However, the method has certain drawbacks. The design procedure requires a permanent decoupling, using weighted linear combinations of the controller outputs as system inputs. This is linked to a robust signal transportation. Furthermore, the transformed system in general not the proposed model structure of a FOTD system, meaning either the linear combination has to be approximated as a FOTD or the collected data of the experiments has to be reused. Since a decoupler is not in every case needed nor wanted, an immense effort designing the algorithm has to be done. Gain Scheduling for a controller would require the diagonal controller and the decoupler to be manipulated.

Imagine the systems gain to be perturbed by a relative error written as $\delta \in \mathbb{C}^{n_y \times n_y}$. The nominal process $\hat{\mathbf{G}}$, on which the decoupler is based, can be written as the real process \mathbf{G} multiplied by a scaling matrix:

$$\hat{\mathbf{G}} = (\mathbf{I} - \delta) \mathbf{G} \quad (4.25)$$

Assuming the error is small in relation to the real process, the maximum singular value of the relative error is bounded by $\bar{\sigma}(\delta) < 1$. Hence, the inverse of the nominal process model can be written as

$$\begin{aligned} \hat{\mathbf{G}}^{-1} &= \mathbf{G}^{-1} (\mathbf{I} - \delta)^{-1} \\ &= \mathbf{G}^{-1} \sum_{i=0}^{\infty} \delta^i \\ &= \mathbf{G}^{-1} + \mathbf{G}^{-1} \delta + \mathbf{G}^{-1} \delta^2 + \dots \end{aligned} \quad (4.26)$$

Eq.4.26 uses the Neumann Series QUELLE to estimate the matrix inverse. Depending on the quality of measurements which result in the perturbation of the matrix, the matrix inverse can vary largely. To illustrate this, the process gain given in REF is perturbed the following:

$$\begin{aligned} \hat{\mathbf{G}}|_{s=0} &= \begin{bmatrix} 1.05 & -0.05 \\ 0.05 & 1.05 \end{bmatrix} \begin{bmatrix} 2 & -1 \\ 5 & 10 \end{bmatrix} \\ &= \begin{bmatrix} 1.85 & -1.55 \\ 5.35 & 10.45 \end{bmatrix} \end{aligned} \quad (4.27)$$

Its inverse can be computed to

$$\hat{\mathbf{G}}|_{s=0}^{-1} = \begin{bmatrix} 0.35 & 0.06 \\ -0.19 & 0.07 \end{bmatrix} \quad (4.28)$$

Multiplying this with the real system gives:

$$\hat{\mathbf{G}}|_{s=0}^{-1} \mathbf{G} = \begin{bmatrix} 1.04 & 0.18 \\ -0.05 & 0.86 \end{bmatrix} \quad (4.29)$$

From Eq.4.29 it is visible that even small changes can make a significant difference in the solution of the inversion. Here an error of 18 percent is given on the influence of the main diagonal.

4.3.2 A Modified Controller Design Based on Åström et.al. - Robust Relative Dynamic Decoupling

To enable the use of the original system, reducing the influence of perturbation and to increase the robustness of the process, another strategy is presented in the following subsection. Building upon

the idea of detuning the first order dynamics of the system, as proposed by [5] and [4], and utilizing mathematical relationships the decoupler is transformed into another form feasible of smoothly enable and disable a decoupling. Furthermore, under certain assumptions the original transfer function model can be used to design the controller. Additionally the detuning process is modified to detune not for the relative gain of the cross couplings, but for the relative process dynamics of the open loop.

First, a decoupler similar to the one presented in Subs.4.3.1 can be deduced. Investigating the product of a matrix multiplication holds:

$$\begin{aligned} \mathbf{G}^A \mathbf{G}^B &= \begin{bmatrix} G_{11}^A & G_{12}^A \\ G_{21}^A & G_{22}^A \end{bmatrix} \begin{bmatrix} G_{11}^B & G_{12}^B \\ G_{21}^B & G_{22}^B \end{bmatrix} \\ &= \begin{bmatrix} G_{11}^A G_{11}^B + G_{12}^A G_{21}^B & G_{11}^A G_{12}^B + G_{12}^A G_{22}^B \\ G_{21}^A G_{11}^B + G_{22}^A G_{21}^B & G_{21}^A G_{12}^B + G_{22}^A G_{22}^B \end{bmatrix} \end{aligned} \quad (4.30)$$

Eq. 4.30 states that the diagonal elements are the sum of two products that either consist of pure diagonal or pure anti-diagonal entries. Anti-diagonal entries are always the mixed product of diagonal and anti-diagonal terms. Via a sufficient interchanging of rows and columns, every matrix can be ordered, such that the main coupling transfer functions are on the diagonal.

Starting with the relation between the transformed, purely diagonal controller \mathbf{K}^* of the transformed system \mathbf{G}^* , the diagonal and anti-diagonal entries of the resulting dense controller \mathbf{K} can be identified:

$$\begin{aligned} \mathbf{D}\mathbf{K}^* &= \mathbf{K} \\ (\mathbf{D}_D + \mathbf{D}_A)\mathbf{K}^* &= (\mathbf{K}_D + \mathbf{K}_A) \\ (\mathbf{D}_D + \mathbf{D}_A)\mathbf{D}^{-1}\mathbf{K} &= (\mathbf{K}_D + \mathbf{K}_A) \end{aligned} \quad (4.31)$$

Eq. 4.31 relates the diagonal controller $\mathbf{K}_D \in \mathbb{C}^{n \times n}$ designed via the diagonal transfer functions g_{ii}^* to the decoupling controller as stated in [5]. Since \mathbf{K}^* is diagonal a direct relationship between the anti-diagonal elements of the controller can be established by using the results of Eq.4.30:

$$\mathbf{K}_A = \mathbf{D}_A \mathbf{K}^*$$

Using the transformation $\mathbf{K}^* = \mathbf{D}^{-1}(\mathbf{K}_D + \mathbf{K}_A)$ holds the two relationships **MICHAEL HAT ANMERKUNG MIT ANDEREN FORMELN -> DISKUSSION:**

$$\begin{aligned} \mathbf{K}_A &= \mathbf{D}_A \mathbf{D}^{-1} (\mathbf{K}_D + \mathbf{K}_A) \\ \mathbf{K} &= \mathbf{D} \mathbf{D}_A^{-1} \mathbf{K}_A \end{aligned}$$

Next, the relation between the diagonal controller \mathbf{K}_D and the anti-diagonal controller \mathbf{K}_A based on the considerations made above is established:

$$\begin{aligned}
K_A &= K - K_D \\
&= D D_A^{-1} K_A - K_D \\
&= [D D_A^{-1} - I]^{-1} K_D \\
&= \Sigma K_D
\end{aligned} \tag{4.32}$$

Eq. 4.32 defines the splitter $\Sigma \in \mathbb{R}^{n \times n}$ which can substitute the anti diagonal controller in Eq.4.31:

$$DK^* = [I + \Sigma] K_D \tag{4.33}$$

HIER EVTL ÄNDERUNG! **The splitter is already a known tool for decoupling, as given in [23, p.190 ff.] explicitly defined in [23, p.193 Eq.(6.19)].** With further investigating the matrix relation given by Eq.4.33, the splitter can be simplified to:

$$\begin{aligned}
\Sigma &= [D D_A^{-1} - I]^{-1} \\
&= [(D_D + D_A) D_A^{-1} - I]^{-1} \\
&= [D_D D_A^{-1} + I - I]^{-1} \\
&= [D_D D_A^{-1}]^{-1} \\
&= D_A D_D^{-1}
\end{aligned}$$

An interesting property of the splitter is the intuitive relation between the main diagonal entries of the system and the anti diagonal entries. Since we can invert a block sufficient conditioned block matrix via:

$$\begin{bmatrix} G_{11} & G_{12} \\ G_{21} & G_{22} \end{bmatrix}^{-1} = \begin{bmatrix} \left[G_{11} - G_{12} G_{22}^{-1} G_{21} \right]^{-1} & -G_{11}^{-1} G_{12} \left[G_{22} - G_{21} G_{11}^{-1} G_{12} \right]^{-1} \\ -G_{22}^{-1} G_{21} \left[G_{11} - G_{12} G_{22}^{-1} G_{21} \right]^{-1} & \left[G_{22} - G_{12} G_{11}^{-1} G_{12} \right]^{-1} \end{bmatrix} \tag{4.34}$$

The splitter given by $D_A D_D^{-1}$ becomes in the notation above

$$\Sigma = \begin{bmatrix} 0 & -G_{11}^{-1} G_{12} \\ -G_{22}^{-1} G_{21} & 0 \end{bmatrix} \tag{4.35}$$

Next, the relation between the controller given by the RGA, K_Λ , is investigated. Assume the relation is given by:

$$\begin{aligned}
GDK^* &= G [I + \Sigma] WK_D \\
&= G_D K_\Lambda
\end{aligned} \tag{4.36}$$

Eq.4.36 states that there exists a weighting matrix $W \in \mathbb{C}^{n_y \times n_y}$ such that the diagonal controller K_D and K_Λ are equal. Solving for the weight holds:

$$\begin{aligned} W &= [\mathbf{I} + \Sigma]^{-1} G^{-1} G_D \\ &= [\mathbf{I} + \Sigma]^{-1} [G_D + G_A]^{-1} G_D \\ &= [\mathbf{I} + \Sigma]^{-1} [\mathbf{I} + G_D^{-1} G_A]^{-1} \\ &= [\mathbf{I} + \Sigma]^{-1} [\mathbf{I} - \Sigma]^{-1} \end{aligned} \quad (4.37)$$

Eq.4.37 gives the perfect decoupler for the system, as given in HIER QUELLEN!. However, since ideal dynamic decoupling requires a precise model, this approach is neglected. Instead, the assumption of a nearly decoupled system is made by setting $W = \mathbf{I}$, hence setting:

$$K_D = K_\Lambda \quad (4.38)$$

Which holds the relative error in dynamics given by:

$$\begin{aligned} G_D^{-1} [G_D^* - G_D] &= G_D^{-1} [G_D + G_A \Sigma - G_D] \\ &= G_D^{-1} G_A \Sigma \end{aligned} \quad (4.39)$$

From Eq.4.39 the relative error dynamics are given in terms of the splitter. Another way to interpret the error is by giving a complex scalar error $\Delta_D \in \mathbb{C}$ with respect to the maximum singular value $\bar{\sigma} \in \mathbb{C}$ and the minimum singular value $\underline{\sigma} \in \mathbb{C}$:

$$\begin{aligned} \Delta_D \sigma(G_D) &\leq \bar{\sigma}(G_A \Sigma) \\ \Delta_D &\leq \frac{\bar{\sigma}(G_A \Sigma)}{\underline{\sigma}(G_D)} \end{aligned} \quad (4.40)$$

Hence, by Eq.4.40 an upper bound is established as well as an indicator for the usefulness. Assuming diagonal dominance requires the elements of the splitter to be small, hence the error is neglectable.

It is clearly visible that the splitter weights the minor with the main diagonals. It can be connected both to feedforward control and disturbance rejection by dividing the system as shown in Fig.4.4 and Fig.4.5. Since the used model used for the estimation of the couplings is crude, a feed forward architecture is better suited since the real delay of the system is not known. Hence, a disturbance rejection based upon a smith predictor would most likely result in an uncontrollable system due to the model error.

Next on the sensitivity of a system designed with and without a decoupling splitter is investigated. Assuming the non decoupled system is less robust, the following relationship holds:

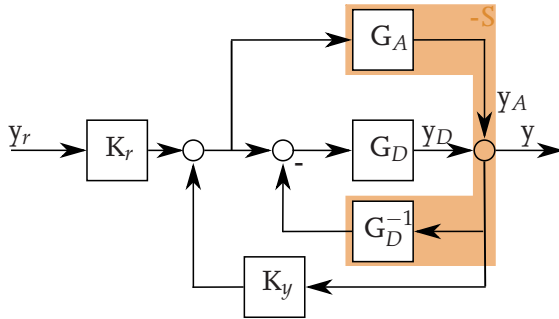


Figure 4.4: Interpretation of the splitter within the disturbance rejection framework

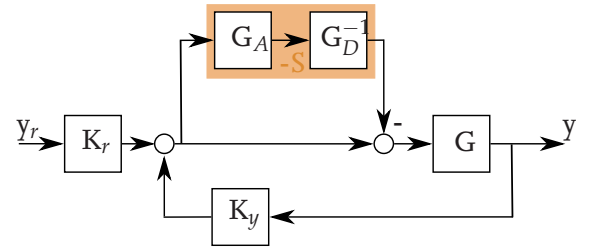


Figure 4.5: Interpretation of the splitter within the feed forward compensation framework

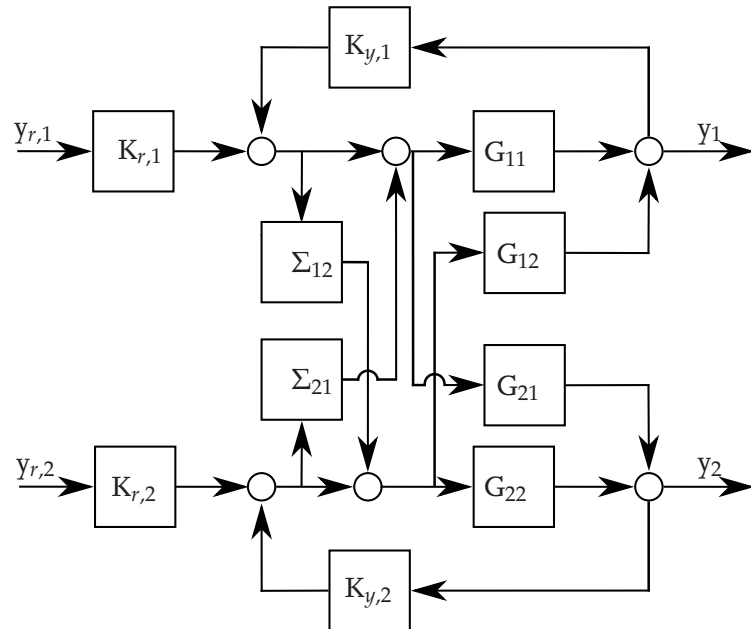


Figure 4.6: Compensator implementation of the splitter in a two input two output system

$$S_\Lambda \geq S^* \quad (4.41)$$

Where S_Λ is the systems sensitivity due to a simple, decentralized controller based on the RGA and S^* is the decoupled systems sensitivity, given by use of the splitter. Starting from the reasoning given in [21, p.443 ff.], the relative magnitude of the off diagonal elements of the transfer function matrix are given by $E \in \mathbb{C}^{n_y \times n_y}$:

$$E = [G - G_D] G_D^{-1} \quad (4.42)$$

Assuming that magnitude of the set-point controller is always less or equal to the feedback controller $|K_R| \leq |K_Y|$, the relation of the magnitude of the complementary sensitivity is given by

$|T| = |maGK_R| \leq |GK_Y|$ and thus $|T| \leq |S - I|$. Hence, a prove of robustness is sufficient for the case $|T| = |S - I|$. Furthermore following [21, p.443], factorization of the Sensitivity holds:

$$S^{-1} = \underbrace{[I - ET_D]}_{\text{Interconnections}} \underbrace{[I - G_D K_D]}_{\text{Individual loops}} \quad (4.43)$$

Hence, the difference between the nominal stability of the diagonal controller is dependent on the factor representing the interconnections given in terms of the complementary sensitivity $T_D = S_D - I$. The sensitivity function is therefore given as the inverse of Eq. 4.43:

$$S = S_D [I - ET_D]^{-1} \quad (4.44)$$

To be able to fulfill the stability conditions in terms of the maximum singular value, Eq. 4.44 needs both the diagonal sensitivity $S_D = I - G_D K_D$ and the factor $I - ET_D$ are both stable. Hence, the general Nyquist theorem requires:

$$\bar{\sigma}(ET_D) < 1 \quad (4.45)$$

Assuming that the controller is tuned for $T_D \leftarrow I$, it can be deduce that:

$$\begin{aligned} \bar{\sigma}(ET_D) &= \bar{\sigma}(E) \bar{\sigma}(T_D) \\ &\approx \bar{\sigma}(E) \\ \bar{\sigma}(E) &\leq 1 \end{aligned} \quad (4.46)$$

Eq. 4.46 can be interpreted the following: If the system is only diagonal, the diagonal sensitivity is equal to the real sensitivity. If couplings are involved, the system will be amplified if the wrong input-output pairings are chosen. The smaller the magnitude of the anti-diagonal described by E , the more robustness is given. Since Eq.4.42 with the use of a splitter becomes:

$$\begin{aligned} E &= [G(I + \Sigma) - G_D] G_D^{-1} \\ &= [G - G_D + G\Sigma] G_D^{-1} \\ &= [G_A + G_D\Sigma + G_A\Sigma] G_D^{-1} \\ &= [G_A - G_A + G_A\Sigma] G_D^{-1} \\ &= G_A\Sigma G_D^{-1} \\ &= -G_A G_D^{-1} G_A G_D^{-1} \\ &= -\Sigma^2 \end{aligned} \quad (4.47)$$

Which is an indicator for the usefulness of the splitter. Eq.4.47 gives a relation between the diagonal process model used for designing the controller and the anti-diagonal entries of the transfer function matrix. For using a static decoupler which leads to all entries of the matrices being real,

the maximum singular value is only greater than one iff the singular values of the anti-diagonal parts of the system are greater than the ones of the diagonal transfer functions.

To illustrate this, lets assume a simple, static transfer function and its RGA given by:

$$\mathbf{G} = \begin{bmatrix} 1 & 1.2 \\ 0.1 & 5 \end{bmatrix}, \Lambda(\mathbf{G}) = \begin{bmatrix} 1.025 & -0.025 \\ -0.025 & 1.025 \end{bmatrix}$$

Obviously, the main diagonal entries are preferred pairings. Investigating the magnitude of the off-diagonal with respect to the main diagonal gives:

$$\mathbf{E} = \left[\begin{bmatrix} 1 & 1.2 \\ 0.1 & 5 \end{bmatrix} - \begin{bmatrix} 1 & 0 \\ 0 & 5 \end{bmatrix} \right] \begin{bmatrix} 1 & 0 \\ 0 & \frac{1}{5} \end{bmatrix} = \begin{bmatrix} 0 & 0.24 \\ 0.1 & 0 \end{bmatrix}$$

And its maximum singular value $\bar{\sigma} = 0.24$. Note that in general the maximum singular value is not equal to any entries of the matrix but since this special case is given by a rotated diagonal matrix, the singular values can be directly seen. Now lets slowly increase the matrix by a gain $K \in \mathbb{R}^+$ acting on the transfer function between input 1 and output 2:

$$\mathbf{G} = \begin{bmatrix} 1 & 1.2 \\ K & 5 \end{bmatrix}$$

And suppose the pairing is staying the same. The interaction gain will be given by:

$$\mathbf{E} = \begin{bmatrix} 0 & 0.24 \\ K & 0 \end{bmatrix}$$

Hence, the maximum singular value will be given as

$$\bar{\sigma}(\mathbf{E}) = \begin{cases} 0.24, & K \leq 0.24 \\ K, & K > 0.24 \end{cases}$$

We can see that the maximum singular value will destabilize the system iff it exceeds value for $K \geq 1$. However, using a decoupler holds for the Eq.4.47:

$$\begin{aligned} \mathbf{E} &= - \begin{bmatrix} 0 & 1.2 \\ 1 & 0 \end{bmatrix} \begin{bmatrix} 1 & 0 \\ 0 & \frac{1}{5} \end{bmatrix} \begin{bmatrix} 0 & 1.2 \\ 1 & 0 \end{bmatrix} \begin{bmatrix} 1 & 0 \\ 0 & \frac{1}{5} \end{bmatrix} \\ &= - \begin{bmatrix} 0 & 0.24 \\ 1 & 0 \end{bmatrix} \begin{bmatrix} 0 & 0.24 \\ 1 & 0 \end{bmatrix} \\ &= - \begin{bmatrix} 0 & 0.24 \\ 0.24 & 0 \end{bmatrix} \end{aligned}$$

Hence, the robustness is increased, since the maximum singular value is not exceeding one. The maximum value for the gain while using the splitter can be estimated roughly as $K \approx 4.167$. Applying this knowledge to the process, one can argue that the maximum sensitivity of the closed loop in presence of a decoupler is decreased, which can already be guessed by Eq. 4.44. Hence, a progressive detuning like Eq. 4.24, since we are much more likely that $E \ll I$, and hence the diagonal sensitivity is equal to the real sensitivity. Also, the use of a setpoint-weight increases the robustness as well, since it decreases the magnitude of the open loop gain.

Since a detuned interaction is wanted, the approximation of the process dynamics via the first order terms of the Taylor Series is used as well. Explicitly the term is given by:

$$\begin{aligned}\Gamma_A &= \left[\frac{d}{ds} [\mathbf{G} [\mathbf{I} + \boldsymbol{\Sigma}]] |_{s=0} \right]_A \\ &= \frac{d}{ds} [\mathbf{G}_A + \mathbf{G}_D \boldsymbol{\Sigma}] |_{s=0}\end{aligned}\tag{4.48}$$

Further investigation of term given in Eq. 4.48 reveals the dependency on the average residence time. Using a decoupler build upon the steady state, the first order dynamics are:

$$\begin{aligned}\Gamma_A &= \frac{d}{ds} [\mathbf{G}_A + \mathbf{G}_D \boldsymbol{\Sigma}] |_{s=0} \\ &= [\mathbf{G}_{A,0} \circ \mathbf{T}_{AR,A} + (\mathbf{G}_{D,0} \circ \mathbf{T}_{AR,D}) \boldsymbol{\Sigma}] \\ &= [\mathbf{G}_{A,0} \circ \mathbf{T}_{AR,A} - \mathbf{G}_A \circ \mathbf{T}_{AR,D}] \\ &= \mathbf{G}_{A,0} \circ [\mathbf{T}_{AR,A} - \mathbf{T}_{AR,D}]\end{aligned}\tag{4.49}$$

With $\mathbf{T}_{AR} = (T_{ar,ij}) = (T_{ij} + L_{ij}) \in \mathbb{R}^{n_y \times n_y}$ being the matrix consisting of the average residence times of the single transfer functions g_{ij} of the process. The operator \circ is the Hadamard Product and stands for the element-wise multiplication. Note that normally, the Hadamard Product is not distributive over multiplication. But since the splitter can be written as a product of a rotation matrix \mathbf{O} and a diagonal matrix $\boldsymbol{\Sigma}_D$, $\boldsymbol{\Sigma} = \boldsymbol{\Sigma}_D \mathbf{O}$, it is possible. From Eq. 4.49 we can see that the first order dynamics acting on the output are related to the difference in the dynamics of the main diagonal and the anti-diagonal terms. This coincides with the statements of e.g. LUNZE, where a static decoupling is described to be able to decouple the dynamics if the dynamic behavior of the process are alike. Using this knowledge, the goal of the detuning can be reformulated to change the controller in such a way that the dynamic behavior of the output is nearly equivalent to the dynamics of the main coupling.

Hence, we relate both dynamics with each other to find the relative dynamic interaction of the process $\Gamma_R \in \mathbb{R}^{n_y \times n_y}$:

$$\begin{aligned}\Gamma_R &= \left| \Gamma_D^{-1} \Gamma_A \right| \\ &= \left| [\mathbf{G}_{D,0} \circ \mathbf{T}_{AR,D}]^{-1} \mathbf{G}_{A,0} \circ [\mathbf{T}_{AR,A} - \mathbf{T}_{AR,D}] \right|\end{aligned}\tag{4.50}$$

Eq.4.50 can be used as a measure of the relative difference between the main coupling on the diagonal and the interaction dynamics. It includes the gain as well, so if the difference in dynamics is high but the gain of the anti-diagonal is small in relation to the diagonal, the process is nearly decoupled. Likewise a high difference of the gains in presence of roughly identical dynamics will have no impact on the process.

With the maximum allowed relative dynamic interaction and sensitivities the detuning formula is explicitly given by:

$$\begin{aligned} \mathbf{H}_{A,Max} &\geq \mathbf{M}_S \boldsymbol{\Gamma}_R \mathbf{K}_r \\ &\geq \det(\mathbf{M}_S) \boldsymbol{\Gamma}_R \mathbf{K}_r \end{aligned} \quad (4.51)$$

Good limits for the upper bound $\mathbf{H}_{A,Max} = (h_{ij,Max}) \in \mathbb{R}^{n_y \times n_y}$ are within the set of [0.1 … 0.5] to ensure the process dynamics are roughly the same.

4.4 Review of the Methods

While being mathematical equivalent, both algorithms diverge with regards to design principles and can be used very differently. Aströms original method uses a decoupled system to derive an optimal controller. The modified variant is able to build upon a controller designed by the original system. Hence, either the RGA can be used as a starting point or a naturally pairing, e.g. valve and pressure, can be build upon. This is illustrated by Fig.

HIER FIG.

The method proposed in Subs. 4.3.1 gives many advantages over a controller design simply based on RGA while holding the number of integrators minimal. The enhancement of performance comes through the interconnection of the controller outputs via the decoupler, which can be viewed as a simple form of model based control. Whilst giving major performance improvements, the presented method has a significant disadvantages.

Depending on the model chosen for identification and the values of the coefficients, the resulting transfer function will in general be of other form than the initial identified model. Hence, algorithms depending on these models to design controllers can not be used naturally, but have to use a simplified or approximated model. This process results in a higher model error and thus in poor performance and robustness of the derived controller.

Hence, an application of the splitter as introduced in Subs.4.3.2 can be used to derive a similar representation while using the original identified functions. An illustrative example will be given in the following chapter pointing to the advantages of the process. In [23] several properties of the splitter are investigated and a design algorithm is given. It can be related to both feed forward control and disturbance rejection control architecture, which allows for usage of either the error in delay dominant systems or for calculating a corrected input from the output for lag dominant systems.

5 Control of Simple Multivariable Processes

The following chapter gives several examples to decouple a FOTD transfer function matrix. The process is explained with all three method to design multivariable controller.

In Sec.5.1 the analytic description of the methods are given, followed by the example taken from literature in Sec. 5.2 and Sec.5.3.

5.1 Analytic Decoupling

Since a FOTD is the model structure chosen for this work a deeper investigation of transfer function matrices based on this model and the corresponding decoupling algorithms is performed. For the following section a simple two input two output model is defined:

$$\mathbf{G} = \begin{bmatrix} g_{11} & g_{12} \\ g_{21} & g_{22} \end{bmatrix}, g_{ij} = \frac{K_{ij}}{T_{ij}s + 1} e^{-L_{ij}s} \quad (5.1)$$

For the system described in Eq. 5.1 three different controller based on PI-structure are defined using the methods presented in the previous chapter. Further restrictions on the systems behavior are given by the Maximum Sensitivity \mathbf{M}_S as a robustness requirement and Maximum Interaction $\mathbf{H}_{A,Max}$ as a decoupling requirement:

$$\begin{aligned} \mathbf{H}_{A,Max} &= \begin{bmatrix} 0 & h_{12,Max} \\ h_{21,Max} & 0 \end{bmatrix} \\ \mathbf{M}_S &= \begin{bmatrix} M_{S,1} & 0 \\ 0 & M_{S,2} \end{bmatrix} \end{aligned} \quad (5.2)$$

Eq.5.2 is given under the assumption that only the diagonal transfer functions are required and the interaction acts on the antidiagonal entries. Furthermore the system will be operating near steady state and hence the frequency used for the RGA analysis and the Taylor Series Expansion is chosen to be $s = 0$.

5.1.1 Controller Design via Relative Gain Array Analysis

To design decentralized controller an adequate pairing has to be chosen and a controller has to be computed by means of a suitable algorithm with the given identified parameters of the transfer

function. Using the RGA as an indicator of interaction, the pairing is to be chosen such that the corresponding element $\Lambda_{ij}(G_0)$ equals the maximum entry of the row. Assuming a sufficient sorting, the structure of the controller is diagonal as well. The PI controller are designed via the AMIGO algorithm as presented in Sec.4.1.

Hence, for every pairing i, j the controller parameter are given by:

$$K_P = \frac{0.15}{\hat{K}} + \left(0.35 - \frac{\hat{L} + \hat{T}}{(\hat{L} + \hat{T})^2}\right) \frac{\hat{T}}{\hat{K}\hat{L}}$$

$$T_I = 0.35\hat{L} + \frac{13\hat{L}\hat{T}^2}{\hat{T}^2 + 12\hat{L}\hat{T} + 7\hat{L}^2}$$

With a minimum requirement for the delay of $\hat{L} \geq 0.3\hat{T}$. The setpoint-weight is chosen according to the normalized time delay $\tau = \frac{\hat{L}}{\hat{L} + \hat{T}}$:

$$b = \begin{cases} 0, & \tau < 0.2 \\ 10(\tau - 0.2), & 0.2 \leq \tau \leq 0.3 \\ 1.0, & \tau \geq 0.3 \end{cases}$$

5.1.2 Controller Design via Åström et. al.

At first the decoupler is designed via the inverse static gain of the system, since the error connected to the steady state measurement can be assumed small with respect to the dynamic error. Hence, the decoupler is given by:

$$\begin{aligned} D &= G_0^{-1} \\ &= \frac{1}{K_{11}K_{22} - K_{12}K_{21}} \begin{bmatrix} K_{22} & -K_{21} \\ -K_{12} & K_{11} \end{bmatrix} \\ &= \frac{1}{\det(G_0)} \begin{bmatrix} K_{22} & -K_{21} \\ -K_{12} & K_{11} \end{bmatrix} \end{aligned} \tag{5.3}$$

The transformed system G^* can thus be calculated as

$$\begin{aligned} G^* &= GD \\ &= \frac{1}{\det(G_0)} \begin{bmatrix} g_{11} & g_{12} \\ g_{21} & g_{22} \end{bmatrix} \begin{bmatrix} K_{22} & -K_{21} \\ -K_{12} & K_{11} \end{bmatrix} \\ &= \frac{1}{\det(G_0)} \begin{bmatrix} K_{22}g_{11} - K_{12}g_{12} & -K_{21}g_{11} + K_{22}g_{12} \\ K_{22}g_{21} - K_{12}g_{22} & -K_{21}g_{21} + K_{11}g_{22} \end{bmatrix} \end{aligned} \tag{5.4}$$

From Eq. 5.4 it is clear that the entries g_{ij}^* are linear combinations of FOTD transfer functions. Due to the properties of the exponential function the superposition principle does not hold. Hence a

controller via the AMIGO algorithm can only be designed if a sufficient approximation of the linear combination as a FOTD can be formulated:

$$\begin{aligned} g_{ij}^* &= \frac{K_{ij}^*}{T_{ij}^* s + 1} e^{-L_{ij}^* s} + \Delta g_{ij}^* \\ &\approx \frac{K_{ij}^*}{T_{ij}^* s + 1} e^{-L_{ij}^* s} \end{aligned} \quad (5.5)$$

Within Eq. 5.5 the main drawback of the method is laid out. As stated earlier, most algorithms for PI(D) design rely on a fixed model structure and hence are not fit to process information given by a combination. To use the function, two methods are proposed to approximate the linear combination of FOTD.

Assuming the results of the experiment used for identifying the process are still available the process approximate model can be found via a weighted sum of the systems output. Calculating the static can as proposed in Ch.3, the linear combination of the TITO system can be fitted to the resulting weighted measurement data, e.g. given by

$$y_{11}^*(t) = \frac{K_{22}y_{11}(t) - K_{12}y_{12}(t)}{\det(\mathbf{G}_0)} \quad (5.6)$$

Eq. 5.6 reuses the experimental data to approximate the systems output. y_{ii} is the i-th output of the system reacting to excitation via the i-th input. With the weighted data given by y_{11}^* , a FOTD model could be fitted according to the already known algorithm presented in Ch. 3. However, this approach is limited to the reuse of data and requires that the process is always weighted by a decoupler.

The second method relies on knowledge about the behaviour of the transfer functions in the time domain. At first, the static gain is given by:

$$\begin{aligned} \mathbf{K}^* &= \lim_{s \rightarrow 0} \mathbf{G}^* \\ &= \mathbf{K} \mathbf{D} \\ &= \mathbf{I} \end{aligned} \quad (5.7)$$

The integral of every part of the experiment, given by a matrix $\mathbf{Y} = (y_{ij}) \in \mathbb{R}^{n_y \times n_y}$ and its transformed counterpart can be rewritten as

$$\begin{aligned} \int_0^\infty \mathbf{Y}^*(\infty) - \mathbf{Y}^*(t) dt &= \int_0^\infty \mathbf{Y}(\infty) - \mathbf{Y}(t) dt \mathbf{D} \\ \mathbf{K}^* \circ \mathbf{T}_{ar}^* &= \mathbf{K}^* \circ (\mathbf{T}^* + \mathbf{L}^*) \\ &= (\mathbf{K} \circ (\mathbf{T} + \mathbf{L})) \mathbf{D} \end{aligned} \quad (5.8)$$

Where \circ denotes the element wise multiplication, also called Hadamard Product. It gives the transformed average residence times T_{ar}^* . Since the Hadamard Product relates to the row and column sum, one can rewrite the transformed average residence time for a static decoupler as

$$\begin{aligned}\sum_{i=1}^{n_y} [(\mathbf{K} \circ (\mathbf{T} + \mathbf{L})) \mathbf{D}]_{i,j} &= \left[\left((\mathbf{T} + \mathbf{L})^T \mathbf{K}^T \right) \mathbf{D} \right]_{j,j} \\ &= \left[\left((\mathbf{T} + \mathbf{L})^T \right) \mathbf{K}^T \mathbf{K}^{-1} \right]_{j,j} \\ &= \left[(\mathbf{T} + \mathbf{L})^T \mathbf{\Lambda}^T (\mathbf{G}) \right]_{j,j}\end{aligned}\quad (5.9)$$

Eq. 5.9 relates the approximation to the RGA as given in Ch. 4. Hence, if the influence of the minor diagonals is small, the approximation is sufficiently good.

To determine the coefficients of the new system a third equation is needed. It is convenient to choose an appropriate value for the new time delay L^* with several options like a weighted sum, the minimum or maximum of all involved delays. A robust method is given by choosing the maximum and hence implement a conservative tuning. Subsequently Eq. 5.8 can be rearranged to

$$\begin{aligned}T^* &= T_{ar}^* - L^* \\ &= T_{ar}^* - L_{Max}\end{aligned}\quad (5.10)$$

Assuming an approximation can be found and the resulting error is sufficiently small the diagonal controller can be designed. Since the main coupling are always on the main diagonal, the RGA has not to be performed. The single, decentralized controllers are design as explain earlier by the use of the AMIGO Tuning rules. A controller is then given by:

$$\begin{aligned}\mathbf{K}_y^* &= \begin{bmatrix} -K_{P1}^* - K_{I1}^* \frac{1}{s} & 0 \\ 0 & -K_{P2}^* - K_{I2}^* \frac{1}{s} \end{bmatrix} \\ \mathbf{K}_r^* &= \begin{bmatrix} b_1 K_{P1}^* + K_{I1}^* \frac{1}{s} & 0 \\ 0 & b_2 K_{P2}^* + K_{I2}^* \frac{1}{s} \end{bmatrix}\end{aligned}\quad (5.11)$$

With parameters $K_{P,i}, K_{I,i} \in \mathbb{R}$ are calculated via the AMIGO tuning rules as described in Sec.4.1. Since the approximation given in Eq.5.5 holds an inevitable error so do the parameter.

Next, the interaction will be used to detune the controller. The first order term of the Taylor series of the antidiagonal entries of the system $\mathbf{G}^* = \mathbf{G}\mathbf{D}$ is given by:

$$\begin{aligned}
\boldsymbol{\Gamma}_A &= \left[\frac{d}{ds} \mathbf{G} \Big|_{s=0} \right]_A s \\
&= \frac{1}{\det(\mathbf{G}_0)} \begin{bmatrix} 0 & -K_{21}K_{11}(T_{11} - L_{11}) + K_{22}K_{12}(T_{12} - L_{12}) \\ -K_{12}K_{22}(T_{22} - L_{22}) + K_{22}K_{21}(T_{21} - L_{21}) & 0 \end{bmatrix}_s \\
&\approx \begin{bmatrix} 0 & K_{12}^*(T_{12}^* - L_{12}^*) \\ K_{21}^*(T_{21}^* - L_{21}^*) & 0 \end{bmatrix}_s
\end{aligned} \tag{5.12}$$

From Eq. 5.12 the dependency of the coupling on the both the static gain of the system and the dynamical behaviour can be observed. This coincides with the statements of [19] declaring that static decoupling is in general easier if the dynamic behaviour of the involved transfer functions is similar.

Detuning the controller with the constrains on the closed loop given by Eq. 5.2 and solving Eq. 4.22 for the controller with setpoint holds:

$$\begin{aligned}
\mathbf{K}_r^* &\leq \boldsymbol{\Gamma}_{A,Max}^{-*} \mathbf{M}_S^{-1} \mathbf{H}_{A,Max}^* \\
&\leq \frac{1}{\det(\mathbf{M}_S)} \boldsymbol{\Gamma}_{A,Max}^{-*} \mathbf{H}_{A,Max}^* \\
&\leq \frac{1}{M_{S,1} M_{S,2}} \begin{bmatrix} \frac{h_{21,Max}}{K_{12}^*(T_{12}^* - L_{12}^*)} & 0 \\ 0 & \frac{h_{12,Max}}{K_{21}^*(T_{21}^* - L_{21}^*)} \end{bmatrix}
\end{aligned} \tag{5.13}$$

A detuning of the controller parameter is performed according to the detuning rules given in Sec.4.1 to ensure the controller is within the limits specified earlier.

Controller Design via Modified Åström

Now the modified algorithm proposed in this thesis is applied to the same system. First, we design the controller as a function of the main diagonal entries g_{ii} once again using the AMIGO tuning rules:

$$\begin{aligned}
\mathbf{K}_y &= \begin{bmatrix} -K_{P1} - K_{I1} \frac{1}{s} & 0 \\ 0 & -K_{P2} - K_{I2} \frac{1}{s} \end{bmatrix} \\
\mathbf{K}_r &= \begin{bmatrix} b_1 K_{P1} + K_{I1} \frac{1}{s} & 0 \\ 0 & b_2 K_{P2} + K_{I2} \frac{1}{s} \end{bmatrix}
\end{aligned} \tag{5.14}$$

The splitter Σ is likewise designed by the steady state of the system as:

$$\begin{aligned}
\Sigma &= \mathbf{D}_A \mathbf{D}_D^{-1} \\
&= \begin{bmatrix} 0 & -\frac{K_{12}}{K_{11}} \\ -\frac{K_{21}}{K_{22}} & 0 \end{bmatrix}
\end{aligned} \tag{5.15}$$

To test for interaction define the maximum interaction and the sensitivity like in Eq. 5.2. The anti diagonal parts of the Taylor series can be calculated to be

$$\begin{aligned}\boldsymbol{\Gamma}_A &= \frac{d}{ds} [\boldsymbol{G}_A + \boldsymbol{G}_D \boldsymbol{\Sigma}] |_{s=0} \\ &= \begin{bmatrix} 0 & K_{12}(T_{12} - L_{12}) - K_{11}\frac{K_{12}}{K_{11}}(T_{11} - L_{11}) \\ K_{21}(T_{21} - L_{21}) - K_{22}\frac{K_{21}}{K_{22}}(T_{22} - L_{22}) & 0 \end{bmatrix} \\ &= \begin{bmatrix} 0 & K_{12}(T_{12} - L_{12} - T_{11} + L_{11}) \\ K_{21}(T_{21} - L_{21} - T_{22} + L_{22}) & 0 \end{bmatrix}\end{aligned}\quad (5.16)$$

To detune the controller solving Eq. 4.22 with for the controller as before holds:

$$\begin{aligned}\boldsymbol{K}_R &\leq \boldsymbol{\Gamma}_A^{-1} \boldsymbol{M}_S^{-1} \boldsymbol{H}_{A,Max} \\ &\leq \frac{1}{\det(\boldsymbol{M}_S)} \boldsymbol{\Gamma}_A^{-1} \boldsymbol{H}_{A,Max} \\ &\leq \frac{1}{M_{S,1} M_{S,2}} \begin{bmatrix} \frac{h_{12,Max}}{K_{12}(T_{12} - L_{12} - T_{11} + L_{11})} & 0 \\ 0 & \frac{h_{21,Max}}{K_{21}(T_{21} - L_{21} - T_{22} + L_{22})} \end{bmatrix}\end{aligned}\quad (5.17)$$

The system is detuned according to the detuning rules of the AMIGO algorithm. In contrast to Aströms decoupling algorithm, the original system is used the original structure of the model is preserved.

5.2 Rosenbrocks Function

First, the example of Rosenbrock's Function will be considered. The system is given by

$$\begin{aligned} \mathbf{G} &= \begin{bmatrix} \frac{1}{s+1} & \frac{2}{s+3} \\ \frac{1}{s+1} & \frac{1}{s+1} \end{bmatrix} \\ &= \begin{bmatrix} \frac{1}{s+1} & \frac{\frac{2}{3}}{\frac{1}{3}s+1} \\ \frac{1}{s+1} & \frac{1}{s+1} \end{bmatrix} \end{aligned} \quad (5.18)$$

The transfer function matrix given in Eq.?? is delay free. The systems time constants and gains are equal for the transfer functions for the input-output pairing $(u_1, y_1), (u_1, y_2)$ and (u_2, y_1) all equal $T = 1 \text{ sec/rad}$ and $K = 1$. The transfer function from input 2 to output 1 has a time constant $T = \frac{1}{3} \text{ sec/rad}$ and a gain of $K = \frac{2}{3}$. Hence, whilst not as influential with respect to gain, g_{21} is acting faster on y_1 than g_{11} .

Rosenbrock's system is a common example. As stated in [5], it looks easy to control but is not stable, since its characteristic equation given in Eq. 5.19 has a pole in the right half plane at $s = 1$.

$$\det(\mathbf{G}) = \frac{1}{(s+1)^2} - \frac{2}{(s+1)(s+3)} \quad (5.19)$$

The system is used as an example in [5], where a controller has been computed using analytical methods. This controller will serve as a reference to the methods developed in Ch. 4.

5.2.1 Decentralized Controller

To determine the system input-ouput pairing the RGA of Eq.5.18 at steady state is computed to be:

$$\Lambda(\mathbf{G})_0 = \begin{bmatrix} 3 & -2 \\ -2 & 3 \end{bmatrix} \quad (5.20)$$

The result of Eq.5.20 advices to control the process using the main diagonal of the system. Following this advice, one is able to design the decentralised controller via the AMIGO tuning rules given in Sec. 4.1. Designing a PI controller by Eq. 4.1 with the system coefficients gives a diagonal controller with

$$\mathbf{K} = \mathbf{K}_P + \frac{1}{s} \mathbf{K}_I \quad (5.21)$$

$$= \begin{bmatrix} 0.725 & 0 \\ 0 & 0.725 \end{bmatrix} + \frac{1}{s} \begin{bmatrix} 0.852 & 0 \\ 0 & 0.852 \end{bmatrix} \quad (5.22)$$

With a set-point weight of $b = 0$, since the normalized time delay $\tau_{ij} = 0 \forall i, j \in [1, 2]$. The parameter of the controller have been computed using an artificial delay of $L = 0.3 T$, since it enables a more robust tuning.

5.2.2 Decoupled Controller based on Åström

At first, the decoupler D is designed based on the steady state gain to be

$$D = \begin{bmatrix} 3 & -2 \\ -3 & 3 \end{bmatrix} \quad (5.23)$$

This results in the transformed system G^* as given in [5]:

$$\begin{aligned} G^* &= G D \\ &= \begin{bmatrix} \frac{3(1-s)}{(s+1)(s+3)} & \frac{4s}{(s+1)(s+3)} \\ 0 & \frac{1}{s+1} \end{bmatrix} \end{aligned} \quad (5.24)$$

From Eq.5.24 it is easy to see that the influence of input 1 to output 2 is already decoupled. The interaction is therefore zero. This relies on the similarities of the dynamics of g_{12} and g_{22} . The first order linearization of g_{21}^* holds:

$$\begin{aligned} \gamma_{12} &= \frac{d}{ds} (g_{21}^*)|_{s=0} \\ &= \frac{4}{3} \end{aligned} \quad (5.25)$$

To design a controller based on the simple tuning rules, the main diagonal transfer functions of the system Eq.5.24 have to be estimated with a FOTD model. According to Eq. 5.8, one can estimate the influence the linear combination of the FOTD model via:

$$\begin{aligned} K^* \circ T_{ar}^* &= K^* \circ (T^* + L^*) \\ &= (K \circ [T + L]) D \\ &= \begin{bmatrix} 2.330 & -1.335 \\ 0.003 & 0.977 \end{bmatrix} \end{aligned} \quad (5.26)$$

Which is consisting of the steady state gain $K^* = I$ and the approximate lag of:

$$\begin{aligned} T^* &= T_{ar}^* - \underbrace{\begin{bmatrix} * \\ 0 \end{bmatrix}}_0 \\ &= T_{ar}^* \end{aligned} \quad (5.27)$$

Hence, the approximated, diagonal system is given by

$$G_D^* \approx \begin{bmatrix} \frac{1}{2.330 s+1} & 0 \\ 0 & \frac{1}{0.977 s+1} \end{bmatrix} \quad (5.28)$$

The transfer function g_{22} of the approximated system given in Eq.5.28 is almost identical with its real counterpart in Eq.5.24. The difference of the first main diagonal entry is however, much more significant. A bode plot of both systems hold

FIGURE

From FIG the conservative character of the approximation can be seen. With regards to the design of a PI controller this results in a more aggressive, more faster controller than the controller based on RGA, since $K_P, T_I \propto \frac{1}{T}$. The controller calculated for the diagonal system is given by:

$$\mathbf{K} = \mathbf{K}_P + \frac{1}{s} \mathbf{K}_I \quad (5.29)$$

$$= \begin{bmatrix} 0.725 & 0 \\ 0 & 0.725 \end{bmatrix} + \frac{1}{s} \begin{bmatrix} 0.363 & 0 \\ 0 & 0.852 \end{bmatrix} \quad (5.30)$$

The set-point weight for the proportional gain is $b = 0$ since $\tau_{ij} = 0 \forall i, j \in [1, 2]$. From the integral gain of the first loop we see the conservative estimation of the approximation.

For the detuning an upper limit regarding the interaction of the process is required. Since a minimal interaction is desired, the upper limit of the interaction is set to $h_{ij} = 0.3 \forall i, j \in [1, 2]$. Iterative detuning of the controller with a decay of $\frac{K_p^{i+1}}{K_p^i} = 0.9$ changes the parameter value to be:

$$\mathbf{K} = \mathbf{K}_P + \frac{1}{s} \mathbf{K}_I \quad (5.31)$$

$$= \begin{bmatrix} 0.725 & 0 \\ 0 & 0.015 \end{bmatrix} + \frac{1}{s} \begin{bmatrix} 0.363 & 0 \\ 0 & 0.108 \end{bmatrix} \quad (5.32)$$

After 45 iterations. The impact of the strong coupling of the second input to the first output of the system is clearly visible in the number of iterations. The controller $k_{R,11}$ is tuned to be much less aggressive than its original designed predecessor.

5.2.3 Decoupled Controller based on Robust Relative Dynamic Detuning

Since the process until the detuning is nearly identical to the controller design by a simple RGA analysis previously, these steps are not discussed. The decoupler of the process is given as the ration of the diagonal and anti-diagonal entries as:

$$\Sigma = \begin{bmatrix} 0 & -\frac{\frac{2}{3}}{\frac{1}{1}} \\ -\frac{1}{1} & 0 \end{bmatrix}$$

$$= \begin{bmatrix} 0 & -0.667 \\ -1.000 & 0 \end{bmatrix}$$

The relative dynamic interaction acting on the process are given from u_2 to y_1 :

$$\begin{aligned}
\gamma_{R,12} &= \left| \frac{K_{12} (T_{12} + L_{12} - T_{11} - L_{11})}{K_{11} (T_{11} + L_{11})} \right| \\
&= \left| \frac{\frac{2}{3} \left(1 - \frac{1}{3}\right)}{1(1)} \right| \\
&= \frac{2}{3} \frac{2}{3} \\
&= \frac{4}{9}
\end{aligned}$$

Within the same limitations for the controller, namely $h_{ij} = 0.3 \forall i, j \in [1, 2]$, the dynamically detuned controller is given by:

$$\begin{aligned}
\mathbf{K} &= \mathbf{K}_P + \frac{1}{s} \mathbf{K}_I \\
&= \begin{bmatrix} 0.725 & 0 \\ 0 & 0.058 \end{bmatrix} + \frac{1}{s} \begin{bmatrix} 0.852 & 0 \\ 0 & 0.324 \end{bmatrix}
\end{aligned}$$

After 24 iterations and a shrinking rate of $\frac{K_P^{i+1}}{K_P^i} = 0.9$. While reflecting the detuning with respect to the purely decentralized controller of the RGA, it is much more aggressive than the controller designed by the previous decoupling algorithm.

5.2.4 Results

To evaluate the performance of the controller, a simulation has been performed. As a reference, the decoupled controller presented by [5] for the same process with the following parameters has been added as well:

$$\begin{aligned}
\mathbf{K} &= \mathbf{K}_P + \frac{1}{s} \mathbf{K}_I \\
&= \begin{bmatrix} 0.245 & 0 \\ 0 & -0.452 \end{bmatrix} + \frac{1}{s} \begin{bmatrix} 0.248 & 0 \\ 0 & 0.075 \end{bmatrix}
\end{aligned}$$

The controller has been designed using analytical methods. It has a setpoint-weight of $b_i = 0, \forall i \in [1, 2]$.

To see the effect of the decoupler, at first the system is simulated without the detuned controller. The initial output is set to zero $y_0 = \mathbf{0}$ and at $t = 0$ s a jump on the reference value $y_{R,1}$ is given. When the system is in a steady state, at $t = 100$ s, the reference value for the second output is set to $y_{R,2} = 1$. The results for all three controller are presented in Fig.5.1. The response of the reference controller is in dashed grey, while the decentralized controller is colored blue, the decoupled controller designed as proposed by Aström is red and the robust relative dynamic detuned controller is given in orange.

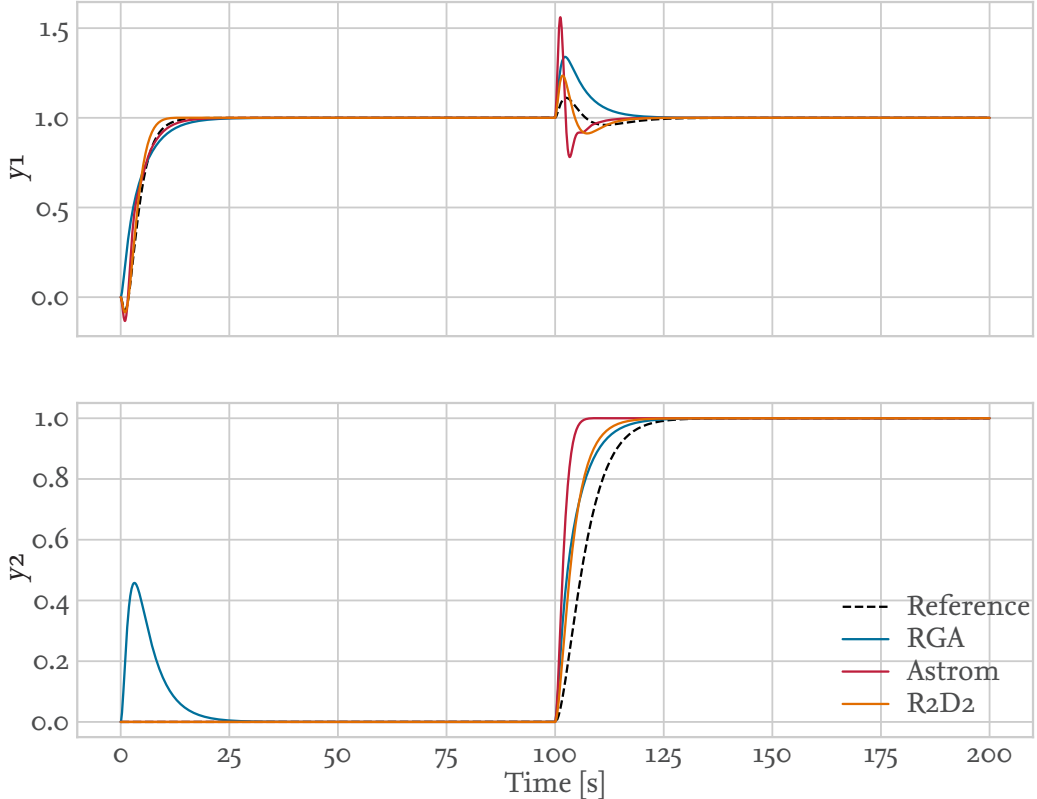


Figure 5.1: Simulation of Rosenbrock's System without detuning

The performance measurements are given in Tab.5.1. The rising time $T_{Rise} \in \mathbb{R}^+$, the overshoot $m_p \in \mathbb{R}^+$ and the settling time $T_{Settle} \in \mathbb{R}^+$ describe the tracking performance of the controller. The rising time describes how fast a controller is able to increase the output from 10% to 90% of the steady state output. The overshoot describes the maximum of the output after it reaches the steady state value for the first time. The settling time measures the time interval which is necessary for the output to stay within $(100 \pm 2) \%$ of the steady state output. Likewise the performance indicators regarding the disturbance rejection are defined. Only the overshoot time $T_P \in \mathbb{R}^+$ is new and gives the time of the maximum overshoot with respect to the signals occurrence.

Table 5.1: Evaluation of tracking performance and disturbance rejection performance of Rosenbrock's system without detuning

		Tracking Performance			Rejection Performance		
		T_{Rise}	m_p	T_{Settle}	T_p	m_p	T_{Settle}
		s	%	s	s	%	s
RGA	y_1	9.40	0.00	17.30	3.10	0.46	83.80
	y_2	9.40	0.00	17.20	2.20	0.34	13.70
Astroem	y_1	6.90	0.00	14.30	0.00	0.00	0.00
	y_2	3.20	0.00	5.50	1.00	0.55	1.30
R2D2	y_1	4.50	0.00	9.10	0.00	0.00	0.00
	y_2	7.70	0.00	14.20	1.60	0.24	2.70

It can be seen that while the decentralized controller is acting fast on its main coupling, the impact due to the coupling of the excited input and the coupled output of y_2 is exalted. The overshoot of the cross coupled output is nearly $m_\Delta(y_2) = 0.46$, while both decoupled controllers are able to suppress the interaction completely. This behavior is induced due to the similar dynamics of the the transfer functions g_{12} and g_{22} . Since both gain and time constant are equal, a simple interconnection is able to completely cancel out the negative effects of the first input excitation.

Observing the input response an undershoot of both decoupled controllers can be seen. This origins in the stationary estimation of the decoupler, which acts instantly and corrects with the full strength of the ratio of the steady state gains. Hence, the signal given onto the second input of the system acts at first to progressive. It is noteworthy that while both the decentralized controller and the controller in combination with the splitter are equal, the last of both is acting faster. This is another effect caused by the decoupling, since the controller does not have to adjust to disturbances due to the systems second output. It can also be observed in weaker form on the fully static decoupler, given as proposed by Aström.

With respect to the reference controller introduced in [5], the auto-tuned controller show nearly identical behavior.

The second output response to a step of its reference value gives interesting results as well. Since both transfer functions acting on the output behave identical with respect to gain and dynamic, the undershoot observed in the second output is missing. Additionally, the controller tuned via the decoupling method proposed by Aström et. al. is clearly acting the fastest referring to input response. The positive effect of the splitter exists but is much weaker than before. Hence, the controller is not notably faster than the decentralized controller.

A clear picture is given by the disturbance acting on the first ouput y_1 due to the excitation of u_2 . The magnitude of the overshoot of the decoupled controller designed with a static decoupler is even worse than its non-decoupled counterpart, reaching nearly $m_\Delta(y_1) = 0.55$. Since the gains

of the system are captured well, the reason for this effect can be found in the controller designed by the analogous model. Since the approximated time constant is twice as much as its original, the controller is not able to act fast enough on the disturbance. Additionally, it amplifies the effect since the processes g_{11} and g_{12} differ from each other dynamically. Afterwards the controller tries to counter the effect and undershoots its target value before slowly reaching a steady state once again.

Oppose to that, the decentralized controller acts more reasonable, slowly reducing the error of the output on a monotone decreasing track. The controller in combination with the splitter reduces the effect of the coupling immensely, but shows small undershoots due to the same reasons as mentioned beforehand. However, it is acting smoother and less drastically than the decoupler based on the static inverse. The reference controller shows only slight influences due to the disturbance and limits the overshoot to $\Delta y_1 = 0.11$. This is reasonable, since it is designed and detuned for that limitation.

Regarding the robustness and the tracking performance, the singular values of the closed loops sensitivity and complementary sensitivity have been calculated. The results can be seen in Fig.5.2.

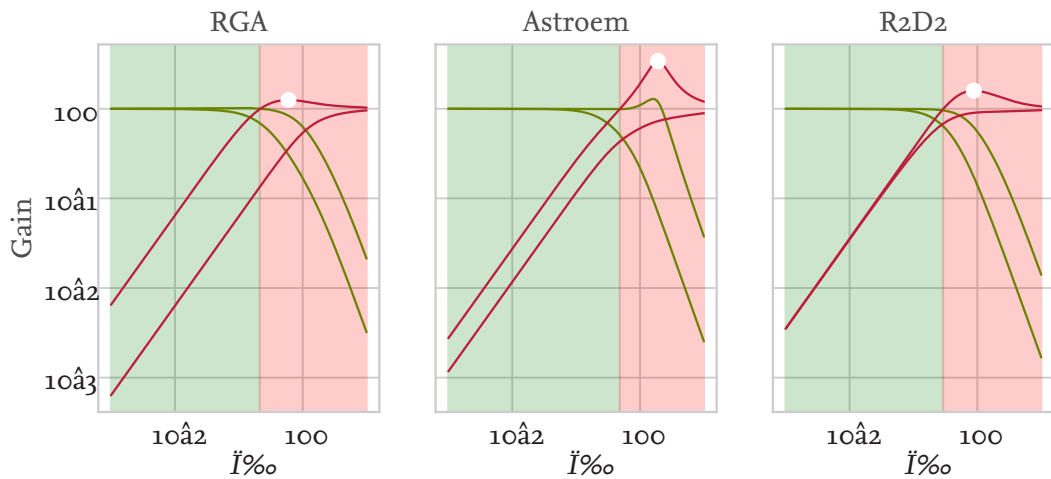


Figure 5.2: Singular values of the sensitivity (red) and complementary sensitivity (green) function of Rosenbrock's system without detuning

The decentralized controller performs reasonably well. Its maximum singular value of the sensitivity is given by $\bar{\sigma} = 1.25$ at the frequency of $\omega = 0.60 \text{ rad/s}$. The process is robust within the frequencies lower than $\omega \leq 0.22$, since this is the first time that the sensitivity exceeds the limit of $\bar{\sigma} \geq 1$. Likewise, the processes tracking performance begins to decrease at that frequency. Until that frequency is reached, the singular values are nearly identical and have a gain of 0 dB, which corresponds to an evenly distributed tracking performance of both outputs.

The singular values of the decoupling controller as proposed by Astrom differ strongly. The maximum singular value of the sensitivity reaches its peak at a frequency of $\omega = 1.91 \text{ rad/s}$ with a magnitude of $\bar{\sigma} = 3.40$. Hence, a more robust complementary sensitivity function with respect to the

bandwidth is given. The maximum singular value exceeds 0 dB around a frequency of $\omega = 0.5 \text{ rad/s}$, which is much higher than the frequency range of the decentralized controller. However, the lower value of the complementary sensitivity decreases faster at hence the outputs are not controllable evenly.

At last, the controller designed by robust relative dynamic decoupling is investigated with respect to its sensitivity and complementary sensitivity. The peak of the sensitivity is given with $\bar{\sigma} = 1.59$ at a frequency of $\omega = 0.88 \text{ rad/s}$. It can be seen that while the decoupler widens the useable frequency range it also amplifies the maximum singular value of the sensitivity function. Furthermore, until the frequency of $\omega = 0.30 \text{ rad/s}$, the singular values are very evenly distributed. This indicates the effect of the decoupler with respect to tracking efficiency and the distribution of noise or disturbances.

Next, the controller are detuned for a maximum interaction of $h_{A,\text{Max}} \leq 0.3$. The simulation results are shown in Fig.5.3 with the same color coding as before. The performance evaluation is given in Tab.5.2

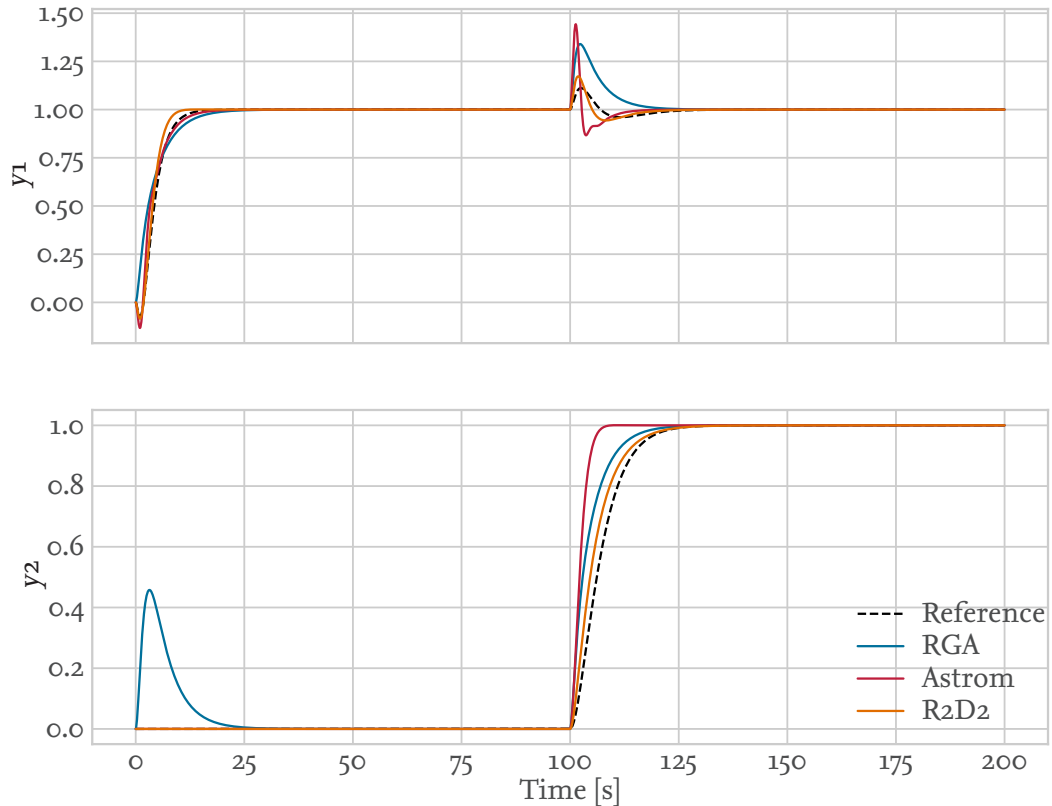


Figure 5.3: Simulation of Rosenbrock's System with detuning

Table 5.2: Evaluation of tracking performance and disturbance rejection performance of Rosenbrock's system with detuning

	Tracking Performance			Rejection Performance		
	T_{Rise}	m_p	T_{Settle}	T_p	m_Δ	T_{Settle}
	s	%	s	s	%	s
RGA	y_1	99.20	0.00	17.30	3.20	0.46
	y_2	99.30	0.00	17.20	2.20	0.34
Astroem	y_1	97.90	0.00	14.30	2.30	0.00
	y_2	99.30	0.00	6.50	1.20	0.43
R2D2	y_1	97.60	0.00	9.10	4.70	0.00
	y_2	98.70	0.00	20.40	1.80	0.17

In comparison to the not-detuned closed loop, both decoupled controller show a less aggressive performance as a result of the much lesser values for the proportional and integral gain. This is visible from the step response of the second output y_2 , where rising times have increased. Likewise,

the detuning reduces the interaction largely. Both decoupled controller have a maximum overshoot of $\Delta y_1 \leq 0.11$.

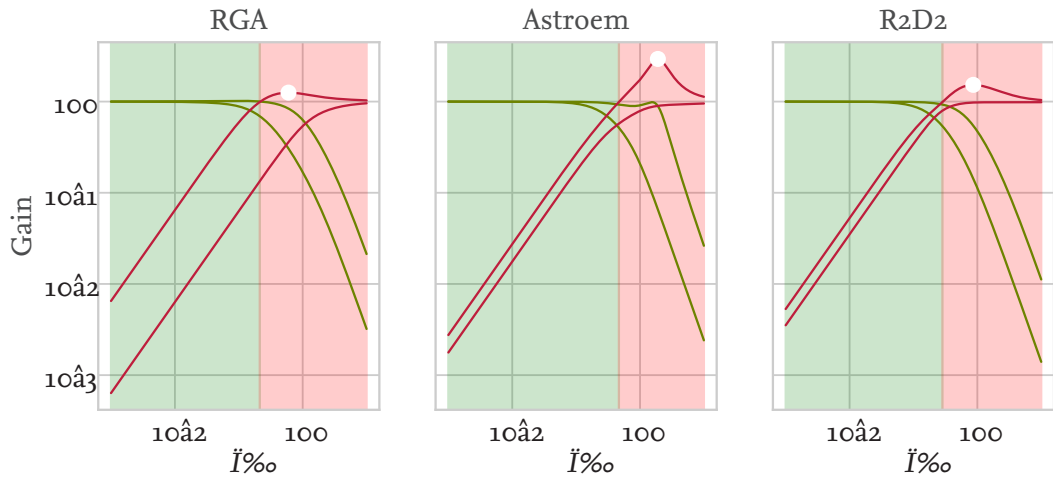


Figure 5.4: Singular values of the sensitivity (red) and complementary sensitivity (green) function of Rosenbrock's system with detuning

The singular values of the decoupled controller designed by Aström also changed, as can be seen in Fig.5.4. While the frequency where the maximum singular value of the sensitivity function occurs changed only little from $\omega = 1.91 \text{ rad/s}$ to $\omega = 1.94 \text{ rad/s}$, the magnitude has decreased to $\bar{\sigma} = 2.61$. But, due to the less aggressive and hence less effective controller, the crossing point of the maximum singular value changed to a lower frequency of $\omega = 0.22 \text{ rad/s}$. Hence, the tracking performance of the controller has a smaller bandwidth than before.

The controller designed by means of R2D2 is not significantly influenced, as can be seen in FIG. Both the frequency of the maximum singular value of the sensitivity and the magnitude change little, given by $\omega = 0.87 \text{ rad/s}$ and $\bar{\sigma} = 1.48$. Opposed to the not detuned controller, a broader spread of the singular values of the sensitivity can be seen. Hence, the tracking performance is already decreasing at lower frequencies, as can be seen from the lower singular value of the complementary sensitivity function. However, the bandwidth of the controller, limited by $\omega = 0.22 \text{ rad/s}$, is nearly identical to before.

5.3 Wood-Berry's Binary Distillation Column

As a second example the model of a binary distillation column, introduced by Wood and Berry REF-ERENZ, and used throughout academia, e.g. [5], RGAMEASURES, [21], will be investigated.

The model is given by the following transfer matrix, consisting of FOTD models:

$$G = \begin{bmatrix} \frac{12.8}{16.7 s+1} e^{-s} & \frac{-18.9}{21.0 s+1} e^{-3s} \\ \frac{6.6}{10.9 s+1} e^{-7s} & \frac{-19.4}{14.4 s+1} e^{-3s} \end{bmatrix}$$

Since the system is under the effect of time delay, the dynamics will be influenced from the average residence time $T_{ar} = T + L$ instead of a pure time constant in the previous section. The processes normalized time is given as following:

$$\tau = \begin{bmatrix} \frac{1}{16.7+1} & \frac{3}{21.0+3} \\ \frac{7}{10.9+7} & \frac{3}{14.4+3} \end{bmatrix} \approx \begin{bmatrix} 0.056 & 0.125 \\ 0.391 & 0.172 \end{bmatrix}$$

Which indicates that most of the transfer functions involved can be controlled without much effort. Only the entry $\tau_{12} \approx 0.391$ is challenging, since the delay has much influence on the outputs behavior. Due to these mixed normalized times, the effectiveness of the AMIGO algorithm in presence of delays can be seen. Furthermore, the effectiveness of the decoupler in presence of delays is to be investigated. At first, the identification is performed. The identified system is given by:

$$\hat{G} = \begin{bmatrix} \frac{12.800}{16.684 s+1} e^{-1.016s} & \frac{-18.899}{20.984 s+1} e^{-3.014s} \\ \frac{6.600}{10.901 s+1} e^{-7.005s} & \frac{-19.400}{14.384 s+1} e^{-3.014s} \end{bmatrix}$$

Since the values are given by a noise free, numerical simulation it is obvious that the identification will perform less optimal in a real environment. Nonetheless, the precision of the method can be seen from the values of the parameter.

The RGA analysis of the system in steady state gain computes to be:

$$\Lambda(G_0) = \begin{bmatrix} 2.01 & -1.01 \\ -1.01 & 2.01 \end{bmatrix}$$

Which indicates the diagonal pairing $u_1 \mapsto y_1, u_2 \mapsto y_2$. Oppose to Sec.5.2, the process of designing the controller will not be explained in its entirety. The parameter for the decentralized control, the decoupling controller based on Aström and the R2D2 are listed in the TABLE!! below for both a not detuned and detuned case.

TABLE

The static decoupler and the splitter are given as:

$$D = \begin{bmatrix} 0.167 & -0.153 \\ 0.053 & -0.104 \end{bmatrix}, \Sigma = \begin{bmatrix} 0 & 1.476 \\ 0.340 & 0 \end{bmatrix}$$

Simulation of the system without detuning, hence representing the effect of the decoupler and splitter, is shown in Fig. 5.5. As before, a reference controller [5] with computational optimized parameters is simulated as well. The performance evaluation is given below in Tab. 5.3.

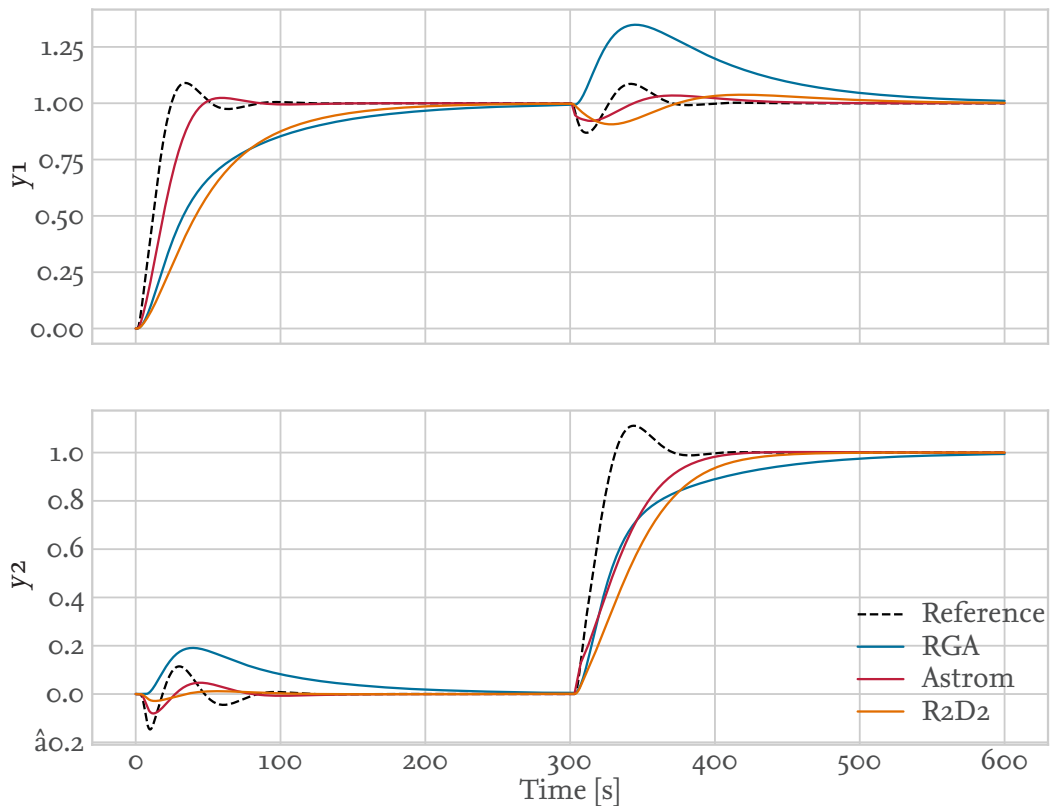


Figure 5.5: Simulation of Wood-Berry's binary distillation column without detuning

Table 5.3: Evaluation of tracking performance and disturbance rejection performance of Wood-Berry's binary distillation column without detuning

		Tracking Performance			Rejection Performance		
		T_{Rise}	m_P	T_{Settle}	T_p	m_Δ	T_{Settle}
		s	%	s	s	%	s
RGA	y_1	110.60	0.00	212.60	30.45	0.19	267.70
	y_2	92.40	0.00	198.90	45.10	0.36	244.15
Astroem	y_1	29.50	0.02	43.90	9.10	0.08	290.80
	y_2	62.80	0.00	97.70	28.75	0.03	8.35
R2D2	y_1	96.70	0.00	180.20	9.95	0.03	114.10
	y_2	75.95	0.00	128.60	43.70	0.04	21.95

From the simulation it can be seen that both the reference controller and the auto-tuned controller as given by Åström are much faster than the ones designed under decentralized assumptions or R2D2. This effect arises from the implementation of the AMIGO algorithm, which states that the delay L_{ij} used for calculations is at least $0.3 T_{ij}$. Since the approximation of the system with an static inverse decoupler holds small time constant, $T_{11}^* = 8.330\frac{1}{s}$ and $T_{22}^* = 9.880\frac{1}{s}$, the process itself is faster and can use the original delay. Opposed to this, the decentralized controller and the R2D2 based controller compute the parameter based on the real time constants, which are much larger, and use a minimum delay. Therefore they perform poorly with respect to the other controller.

Another effect caused by this inequality can be observed from the rejection behavior of y_1 . The faster controller causes and reduces the overshoot in less time than the relative dynamic decoupled controller.

However, the induced disturbance of both decoupled controllers on the outputs y is much less than the effects caused by the reference controller. Additionally, both controller outperform the decentralized architecture with respect to tracking performance and the reference with respect to overshoot.

In Fig.5.6 the effect on overall tracking and rejection performance is given by the singular values of the complementary sensitivity and sensitivity function. All processes show similar properties regarding bandwidth and maximum singular values of the sensitivity. Here both the decentralized controller and the static inverse decoupled controller outperform the proposed splitter architecture.

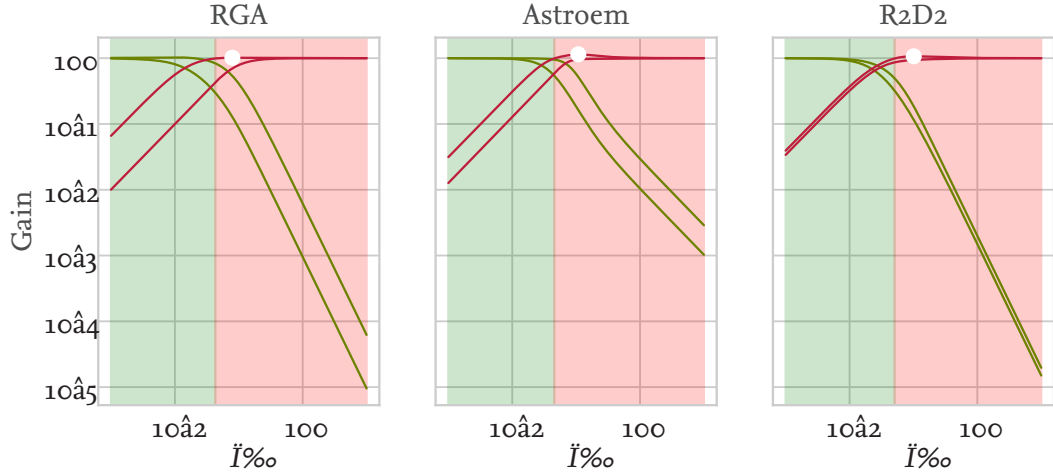


Figure 5.6: Singular values of the sensitivity (red) and complementary sensitivity (green) function of Wood-Berry's binary distillation column without detuning

A clear distinction is given in terms of the relative difference between the upper and lower bounds of the singular values, which is a measure for the evenly distributed maneuverability of the outputs. As shown before, the R2D2 controller distributes tracking and sensitivity much more even than the other controller. With respect to this fact, it can be seen that the both decentralized and static inversely decoupled control enable the steering of an output while the sensitivities upper bound outperforms the other. Hence, the usefulness of these frequency ranges are arguable.

Next, the simulation of the detuned system is shown in Fig.5.7 accompanied by the performance evaluation in Tab.???. The R2D2 controller already acts within the dictated limits of interaction, while the performance of the controller as computed by AStröm has decreased dramatically.

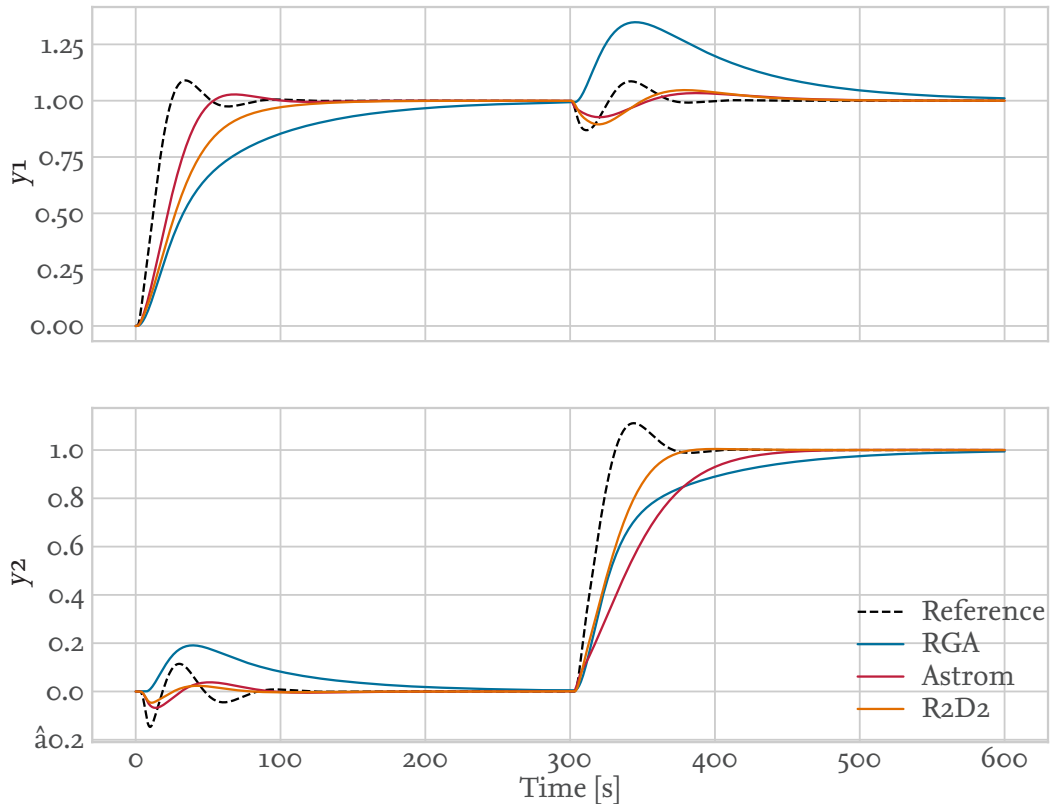


Figure 5.7: Simulation of Wood-Berry's binary distillation column with detuning

While both decoupler outperform the RGA, the splitter clearly dominates the controller decoupled via static inverse in the overall performance. Since the slowness of the controller is originating directly from the lower bound on the delay for computation, a less conservative bound would increase the performance and interaction.

Fig. 5.8 shows the singular value band of the processes. Due to the detuning the usable bandwidth of the Aström controller has decreased while the complementary sensitivity is behaving like the decentralized controller.

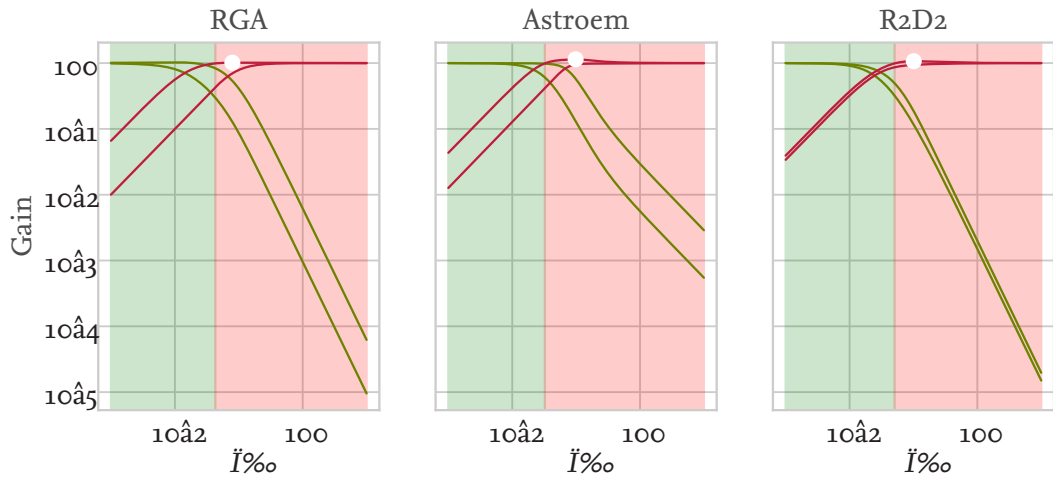


Figure 5.8: Singular values of the sensitivity (red) and complementary sensitivity (green) function of Wood-Berry's binary distillation column with detuning

To conclude the evaluation of the process, both advantages and disadvantages of the decoupling controller can be noted. With a system varying in dynamics and sign of the gain, the effective system due to an approximation is able to be controlled more aggressively. This is shown by the not detuned controller decoupled by a static inverse, which assumes faster process on the main diagonal with a slower disturbance acting as interconnections. Due to this effect, the R2D2 is outperformed. However, if an upper limitation on the interaction is given, the advantages of evenly distributed dynamics are clearly visible. The limitation on the interaction has been adhered without detuning the controller.

5.4 McAvoy et. al.

The system in the following subsection has been introduced by REFERENz and reused for theoretical research since, e.g. REFERENZ INTERACTION. It is given by the following transfer function matrix:

$$\mathbf{G} = \begin{bmatrix} \frac{5}{100s+1} e^{-40s} & \frac{1}{10s+1} e^{-4s} \\ \frac{-5}{10s+1} e^{-4s} & \frac{5}{100s+1} e^{-40s} \end{bmatrix}$$

The RGA holds a diagonal pairing within the steady state, since y_1 is mainly dominated by g_{11} in the steady state. For dynamic control it can be shown that a cross coupling consisting of the pairing (y_1, u_2) and (y_2, u_1) is more suitable, QUELLE. This approach clearly relies on the corresponding delays, which enable to react much faster.

Furthermore it can be seen that the coupling is strong, since y_2 is influenced both by g_{21} and g_{22} with the same magnitude. The not detuned controller used are given by the following parameter:

HIER TABLE

The simulation is of the closed loop is shown in Fig. 5.9. The interaction from u_1 to y_2 are clearly visible. While not able to fully compensate the dynamic effects, both the controller designed by a fully static decoupling and the compensator are able to reduce the magnitude of the interaction. However, the dynamic effects provoked by the decentralized controller are much faster to be decay.

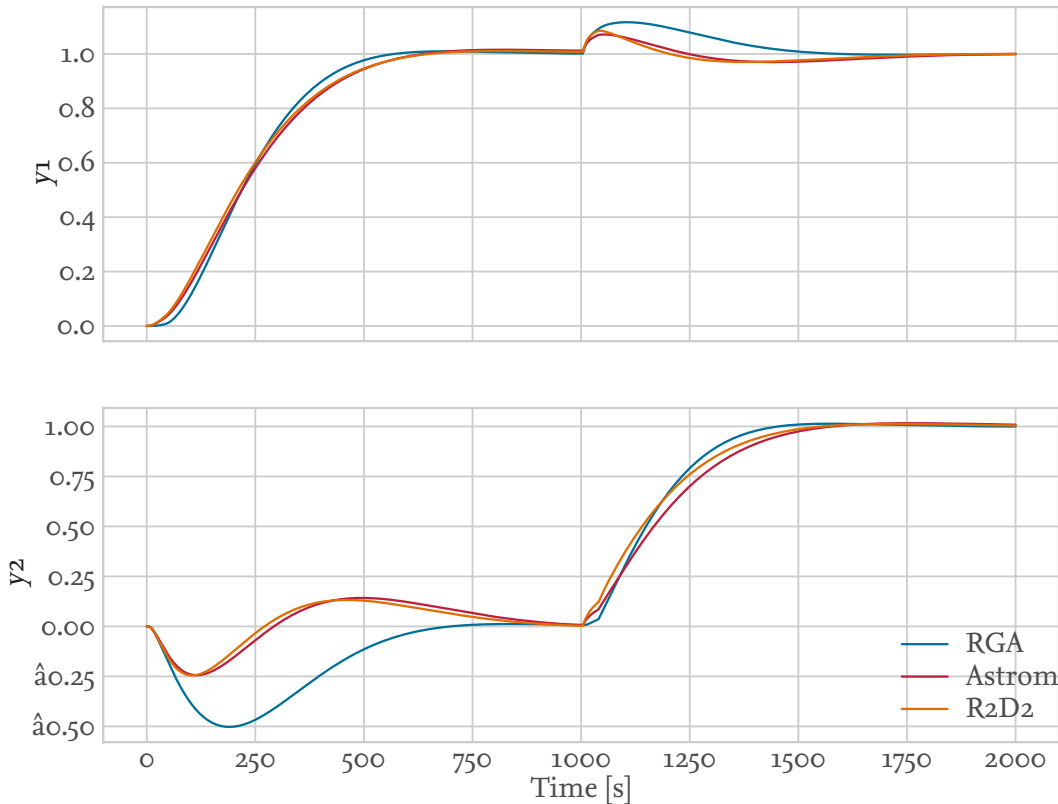


Figure 5.9: Simulation of McAvoy's system without detuning

The tracking and disturbance performance is shown in Tab.5.4. The reasoning for the poor performance of the decoupling and compensation lies within the difference of the dynamics. While the main diagonals are dominant in lower frequencies it loses declines much faster than the minor diagonals. Hence, the static decoupling will not work properly, since the effects transferred via the main diagonals are scaled down significantly.

Table 5.4: Evaluation of tracking performance and disturbance rejection performance of McAvoy's system without detuning

		Tracking Performance			Rejection Performance		
		T_{Rise}	m_P	T_{Settle}	T_p	m_Δ	T_{Settle}
		s	%	s	s	%	s
RGA	y_1	185.05	0.00	293.75	805.20	0.39	0.00
	y_2	259.45	0.01	1103.95	190.20	0.50	0.00
Astroem	y_1	202.35	0.00	293.25	752.35	0.38	0.00
	y_2	1016.05	0.01	1234.95	114.95	0.24	164.65
R2D2	y_1	204.45	0.00	292.75	739.95	0.38	0.00
	y_2	999.25	0.01	1194.80	104.50	0.25	153.70

The singular values of the complementary sensitivity and sensitivity transfer function matrices are shown in Fig.5.10. With respect to the bandwidth, the decoupled and compensated controller show better performance and lower the magnitude of the maximum sensitivity. However, while both processes seem more balanced with respect to the tracking performance near the steady state, but lose influence much faster.

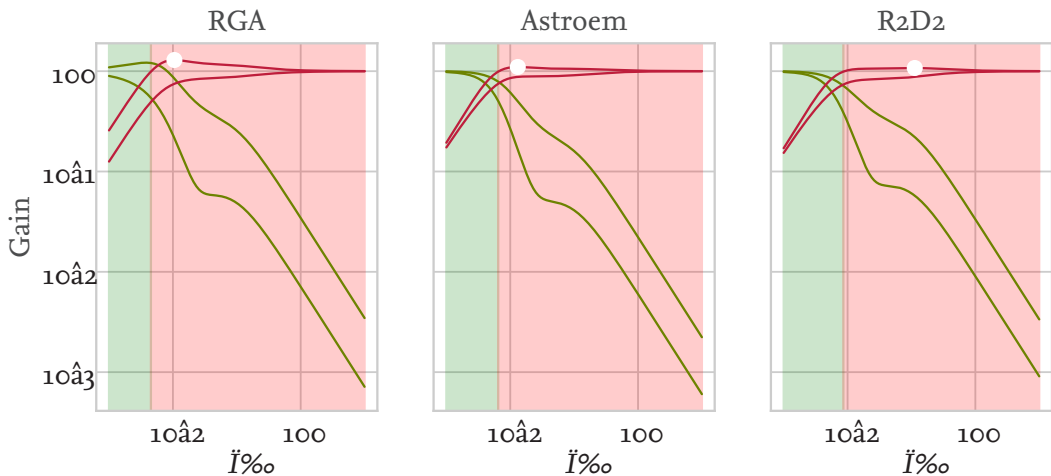


Figure 5.10: Singular values of the sensitivity (red) and complementary sensitivity (green) function of McAvoy's system without detuning

Next, the system will be detuned to a maximum interaction of $h_{ij} \leq 0.5, \forall i \neq j [0, 1]$ with a maximum iteration counter of 5. The parameter for the controller are given in the Tab. TABELLE! below.

TABELLE

The simulation of the closed loop is shown in Fig.5.11, the tracking behavior and disturbance rejection evaluation is given in Tab.5.5. It is clearly visible that both detuned controller are significantly

slower while only slightly decreasing the interaction of both loops.

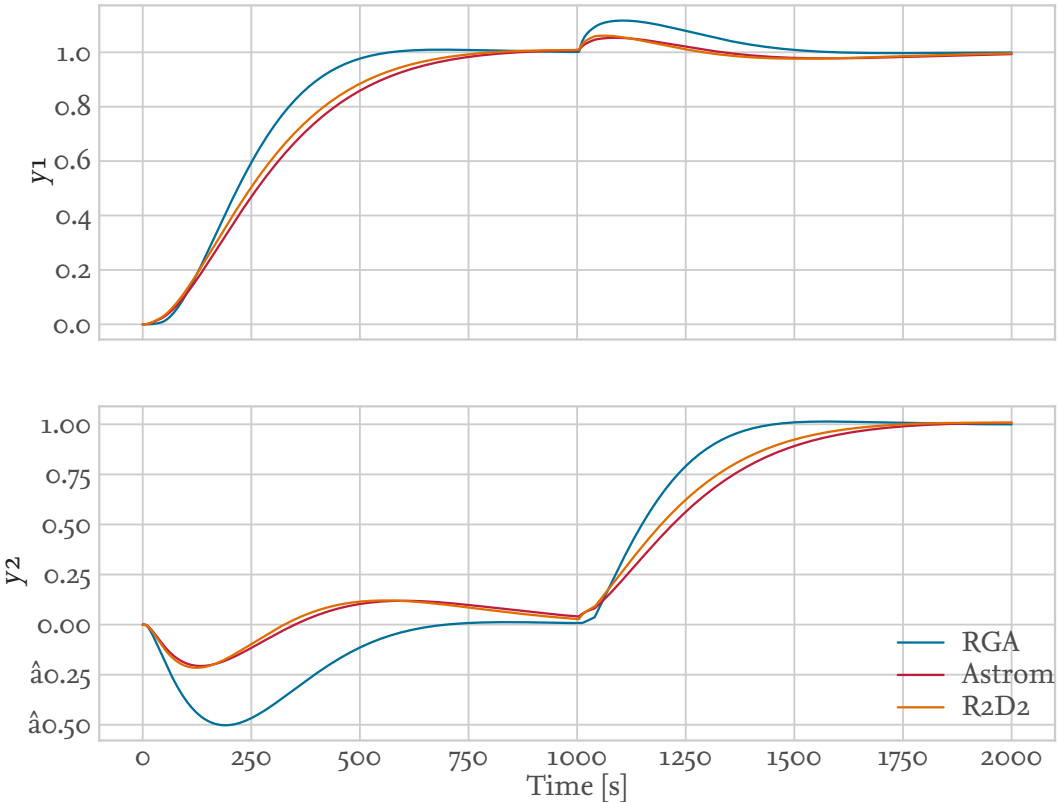


Figure 5.11: Simulation of McAvoy's system with detuning

Table 5.5: Evaluation of tracking performance and disturbance rejection performance of McAvoy's system with detuning

	Tracking Performance			Rejection Performance		
	T_{Rise}	m_P	T_{Settle}	T_p	m_Δ	T_{Settle}
	s	%	s	s	%	s
RGA	y_1	214.45	0.00	293.75	805.20	0.39
	y_2	945.35	0.01	1103.95	190.20	0.50
Astroem	y_1	230.45	0.00	294.20	760.15	0.50
	y_2	1525.95	0.00	1231.60	123.50	0.19
R2D2	y_1	231.20	0.00	293.90	760.85	0.45
	y_2	1544.75	0.00	1371.05	124.20	0.22

These results are underlined by the evaluation of the singular values of both the complementary

sensitivity and sensitivity function, as shown in Fig 5.12. Both bandwidth are reduced while the maximum singular value of the sensitivity is increased. The tracking behaviors balancedness, given by the singular values of the complementary sensitivity, decreases at much lower frequencies than before.

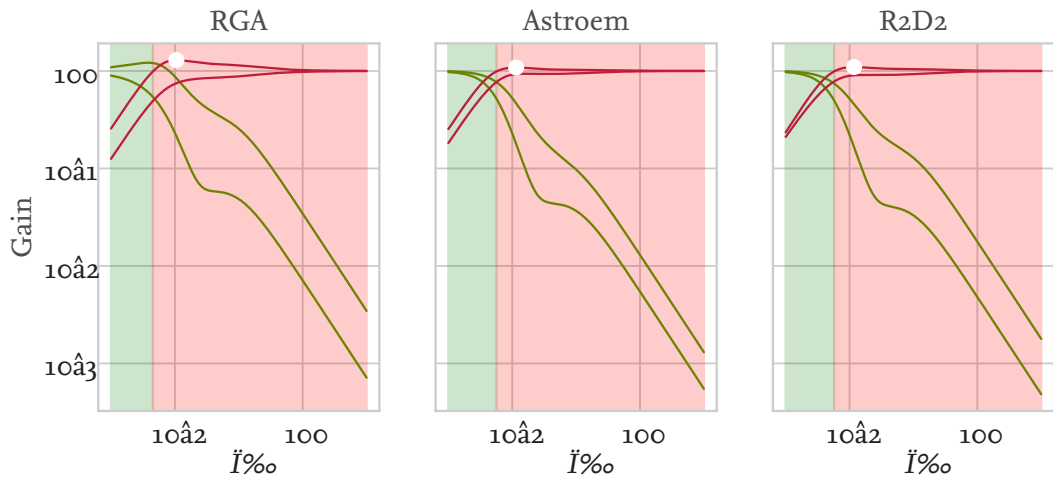


Figure 5.12: Singular values of the sensitivity (red) and complementary sensitivity (green) function of McAvoy's system with detuning

The evaluation of Mc Avoy's system shows the limits of both a static decoupling and the compensator. With near dynamics, the static methods can be used to enhance the controllers performance and the dampen the effects of measurement noise and output disturbances. However, from the dynamics of the current example it can be seen that the presented methods are much likely to have no beneficial effect.

5.5

Working point 2

5.6 Performance Review

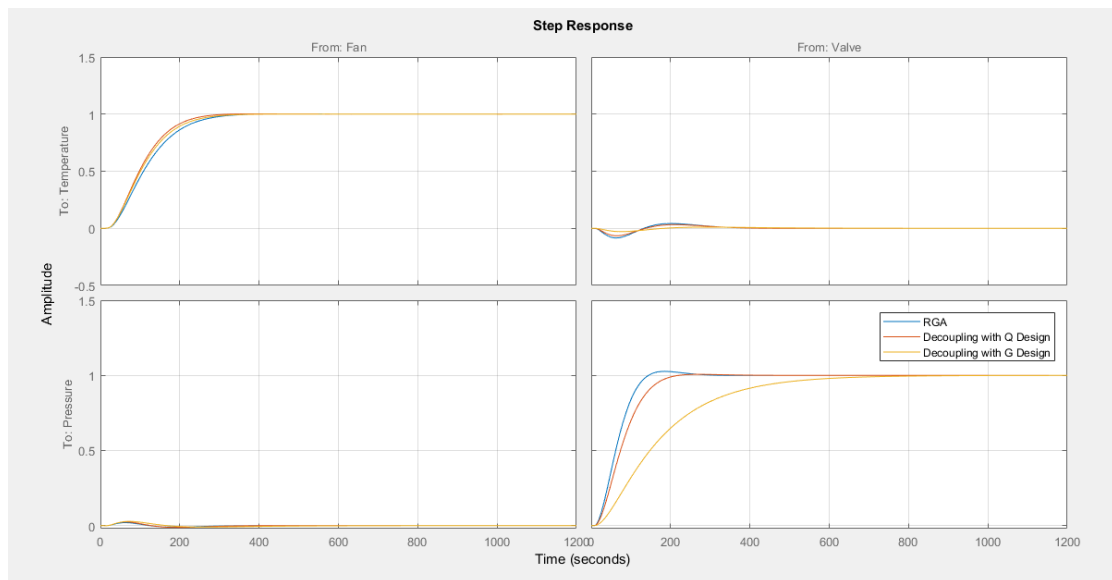


Figure 5.13: Step of the MIMO

6 Robustness Study Using Monte Carlo Methods

To benchmark the robustness of the proposed method, a simulation study based on Monte Carlo Methods is performed. Monte Carlo Methods rely on the statistical interpretation and evaluation of problems, which are not necessarily fully describable by precise terms. To perform a simulation, pseudo random numbers within the parameter limits are generated in a sufficiently large amount and used as an input to the process. Afterwards, the outcome can be evaluated and the distribution of possible outcomes can be achieved. Examples for the usage of these methods are statistical thermodynamics, quantum mechanics, population simulation and even the simulation of structural mechanics.

Basically, Monte Carlo Methods enable the exploration of uncertain systems, which is not describable by in terms of deterministic methods. Imagine a the classical experiment of throwing an ideal coin. The outcome for large samples is given by the probability distribution of heads and tails. If the sample size is small, the outcome will be predicted with a certain bias, e.g. heads is more likely than tails. For large sample sizes, the outcome will be describable as a balanced distribution of heads and tails.

The motivation behind the simulation is to get a picture of the overall process of identification, controller tuning, decoupling and detuning. To better understand these steps, the problem is divided into a simulation study for simple, scalar transfer functions and multivariable transfer function matrices.

The first section of this chapter gives an overview about the main topics of the evaluation. Parameter distributions, statistical methods and the parameter boundaries are explained as well as the methods used to create them.

In Sec. ?? the evaluation of single input single output systems is performed. The maximum sensitivity of an ideal model and the real model is connected and.

6.1 Definition of Parameter Boundaries and Evaluation Methods

To determine the effectiveness of the algorithms, the space of all possible parameters needs to be bounded. To establish these boundaries, both physical assumptions and choosing of boundaries based on best guesses are build upon.

The process itself is governed by the laws of thermodynamics. Due to this, the process is stable. This originates in the conservation of energy, which states that energy can not be destroyed nor created but simply converted. The energy in the system will reach a stable equilibrium when all transportation processes are decayed. Hence, both temperature and pressure will reach a stable configuration. Likewise, the system is causal since it will rest in its equilibrium until an external input of energy occurs.

Furthermore, observations of the systems step response show that the output of a given signal is monotonic in its behavior. Due to this the process is modeled as a simple transfer function with delay described by:

$$g_{ij} = \frac{K_{ij}}{\prod_{k=1}^m s - p_k} e^{-Ls}, \operatorname{Re}(p_k) \leq 0 \quad \forall p_k$$

To further discuss the pseudo random parameters, the terms of distribution, mean and variance in the terms of statistics need to be introduced. A distribution describes the outcome $\nu \subset \mathbb{A}$, where \mathbb{A} denotes the set of all possible outcomes, of a random event $\eta \in \mathbb{H}$, where \mathbb{H} denotes all possible events. The probability $P(\nu) \in [0, 1]$ describes the likelihood by which a specific outcome will occur. Distributions can either be continuous or discrete.

The expected value $\mu(\eta) \in \mathbb{R}$ of all possible outcomes, also called the mean or first statistical moment, describes the center of gravity of a given distribution. Explicitly, it can be calculated for continuous and discrete distribution by:

$$\begin{aligned} \mu(\nu) &= \int_{-\infty}^{\infty} \nu \eta(\nu) d\nu \\ &= \frac{1}{N-1} \sum_{i=1}^N \nu_i \end{aligned} \tag{6.1}$$

Furthermore, the second centralized moment $\mu_2(\eta)$ of a distribution is given by the mean of the deviation with respect to the expected value, and the variance $\sigma(\eta)$ can be defined:

$$\begin{aligned}
\mu_2(\nu) &= \mu((\nu - \mu)^2) \\
&= \int_{-\infty}^{\infty} (\nu - \mu)^2 \eta(\nu) d\nu \\
&= \frac{1}{N-1} \sum_{i=1}^N (\nu_i - \mu)^2 \\
&= \sigma^2
\end{aligned} \tag{6.2}$$

To investigate the dependency of two random variables, ν_X and ν_Y , the correlation coefficient $\varsigma_{XY} \in [-1, 1]$ is given in terms of the covariance σ_{XY} :

$$\begin{aligned}
\varsigma_{XY} &= \frac{\sigma_{XY}}{\sigma_X \sigma_Y} \\
&= \frac{\mu(\sigma(\nu_X) \sigma(\nu_Y))}{\sigma_X \sigma_Y}
\end{aligned} \tag{6.3}$$

The correlation describes the dependency of two outcomes. If they are strongly correlated, meaning $\nu_X = \nu_Y$, than $\varsigma_{XY} = 1$. Likewise, if $\nu_X = -\nu_Y$, than $\varsigma_{XY} = -1$. If $\varsigma_{XY} \approx 0$ than both samples are nearly unrelated to each other.

Next on, the generation of the pseudo random samples is described. Since no prior knowledge of the process is given, a general uniform distribution of all parameters is chosen. This means that every value in the interval is equally likely to be drawn from within the boundaries.

The gain is scalable, and hence the interval can be selected freely as long as its symmetric to zero. These relies on the fact that the likelyhood to choose a process gain with a negative or positive sign. With that, the gain can be describes to be:

$$K \in [-10, 10], \mu(K) = 0, \mu_2(K) = \frac{20^2}{12}$$

The system's lag holds more difficulties to generate. Several cases can be imagined and must be taken to account. Therefore, three simulation scenarios are devised.

The first process model of order m is given by a constant sum time $T_\Sigma = \sum_{k=1}^m = 100$, hence the rise time of the process will be hold constant. The poles of the system are divided by dividing the sum time in several distances. Therefore, the system can be described by:

$$\begin{aligned}
g_{ij} &= \frac{K_{ij}}{\prod_{k=1}^m s - p_k} e^{-Ls} \\
&= \frac{K_{ij}}{\prod_{k=1}^m (T_k s + 1)} e^{-Ls} \\
&= \frac{K_{ij}}{\prod_{k=1}^m (T_\Sigma t_k s + 1)} e^{-Ls}
\end{aligned}$$

With $t_k \in [0, 1], \sum_{k=1}^m t_k = 1$. Hence, the process can variate strongly in the individual time constants but behaves similar with respect to its step response.

To generate the delay of each system, the samples are drawn from a uniform distribution which can be characterized by the following key figures:

$$L \in [1, 10], \mu(L) = 5.5, \mu_2(L) = \frac{9^2}{12}$$

Second, the process model of order m is modified to be given by:

$$\begin{aligned} g_{ij} &= \frac{K_{ij}}{\prod_{k=1}^m s - p_k} e^{-Ls} \\ &= \frac{K_{ij}}{\left(\frac{T}{m}s + 1\right)^m} e^{-Ls} \end{aligned}$$

Which is equal to a system with a pole multiplicity of m at $s = -\frac{T}{m}$. The time constant T is drawn from a random distribution described by:

$$T \in [50, 100], \mu(T) = 75, \mu_2(T) = \frac{50^2}{12}$$

By dividing the time constant by its order, a bounded rising time of the step response is given. In other words, the sum time constant $T_\Sigma = \sum_{k=1}^m T_k$ is bounded within the limits of T . Systems with pole multiplicity are hard to control, since the poles come in complex conjugated pairs which represent the damping. An example is given by Fig.6.1, where the poles of a system described by the process model with $T = 90$ is shown for $m \in [1, 9]$.

To generate the delay of each system, the samples are drawn from a uniform distribution which can be characterized by the following key figures:

$$L \in [15, 30], \mu(L) = 22.5, \mu_2(L) = \frac{15^2}{12}$$

The last parameter study draws the lag from a uniform distribution described by:

$$T \in [1, 20], \mu(T) = \frac{19}{2}, \mu_2(T) = \frac{21^2}{12}$$

Hence, both sum time constant T_Σ and hence the rising time can show significant variation. The delay distribution is given by:

$$L \in [1, 20], \mu(L) = 11.5, \mu_2(L) = \frac{19^2}{12}$$

All three cases described above can be used to evaluate the closed loop behavior with regards to several key figures such as the maximum sensitivity, maximum complementary sensitivity, sum time constant, delay and normalized time delay.

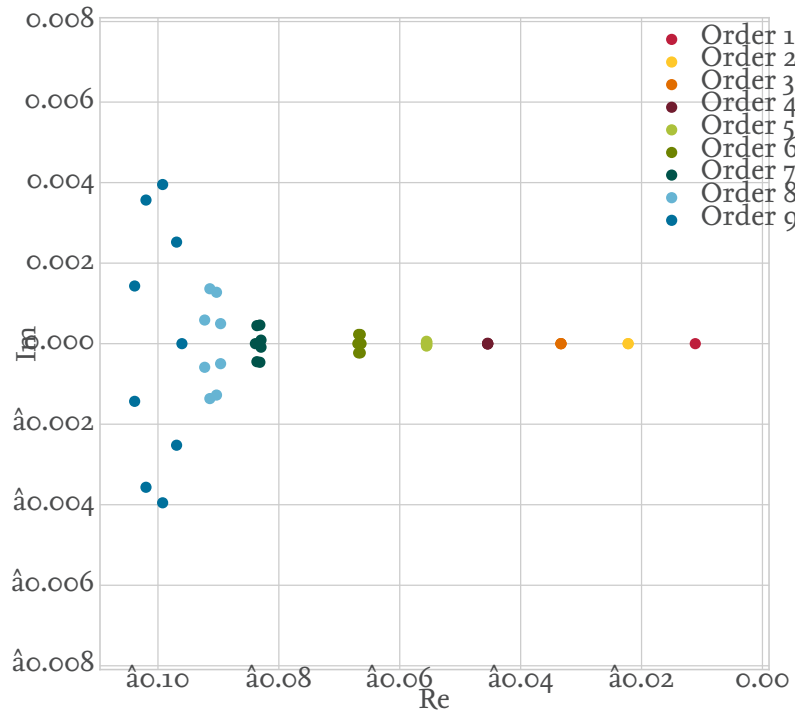


Figure 6.1: Example of a system with pole multiplicity

6.2 Robustness of SISO Systems

The following section describes the results of samples containing SISO systems. All three lag generation methods have been investigated to observe the robustness within the variation of single time constants and sum time. The gain and delay have been chosen according to the description above.

6.2.1 Constant Sum Time

The first simulation run contains the results of the systems described by a constant sum time. In Fig.6.2 the maximum sensitivity of the closed loop with the identified FOTD model is shown over the maximum sensitivity of the closed loop with the real transfer function. The sample size is 9000 systems from order one to nine. Therefore, every order itself contains 1000 system samples.

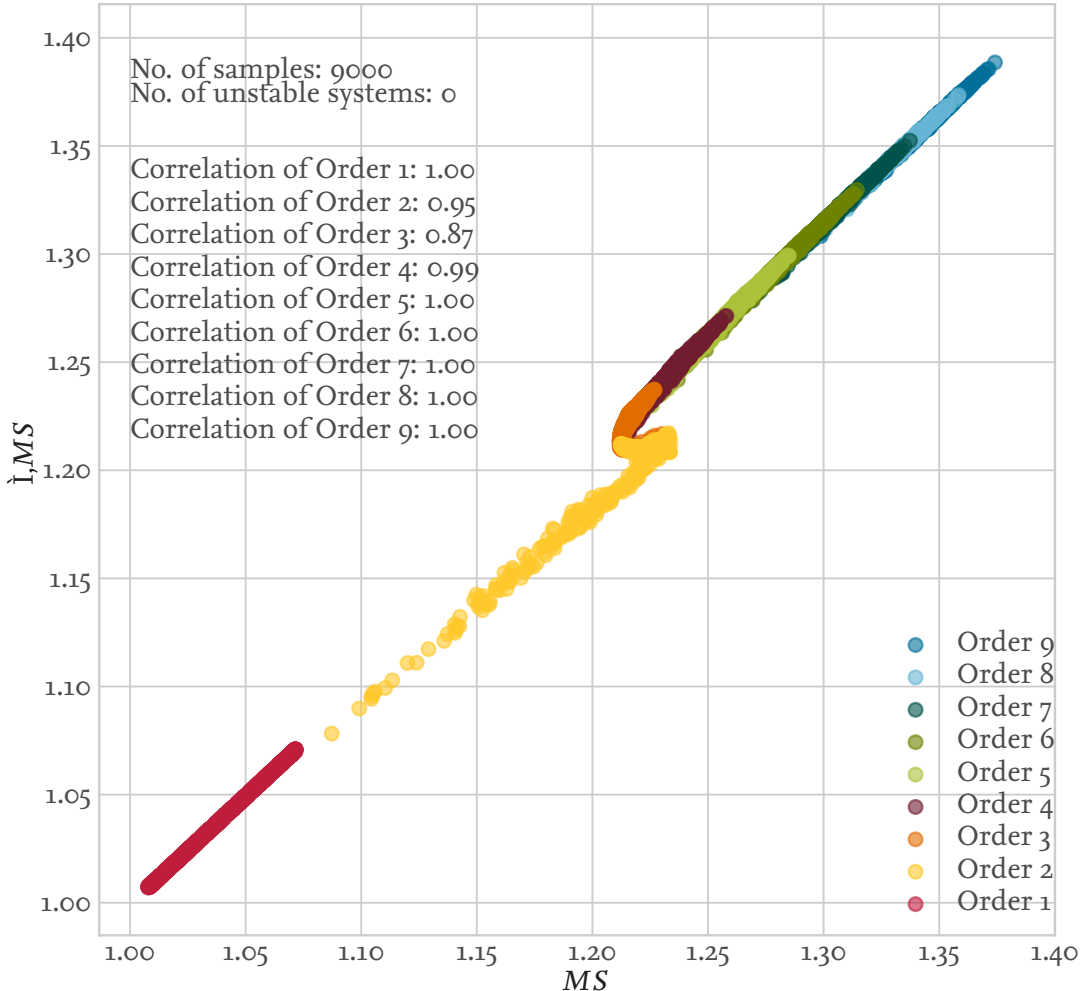


Figure 6.2: Results of the robustness study, maximum Sensitivity of the real System and the identified system

The robustness in terms of the maximum sensitivity never exceeds the value of $M_S \leq 1.40$. Hence, the minimum distance to the critical point of the open loop is given by $s_M \geq \frac{1}{1.40} = 0.7143$. From Fig.6.2 it is obvious that the values of M_S are increasing with the order. Moreover, from the correlation of the real and identified system a nearly identical behavior is given, with $\zeta \in [0.87, 1.00]$. It can be seen that lower order are tendentially more robust and second and third order processes are distributed more widely and show less correlation. This can be explained with regards to the limitation of a minimal delay for the controller parameter estimation, $L \geq 0.3T$. This bound can be equally expressed in terms of the normalized time delay $\tau = \frac{L}{T+L} = \frac{0.3T}{1.3T} = 0.231$. Fig.6.3 shows that below that value a significant change in the robustness of the process occurs.

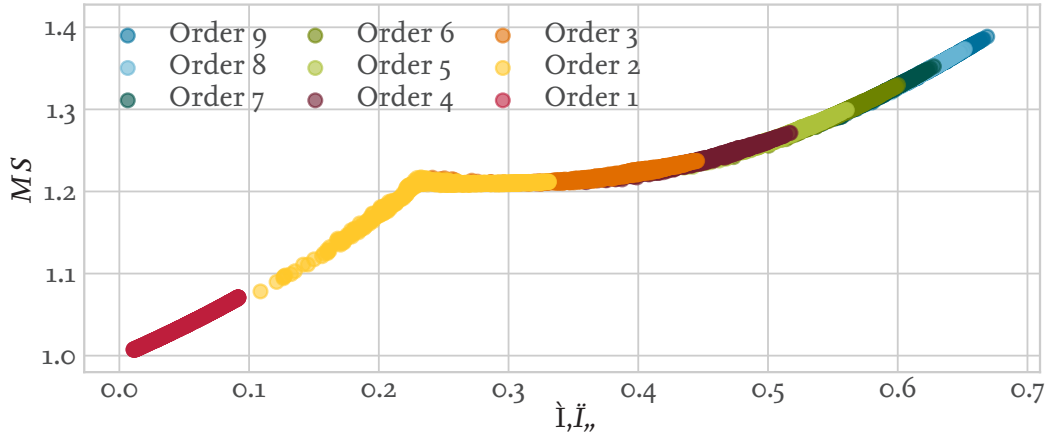


Figure 6.3: Results of the robustness study, maximum sensitivity of the real System over normalized time delay

Furthermore, the distribution over the process lag and delay will be investigated. In Fig.6.4 the model time constant of the FOTD is shown over the maximum time constant of the process $T_{Max} \geq T_k \forall k \in [1, m]$ in addition to the model delay and the real systems delay. It can be seen that the model lag is estimated correctly for first order systems, but spreads more widely for higher orders $m \geq 2$.

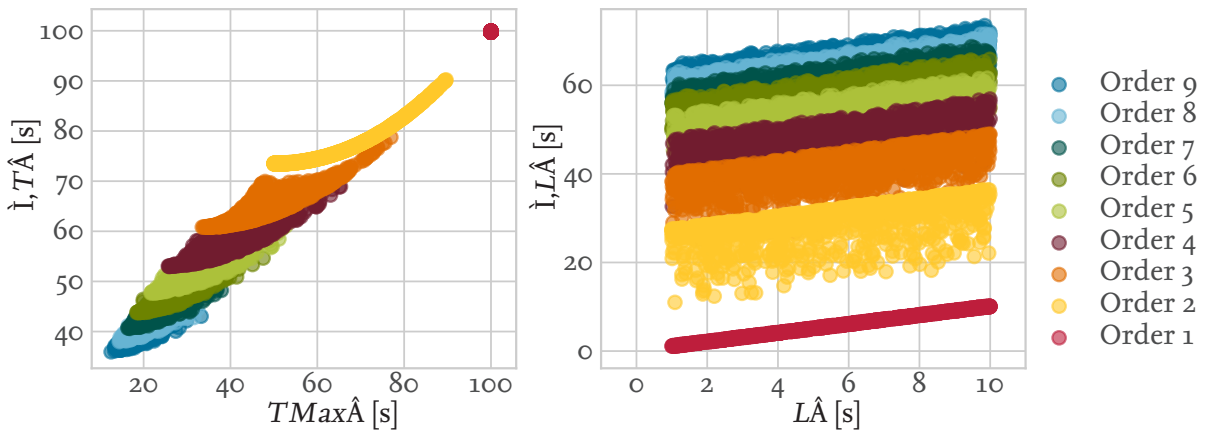


Figure 6.4: Results of the robustness study, model delay and lag over the process parameter

It is visible that the real delay estimated correctly for first order systems while a higher order adds an offset to it, which indicates the compensation of high order dynamics via the model delay. This observation can also be expressed in terms of Fig.6.5 where the normalized time delay of the real process with respect to the sum time constant and the FOTD model is shown. Additionally the probability distribution over the order is given along with its interquartile marked by the box.

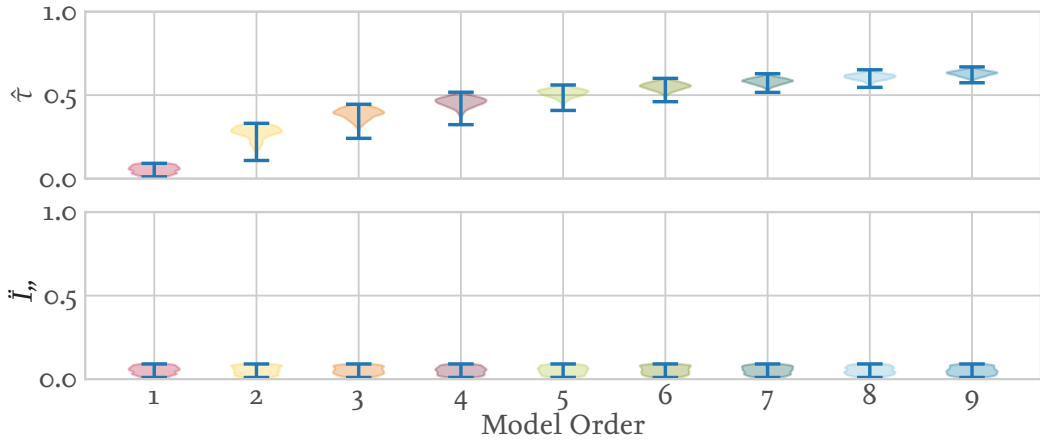


Figure 6.5: Results of the robustness study, normalized time delay of the real system and the FOTD model

6.2.2 Pole Multiplicity

The following subsection describes the results of the study performed by the process model described with multiple poles of random time constants. Hence T_Σ will vary and the performance for different process speeds is given. In Fig. 6.6 the maximum sensitivity of the model systems closed loop over the closed loop with the real system model is shown. The results coincide with the results shown given in SS.6.2.1. Only the second order model is more concentrated, but shows a strong correlation nonetheless.

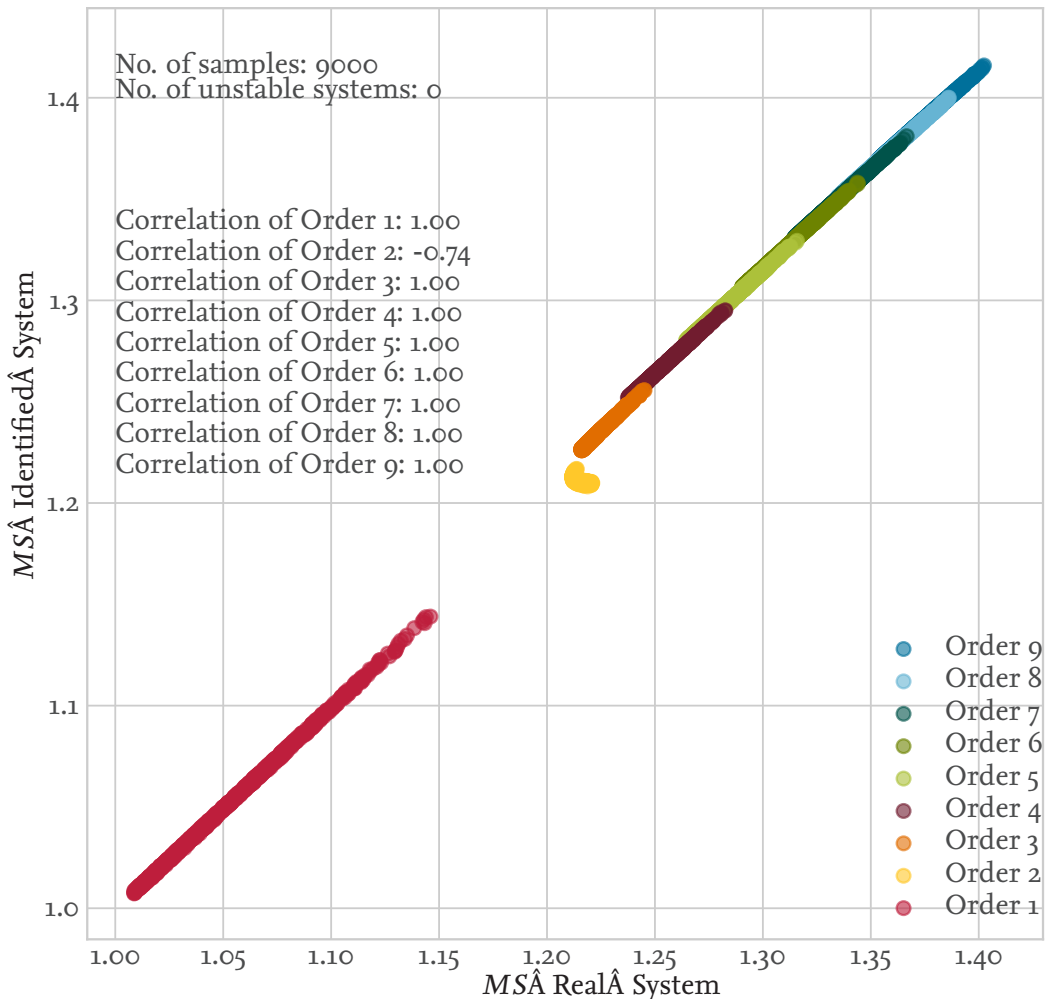


Figure 6.6: Results of the robustness study, maximum sensitivity of the model system over the maximum sensitivity of the real system

Likewise the model parameter estimated do not differ significantly from the previous results, as shown in Fig.6.7. Neither do other results, which will not be discussed further.

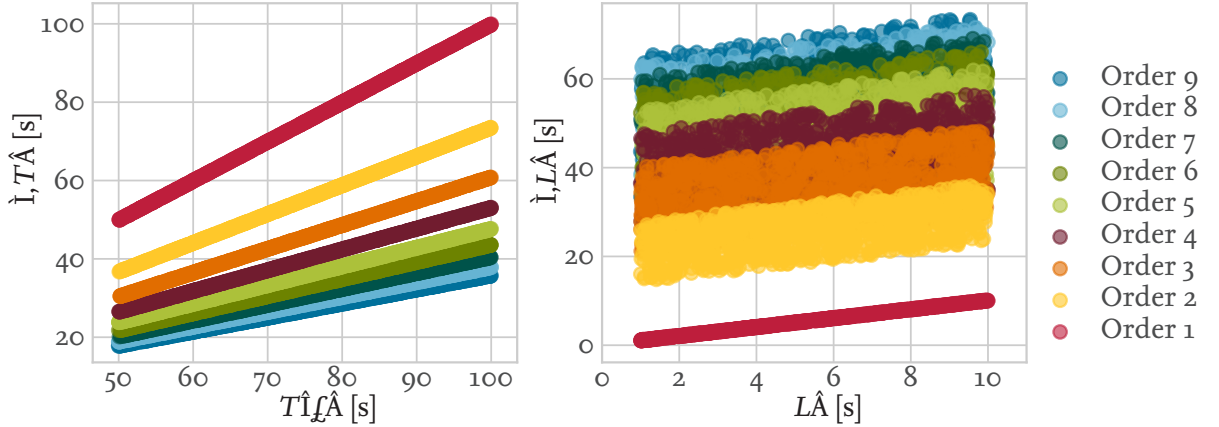


Figure 6.7: Results of the robustness study, model delay and lag over the process parameter

6.2.3 Random Time Constants

Next, the results given by processes with pole multiplicity as described earlier are investigated. At first, the correlation analysis between the maximum sensitivity of the FOTD model and the real process as shown in Fig.6.8 is examined. With respect to the results above, the sensitivity is spread more widely. With the exception of first, second and third order systems, which range between $[1.0, 1.5]$, the systems maximum sensitivity is bounded within $[1.2, 1.5]$. The correlation coefficient of all samples is $\zeta = 1.0$, which indicates that the sensitivity of the real system and model system are identical.

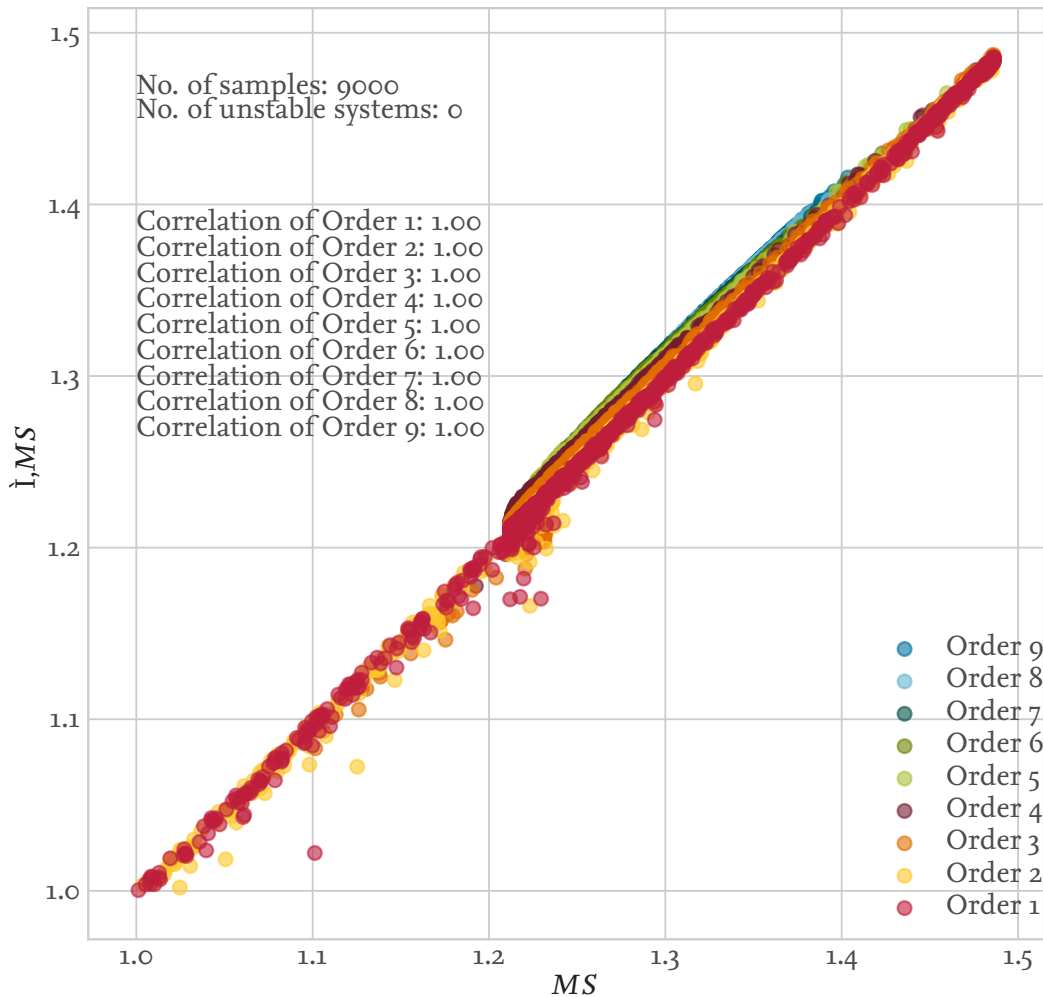


Figure 6.8: Results of the robustness study, maximum sensitivity of the real system and the identified system

These observations can be confirmed by the cumulative density plot of the system, shown in Fig.6.9. The distribution of samples over the maximum sensitivity of the closed loop is shown as fraction of the total sample size. It can be seen that nearly 90 % of all systems maximum sensitivity is less than 1.4 .

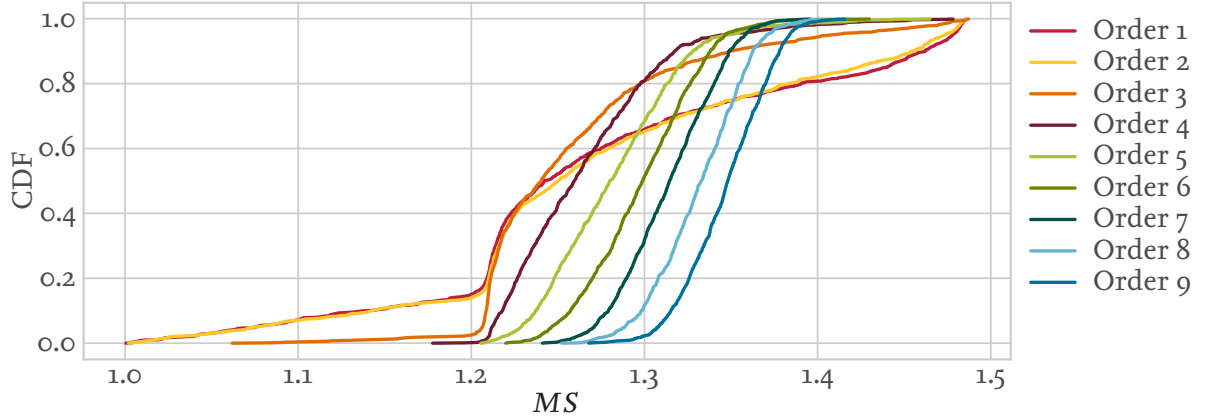


Figure 6.9: Results of the robustness study, cumulative density plot of the maximum sensitivity of the real system

Like earlier, the distribution of the delay and the sum time are shown below. Both model parameter vary much more than before, as shown in Fig. 6.10.

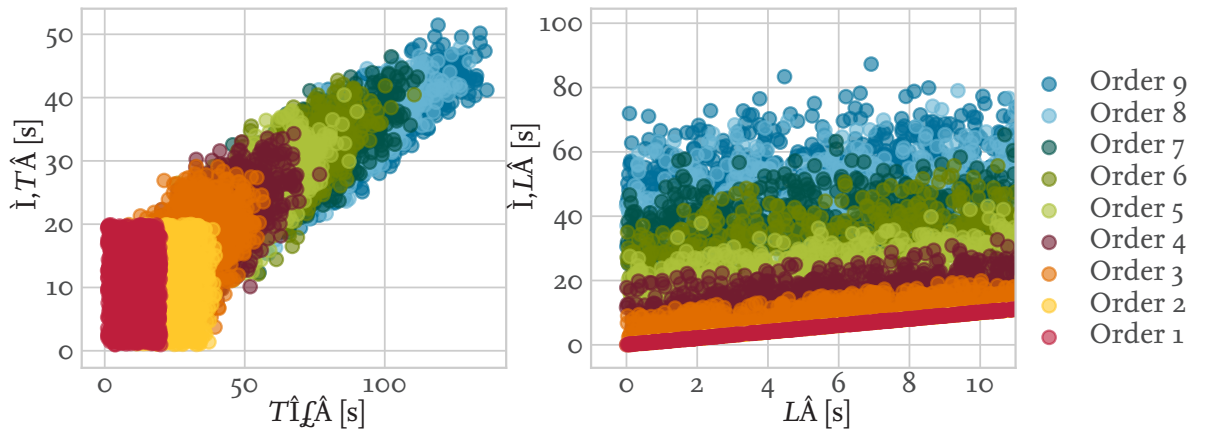


Figure 6.10: Results of the robustness study, model delay and lag over the process parameter

6.3 Robustness of Multivariable Systems

Likewise, multiple input multiple output systems have been investigated with respect to the robustness, e.g. the maximum singular value $\bar{\sigma}$ of the sensitivity function. Furthermore, the effect of detuning is examined by varying the upper boundary of interaction $h_{ij,Max}$ for every control loop.

As before, the transfer functions are created by a constant sum time T_Σ and by drawing a random system with pole multiplicity. The maximum allowed interaction for both cases is limited to either $h_{ij,Max} \leq 0.5$ or $h_{ij,Max} \leq 0.1$. The system order ranges from first to ninth order.

6.3.1 Constant Sum Time

First, the maximum singular value of the sensitivity $\bar{\sigma}$ and the corresponding frequency $\omega(\bar{\sigma})$ of all three multivariable control algorithms is investigated. The results for a purely decentralized control are given in Fig.6.11. Since the controller is not subject to detuning, this result is valid for all h_{ij} .

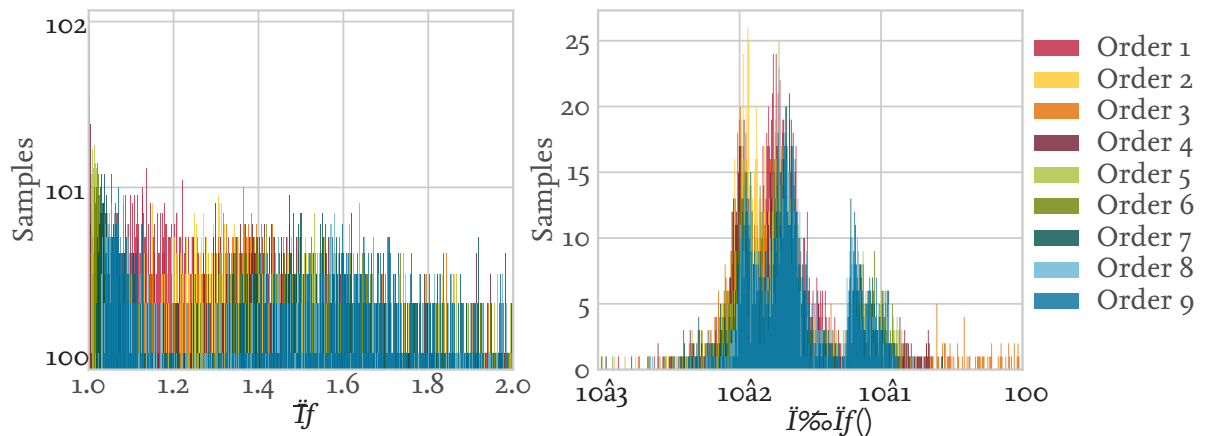


Figure 6.11: Results of the robustness study,maximum singular values and corresponding frequency for decentralized control

It can be observed that the results with regard to the magnitude of the maximum singular value range widely in the interval. The corresponding frequencies show a concentration between the values of $\omega(\bar{\sigma}) \in [10^{-2}, 10^{-1}]$, where they are most likely to occur around $\omega(\bar{\sigma}) \approx 2 \cdot 10^{-2}$.

In Fig.6.12 the results for a static decoupled system, as proposed by Aström, are shown with a maximum interaction of $h_{ij,Max} \leq 0.5$.

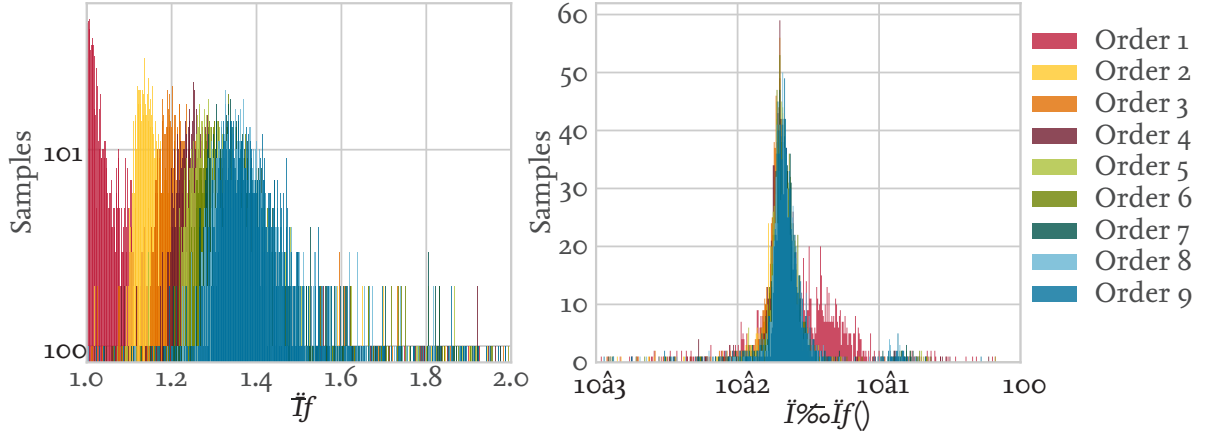


Figure 6.12: Results of the robustness study, maximum singular values and corresponding frequency for static decoupled control, $h_{ij,Max} \leq 0.5$

The results show a much more concentrated distribution over the samples. Most maximum singular values are within $\bar{\sigma} \leq 1.4$, while the corresponding frequency is highly concentrated around $\omega(\bar{\sigma}) \approx 1.5 \cdot 10^{-2}$. In comparison to purely decentralized control, the controller tends to reduce the uncertainty of the systems characteristics with respect to robustness.

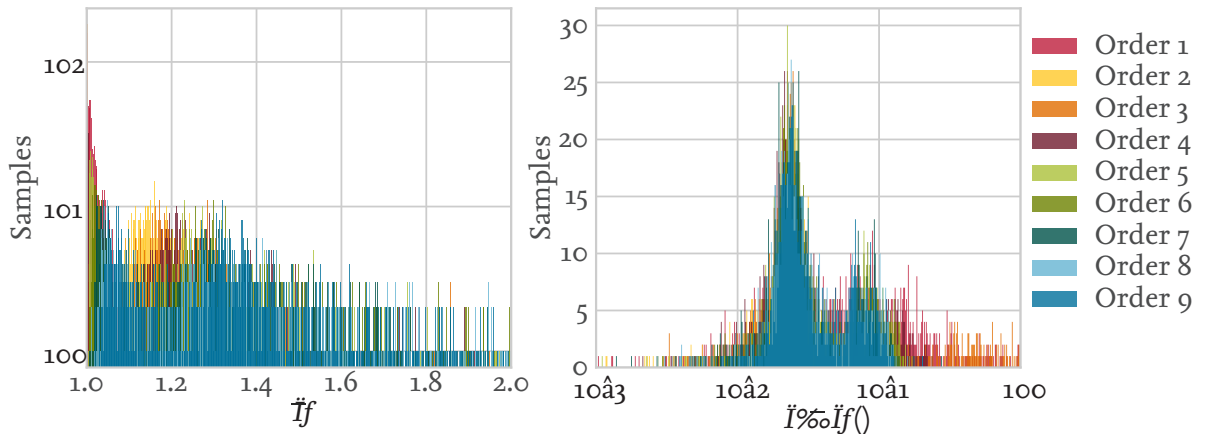


Figure 6.13: Results of the robustness study, maximum singular values and corresponding frequency for R2D2 control, $h_{ij,Max} \leq 0.5$

In Fig.6.13 the same sample systems are controlled using the developed robust routine. It can be seen that the maximum singular values of the sensitivity function are distributed more widely with respect to the static decoupled system but more precise than using just decentralized control. This observation is also visible in the distribution of the occurrence frequency of the maximum singular value.

These conclusions can be confirmed by using the cumulative density functions off the three methods, shown in Fig. 6.14 below. Here, the relative distribution of all samples over the maximum singular values is shown. The green area shows the limits which hold 80% of all sample systems.

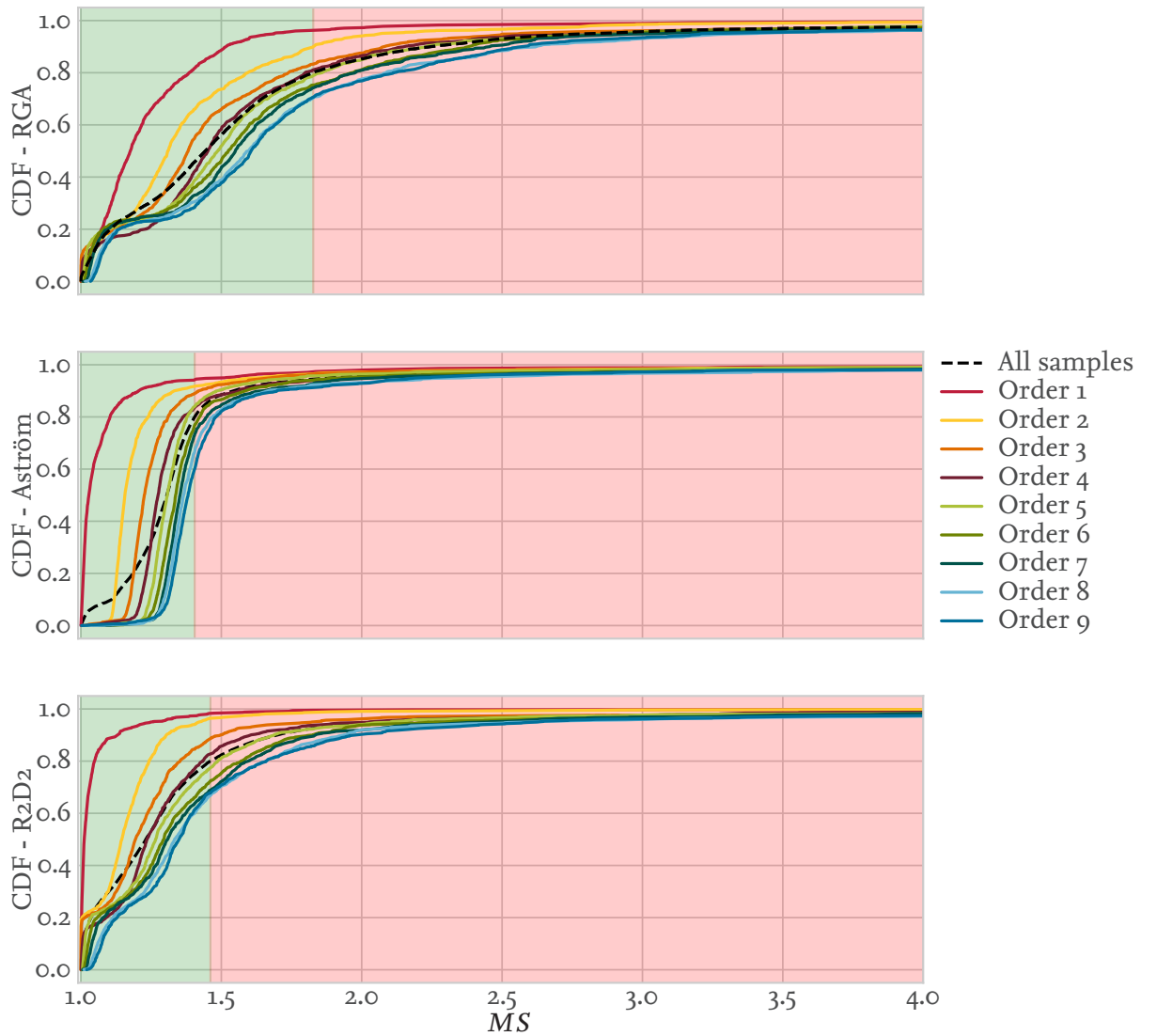


Figure 6.14: Results of the robustness study,maximum singular values cumulative densities of all methods,
 $h_{ij,Max} \leq 0.5$

From Fig.6.14 it can be seen that the static decoupling improves the robustness of the systems

drastically with respect to purely decentralized control. Likewise the distribution of the sensitivity is less fuzzy, but instead shows clear limits per order. The proposed method is less precise in the distribution of the individual orders, but nonetheless show a major improvement with respect to the decentralized controller design based on RGA. This is clearly visible by examining the first order sample systems. The decentralized controller maximum singular value are within the range of $\bar{\sigma} \in [1.0, 2.25]$, while R2D2 limits the gain to $\bar{\sigma} \in [1.0, 1.65]$. Attenuated behaviors can be observed for all orders. Another remark with respect to the relative distribution of the maximum singular value can be made comparing decentralized, static and simple decoupled control. The relative density of systems around $\bar{\sigma} \approx 1$ is much higher for the purely RGA controller and the corresponding controller extended by a compensation. Nearly 20% of all systems are concentrated at the beginning of scale, hence much more robustness is given.

To investigate the effect of detuning, the cumulative density functions detuned for a maximum interaction of $h_{ij,Max} \leq 0.1$ are shown in Fig.6.16. The effect on the static decoupled systems is obvious, tightening the bounds of the maximum singular values. The controller using a simple decoupler is much less. This relies mostly on the constant sum time for all processes, which results in small differences between the average residence times of the coupled systems. Hence, the dynamic difference between the processes is small and hence not detuned. Therefore, only the maximum singular values of the static decoupled system are shown in Fig.6.15, where the effect is also visible.

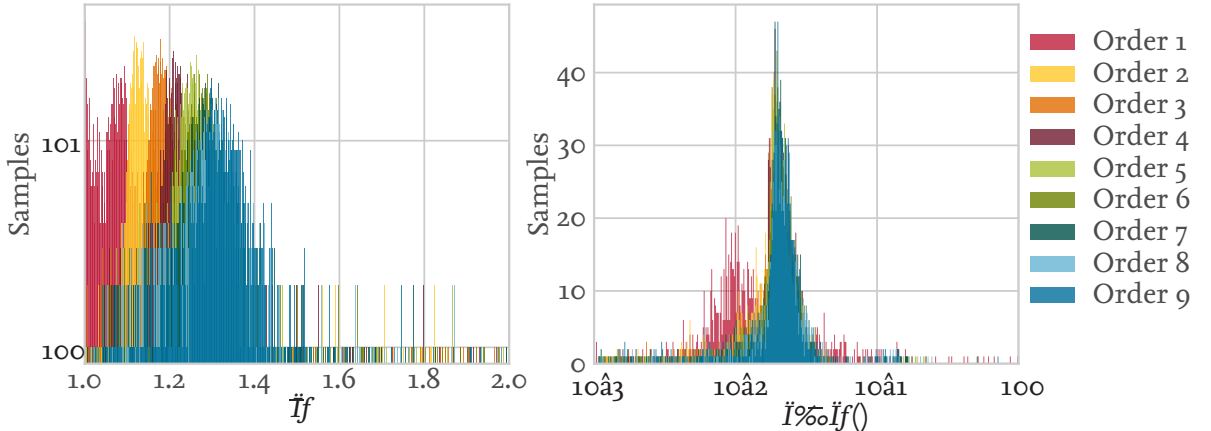


Figure 6.15: Results of the robustness study, maximum singular values and corresponding frequency for static decoupled control, $h_{ij,Max} \leq 0.1$

From Fig.6.15 the effect on the corresponding frequencies is also visible. The frequencies tend to get smaller with detuning, which can be concluded from the connection between the sensitivity and complementary sensitivity function. Hence, if the controller is detuned, the bandwidth of the tracking performance is reduced and likewise the maximum singular value is located at lower frequencies.

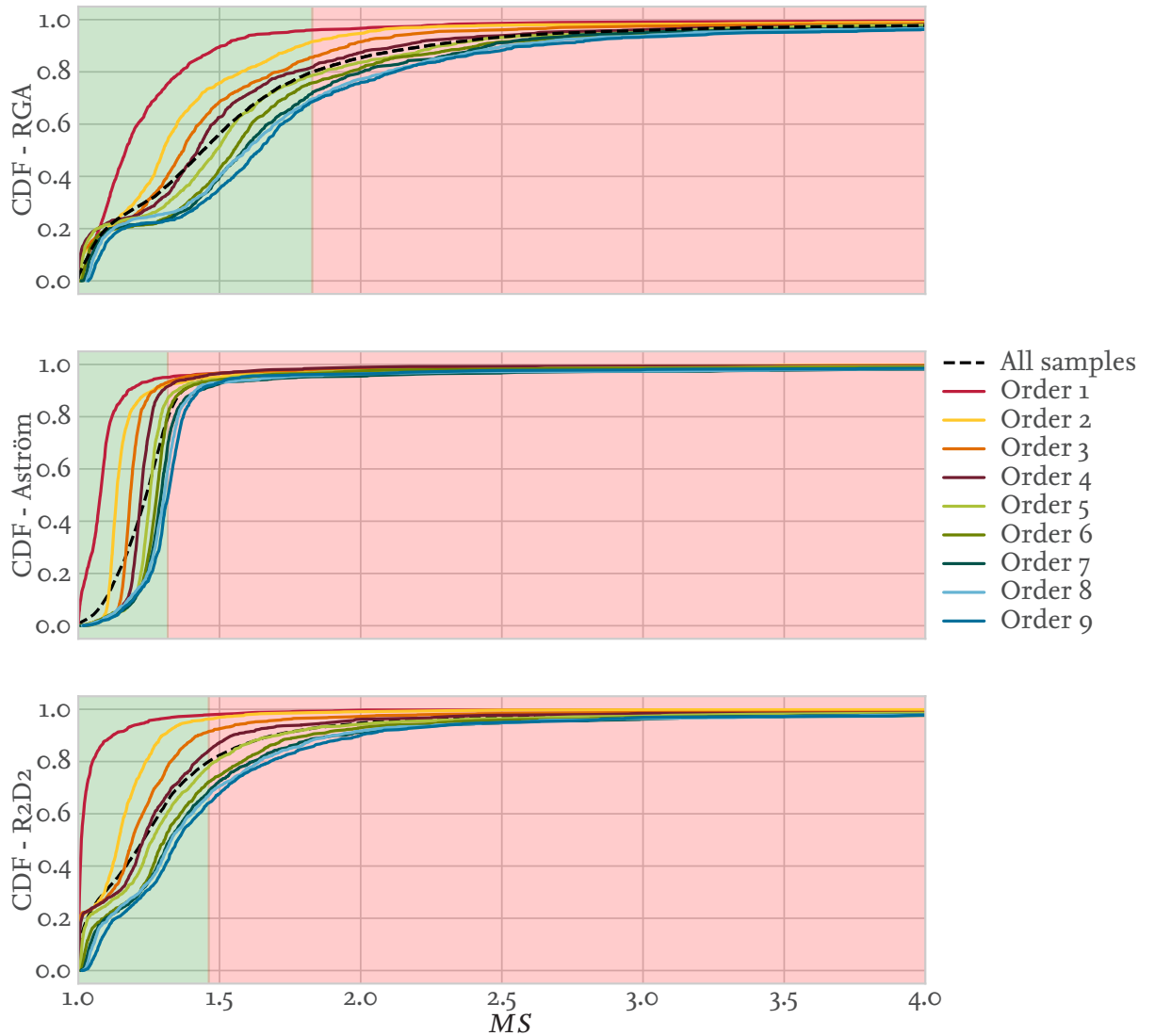


Figure 6.16: Results of the robustness study, maximum singular values cumulative densities of all methods,
 $h_{ij,Max} \leq 0.1$

6.3.2 Random Pole Multiplicity

The simulation study has also been performed with a random sum time constant with a pole multiplicity. The maximum singular values and the corresponding frequencies of a decentralized control are shown in Fig.6.17. Like earlier, the maximum magnitude of the sensitivity function is distributed highly over the sample systems. The frequency $\omega_{\bar{\sigma}}$ has significant peaks, the first at 10^{-2} for first order time delay systems. The other peaks occur at $9 \cdot 10^{-3}$, $1.5 \cdot 10^{-2}$ and $8 \cdot 10^{-2}$ and are distributed more evenly.

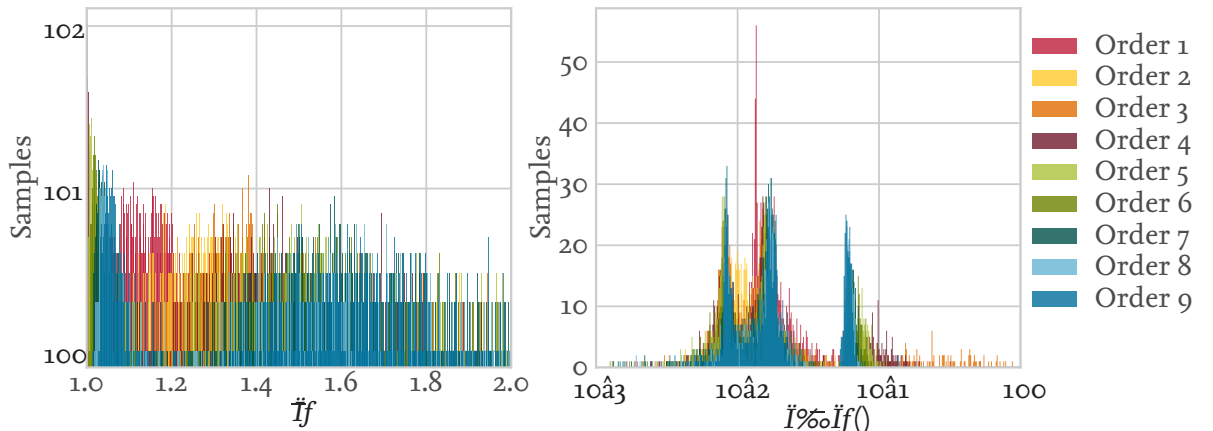


Figure 6.17: Results of the robustness study,maximum singular values and corresponding frequency for decentralized control, $h_{ij,Max} \leq 0.5$

The corresponding systems characteristics with a static decoupler are shown in Fig.6.18. The distribution of $\bar{\sigma}$ is dense in the range of $\bar{\sigma} \in [1.0, 1.4]$. The corresponding frequencies show a dominant peak around $1.4 \cdot 10^{-2}$ and for FOTD systems a peak at 10^{-2} . Hence, a more precise bandwidth is given while concentrating the maximum singular values within denser limits.

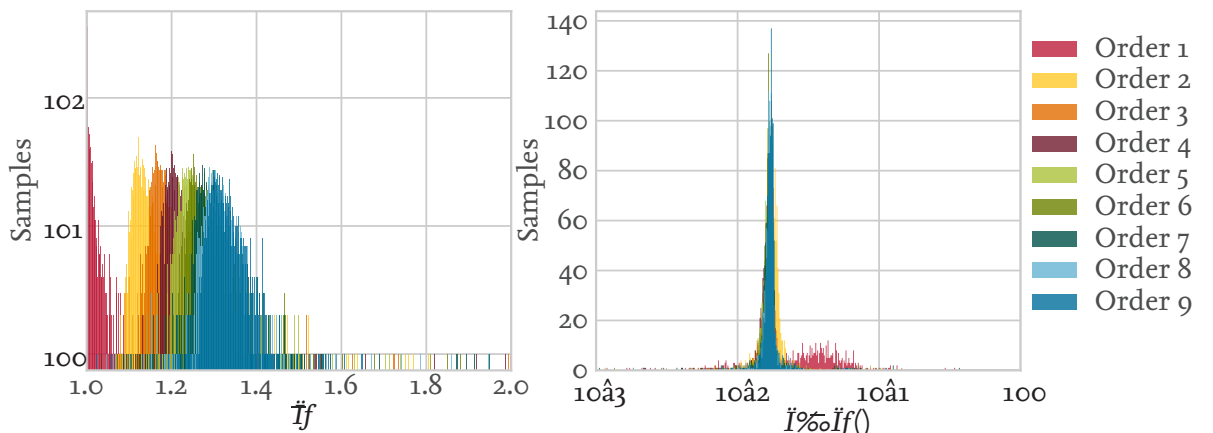


Figure 6.18: Results of the robustness study,maximum singular values and corresponding frequency for static decoupled control, $h_{ij,Max} \leq 0.5$

For the sample systems controlled with a simple decoupler show a less precise distribution of the maximum singular values, but nonetheless a better performance than the decentralized control. The results are shown in Fig.6.19. The corresponding frequencies that nearly all systems have $\omega_{\bar{\sigma}} \geq 1.3 \cdot 10^{-2}$, the location of the dominant peak. Another peak, which is less dense, occurs at $9.0 \cdot 10^{-1}$. Hence, the system concentrates the maximum singular value within stricter bounds and at higher frequencies.

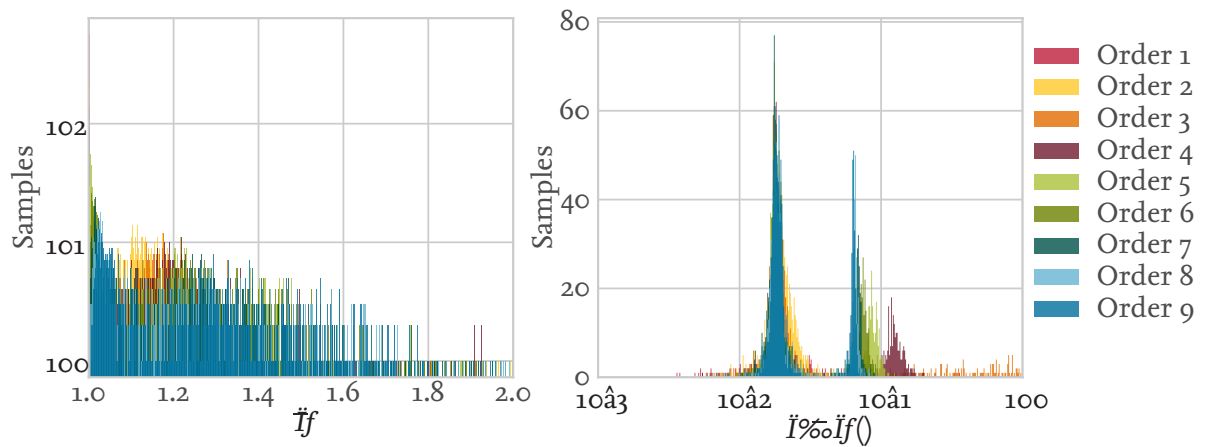


Figure 6.19: Results of the robustness study, maximum singular values and corresponding frequency for simple decoupled control, $h_{ij,Max} \leq 0.5$

The results can be also shown through the cumulative density functions, shown in Fig.6.20 below. Like earlier, the green area marks 80% of all sample systems. It is obvious that R2D2 is much more robust than the purely decentralized control but less precise in terms of the distribution of the samples than a static decoupled system.

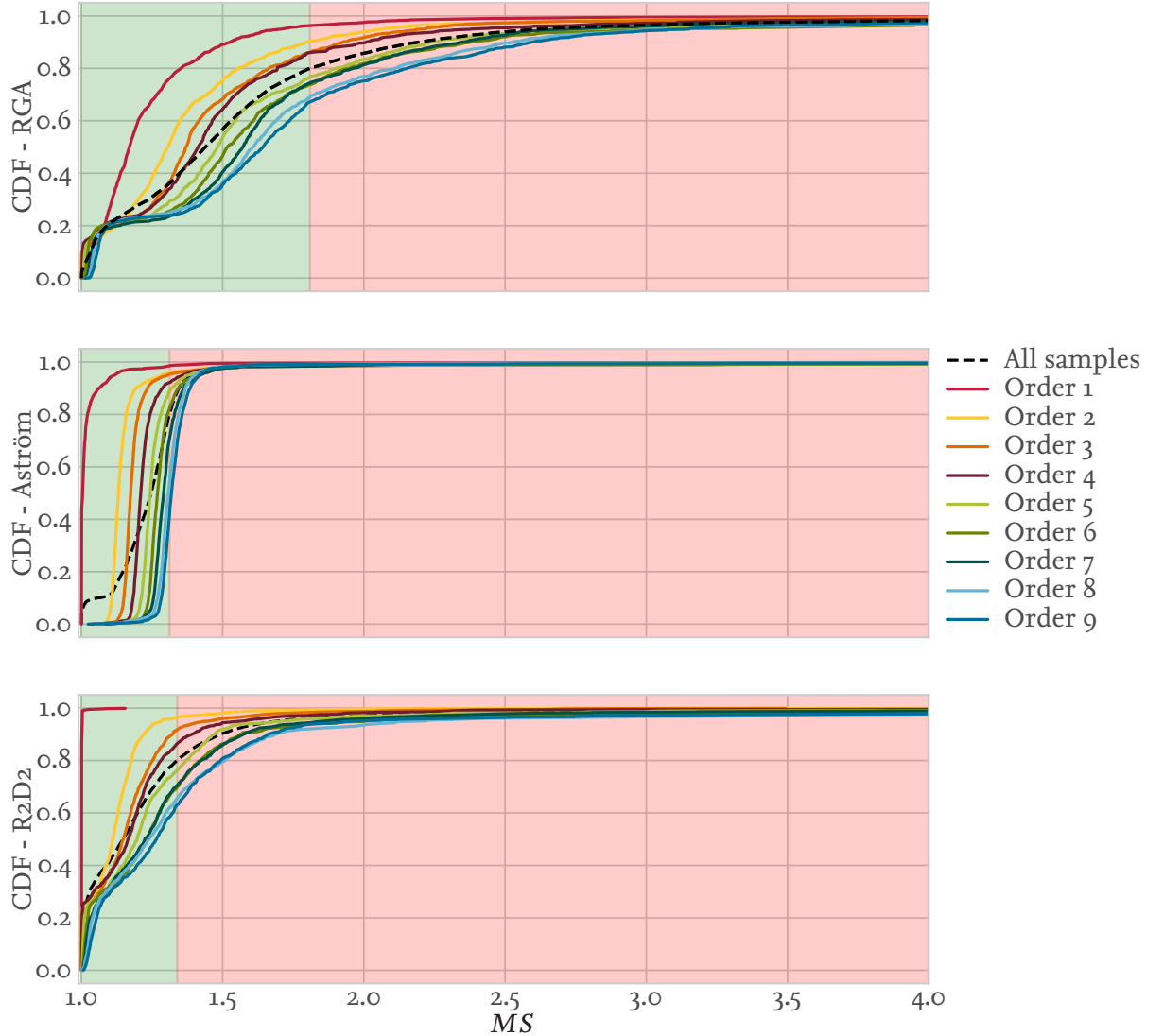


Figure 6.20: Results of the robustness study, maximum singular values cumulative densities of all methods,
 $h_{ij,Max} \leq 0.5$

Next, the effects of the detuning with a maximum allowed interaction of $h_{ij,Max} \leq 0.1$ are discussed. Since the dynamics of the interacting transfer functions differ, both the static decoupled system described by Aström and R2D2 are affected. Fig.6.21 show the maximum singular values and the corresponding frequencies for a static decoupled and detuned system. In comparison to Fig.6.18 the frequency spectrum is slightly more balanced around the peak at $1.3 \cdot 10^{-2}$. Hence, the

minimization of interaction leads to a limited bandwidth of the tracking performance as discussed earlier.

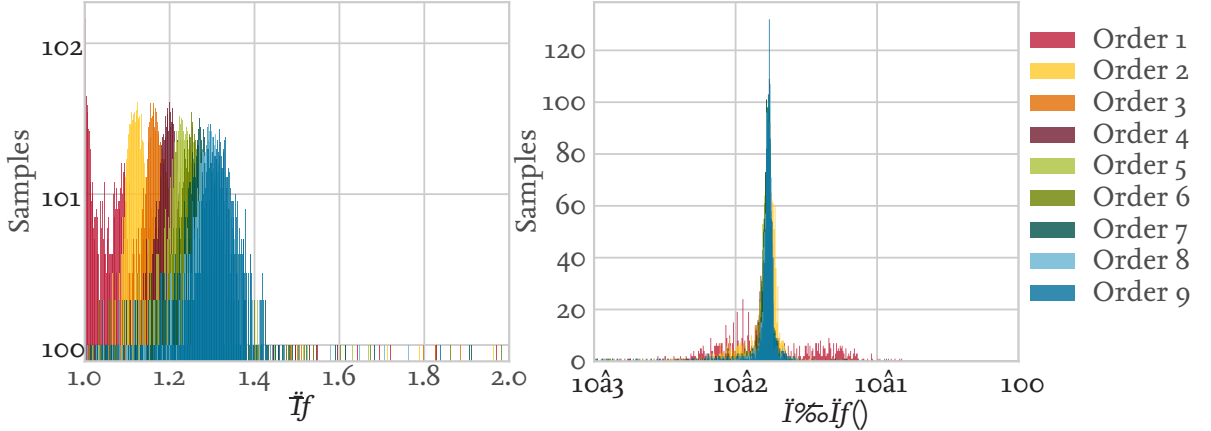


Figure 6.21: Results of the robustness study, maximum singular values and corresponding frequency for static decoupled control, $h_{ij,Max} \leq 0.1$

In Fig.6.22 the characteristics of the sensitivity function for the sample systems with a detuned simple decoupler are shown. Like above, the frequency spectrum is shifted to lower frequencies and is much less concentrated around the appearing peaks.

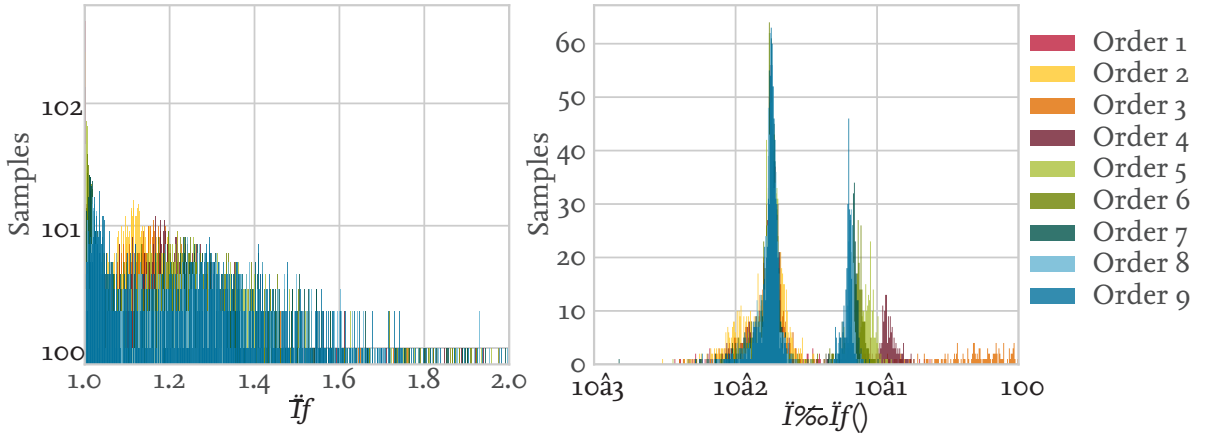


Figure 6.22: Results of the robustness study, maximum singular values and corresponding frequency for simple decoupled control, $h_{ij,Max} \leq 0.1$

The cumulative density function for all processes have been plotted in Fig.6.23. It can be seen that the influence of detuning is much more significant to the static decoupled system, while its influence within R2D2 is only of lesser importance to the maximum singular value distribution. Like before, the distribution of $\bar{\sigma} \approx 1$ is much higher for the controller given by the RGA and R2D2.

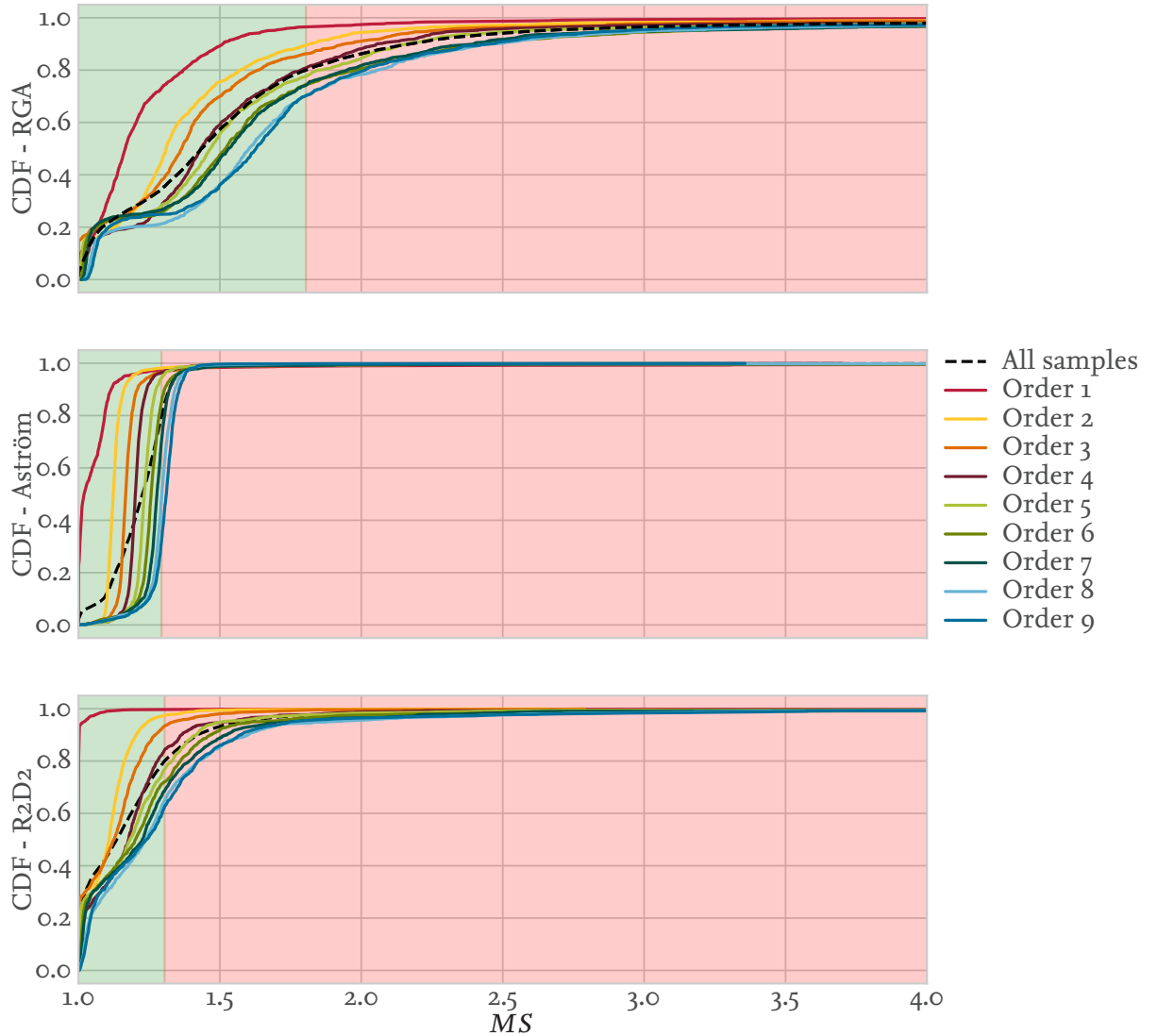


Figure 6.23: Results of the robustness study, maximum singular values cumulative densities of all methods,
 $h_{ij,Max} \leq 0.1$

6.4 Review

It could be seen that the identification process in addition to the AMIGO tuning rules gives good results. The correlation of the models maximum sensitivity and its corresponding sensitivity of the real system is strongly correlated. Hence, the robustness of the algorithm for the class of systems with the anticipated behavior could be shown.

The multivariable robustness study show a significant influence with regards to the bounds of the maximum singular values. While a simple decentralized controller shows a strong usually a strong concentration around $\bar{\sigma} \approx 1.0$ it also spreads widely to much higher values.

The controller designed with a static decoupler and an approximated FOTD from a linear combination of two FOTD tend to give a more stricter bound within the maximal magnitude of the sensitivity function. But the values are usually dense around the middle of the spectrum.

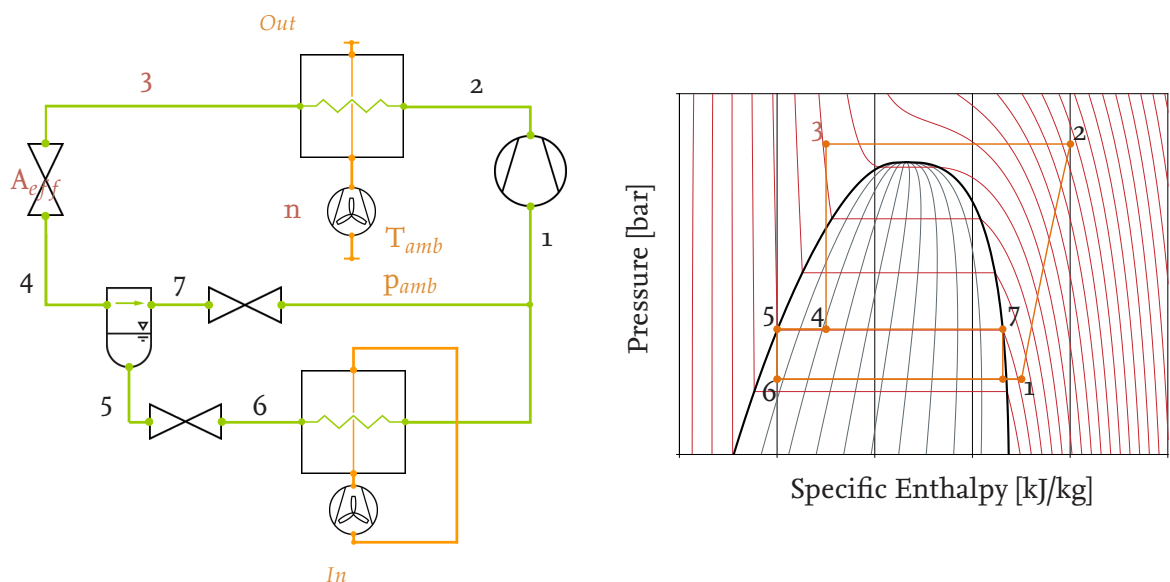
The robust routine for decoupled detuning combines both aspects. Hence, a strong concentration around the lower bound of the maximum singular value is given in addition to much less higher bound. Hence, both performance and robustness can be assumed.

7 Application to Physical Process Models

7.1 Process Description and Problem Statement

The aim of engineering thermodynamics is - as stated earlier in Chap. 1 - to understand and optimize the behaviour of technical systems used for energy transformation and transportation. Hence, a connection to the field of optimal control is a logical extension to maximize the efficiency. As described in sec. ?? the systems states are general interconnected by both physical components and physical phenomena. In the following section the coupling due to physical phenomena will be investigated.

The process at hand is an anticlockwise refrigeration process, shown in Fig.7.1 in technical schematics and in Fig.7.1 in the pressure-specific enthalpy diagram. The model used for simulation in the scope of this work was provided and consists of a simple valve, according to Eq.7.6, heat exchanger model fitted to experimentation data and a compressor modeled with a linear efficiency.



Starting at the inlet of the compressor, Point 1, mechanical energy is given into the refrigerant increasing pressure and specific enthalpy in an isentropic process. Then, energy is subtracted isobaric in form of heat between the point 2 and 3 via a heat exchanger, called gascooler. Afterwards, the pressure drops to via a throttle valve from point 3 to point 4 isothermal, where it reaches a settling tank. There, the fluid phase is separated from the gas phase. The purely gas phase is transported to

the inlet of the compressor via another isothermal throttle between point 7 and 1. The pressure of the liquid phase is also reduced via a throttle between point 5 and 6, before another heat exchanger adds energy isobaric to the system.

The problem description from a control perspective involves the control of five variables, the high pressure, medium pressure, the overheating and undercooling. In the scope of this work, the control of high pressure and undercooling is investigated. This is conducted via the revolutions of the fan to control the difference in temperature between point 2 and 3 and the effective area of the valve, which controls the pressure drop between point 3 and 4.

At first, the theoretical properties of the individual parts are investigated. The process can be divided in three basic processes:

- Isobaric process with heat supply
- Adiabatic isenthalpic process
- Isentropic process with exchange of (mechanical) work

These processes can be characterized using the First Law of Thermodynamics in differential form, see e.g. [24, p.25]:

$$\begin{aligned} du &= d(h - pv) \\ &= dh - vdp - pdv \\ &= \delta q + \delta w_{diss} - pdv \end{aligned} \tag{7.1}$$

Which states that the change in inner energy $u \in \mathbb{R}$ is equal to the sum of heat $\delta Q \in \mathbb{R}$ and dissipated work $\delta w_{diss} \in \mathbb{R}$ minus the pressure-volume work, depending on the pressure $p \in \mathbb{R}^+$ times the change in specific volume $v \in \mathbb{R}^+$. The internal energy can be related to the specific enthalpy $h = u + pv \in \mathbb{R}$.

The Second Law of Thermodynamics as formulated by Gibbs [22, p.59] is given by:

$$\begin{aligned} Tds &= du + pdv \\ &= d(h - pv) + pdv \\ &= dh - vdp \end{aligned} \tag{7.2}$$

Defining two independent to be state variables the specific volume v and temperature T and substitute Eq.7.1 in Eq.7.2:

$$\begin{aligned} Tds &= du + pdv \\ &= \delta q + \delta w_{diss} \end{aligned} \tag{7.3}$$

Since the total differential of the inner energy is given by

$$du = \left(\frac{\partial u}{\partial T} \right)_v dT + \left(\frac{\partial u}{\partial v} \right)_T dv \quad (7.4)$$

Substitute Eq. 7.4 in 7.3 while using the definition for the specific heat capacity at constant volume $c_V = \left(\frac{\partial u}{\partial T} \right)_v \in \mathbb{R}^+$ holds:

$$\begin{aligned} Tds &= \left(\frac{\partial u}{\partial T} \right)_v dT + \left(\frac{\partial u}{\partial v} \right)_T dv + pdv \\ &= c_V dT + \left[p + \left(\frac{\partial u}{\partial v} \right)_T \right] dv \end{aligned}$$

Using the relation [22, p.375] $T \left(\frac{\partial s}{\partial v} \right)_T = \left(\frac{\partial u}{\partial v} \right)_T + p$ and the Maxwell Relation $\left(\frac{\partial s}{\partial v} \right)_T = \left(\frac{\partial p}{\partial T} \right)_v = \frac{\beta}{\kappa}$ the equation becomes:

$$\begin{aligned} Tds &= \left(\frac{\partial u}{\partial T} \right)_v dT + \left(\frac{\partial u}{\partial v} \right)_T dv + pdv \\ \delta q &= c_V dT + T \frac{\beta}{\kappa} dv \end{aligned} \quad (7.5)$$

The coefficient of thermal expansion at constant pressure $\beta \in \mathbb{R}$ is defined by $\frac{1}{v} \left(\frac{\partial v}{\partial T} \right)_p = \beta$ and the compressibility $\kappa = \left(\frac{\partial v}{\partial p} \right)_T \in \mathbb{R}^+$ substitute the differential change of pressure due to temperature at constant volume via the chain rule.

Eq. 7.5 states that the exchange of heat in the isobaric process results in a change of specific volume and temperature.

The massflow $\frac{dm}{dt} = \dot{m} \in \mathbb{R}$ from A to B through a throttle can be described by a function of the density $\rho = \frac{1}{v} \in \mathbb{R}^+$, the effective area $A_{eff} \in \mathbb{R}^+$ and the difference in pressure

$$\dot{m} = A_{eff} \sqrt{2\rho_A (p_A - p_B)} \quad (7.6)$$

which directly relates the difference pressure $p_A - p_B = \Delta p > 0$ to the exchange of heat. Assume a constant mass flow, a constant effective Area and a constant pressure niveau p_B due to perfect controller of the system, the energetic coupling between fan and pressure can be seen. If heat is added before A as described by Eq. 7.5 the Temperature in A will be influenced as well the pressure due to the change in the specific volume and therefore the density via Eq.7.6.

The isenthalpic, adiabat throttling process can be described by the Joule-Thomson Coefficient [22, p.387]. The equation relates the change in temperature and pressure to each other via

$$\begin{aligned} \left(\frac{\partial T}{\partial p} \right)_h &= -\frac{1}{c_p} \left(\frac{\partial h}{\partial p} \right)_T \\ &= \frac{v}{c_p} (T\beta - 1) \end{aligned} \quad (7.7)$$

Where $c_p = \left(\frac{\partial h}{\partial T} \right)_p \in \mathbb{R}^+$ is the specific heat at constant pressure which relates the change in entropy due to a change in temperature. Eq. 7.7 and Eq. 7.6 relate the change in pressure via variation of the effective Area to the change in temperature.

Eq. 7.5, 7.6 and 7.7 show the thermodynamic coupling of the system. They are highly nonlinear and give an ideal coupling for the quasi stationary processes and the chosen states pressure and temperature. Since both couplings take effect at the same time, a reasonable estimation of the process trajectory is difficult.

An important fact is that none of the equations above depend explicitly on the time. Rather, all coefficients above are functions of the thermodynamic states p, v, T, s which are depending on time. Assuming quasi stationary behavior of the system for every coefficient $c \in \{\beta, \kappa, c_v, c_p\}$ can be related to the static gain of the couplings.

7.2 Identification of the FOTD model

In the following section, the identification process is laid out and investigated within the simulation model. At first, some basics of the behavior shall be discussed. In Sec.7.1 the thermodynamic properties of the gain has been investigated. The relations established before can be qualitatively extended to the whole technical system including the valve and the fan.

To estimate the effects of a change in input, the energy of Point 3 is evaluated. Assuming that the initial change in input result in a change of the internal energy at the outlet of the gascooler, the energy conservation can be formulated as:

$$\begin{aligned} \int \left(\dot{m}c_p T_3 + \frac{\dot{m}}{\rho} p_3 \right) dt &= \int \left(\dot{m}c_p T_{3'} + \frac{\dot{m}}{\rho} p_{3'} \right) dt \\ \rho c_p (T_3 - T_{3'}) + p_3 - p_{3'} &= 0 \\ \rho c_p \Delta T_u + \Delta p_u &= 0 \end{aligned}$$

From which can be concluded that the pressure and temperature change due to an external input $\Delta p_u, \Delta T_u \in \mathbb{R}$ are of opposite sign.

Increasing the revolution speed of a fan will increase the amount of heat transported out of the systems boundaries. Hence, the gain will be negative, since the temperature will decrease. If the temperature will decrease $\Delta T_u > 0$ and therefore the pressure at Point 3 will decrease to ensure that

the energy of the system is conserved by $\Delta p_u < 0$.

Likewise, if the effective area of the throttle is increased, the pressure at the outlet of the gascooler will decrease, meaning $\Delta p_u > 0$. Hence, $\Delta T_u < 0$, meaning that the temperature after the excitation of the valve must be greater than before.

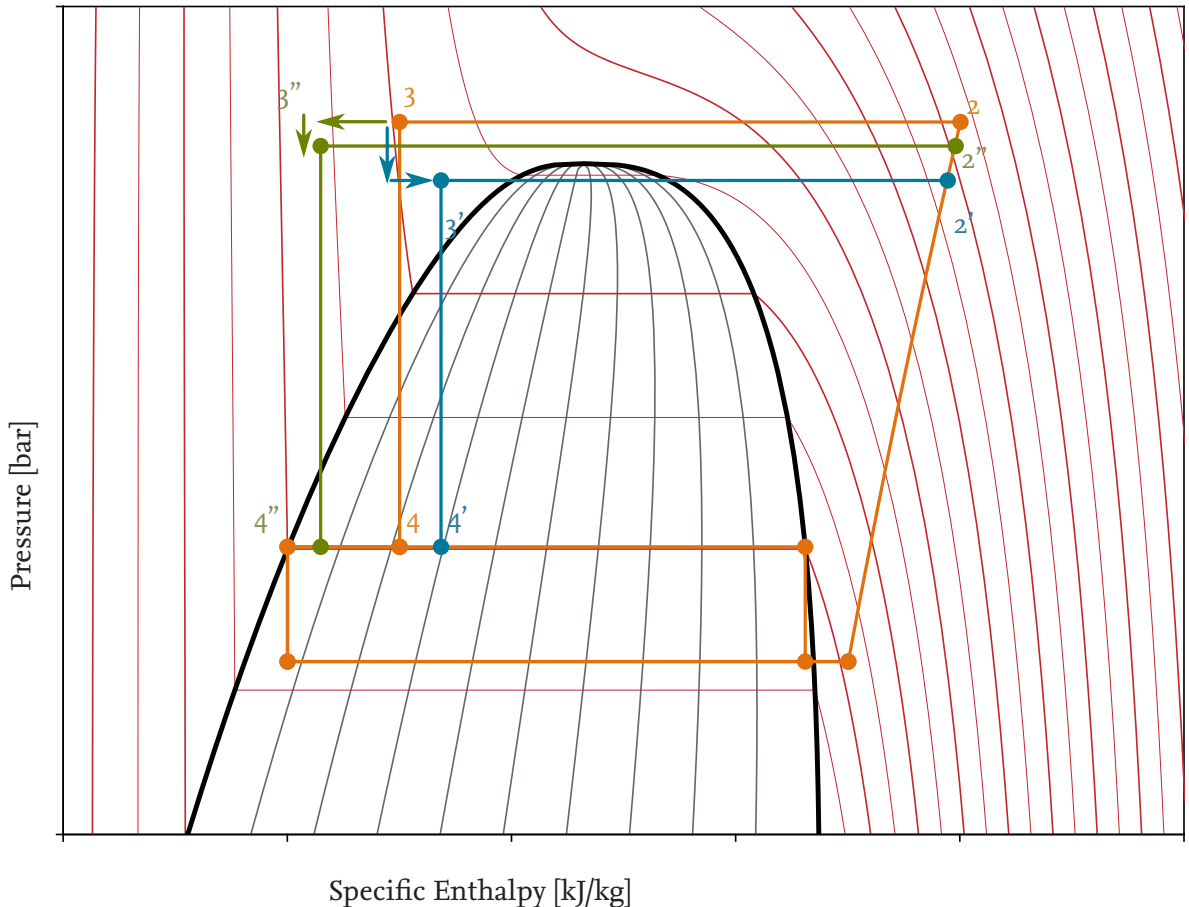


Figure 7.1: Pressure over specific enthalpy diagram of the refrigeration cycle, Effects of an increase in A_{eff} (blue) and n (green)

This is illustrated in Fig. 7.1, where both processes are given qualitatively. In terms of the steady state gain of the transfer function matrix, this can be written as:

$$\text{sign} (G_0) = \begin{bmatrix} -1 & +1 \\ -1 & -1 \end{bmatrix}$$

This effect can be seen in Fig. 7.2, where a simulation of the system with an identification has been performed. Both the rotational speed of the fan and the effective area have been decreased to avoid crossing the saturated liquid line. The full line shows the impact of a change in the effective area on both the pressure and the temperature while the dashed line represents the influence of a change

in the rotational speed of the fan. The identification has been performed at a ambient temperature $T_{amb} = 295K$ with a heat of $\dot{Q}_{In} = -60kW$ applied to the system. This results at an optimal working point of $(p_2, T_2) = (76.60bar, 298.00K)$ which is calculated using an formula based on optimization studies.

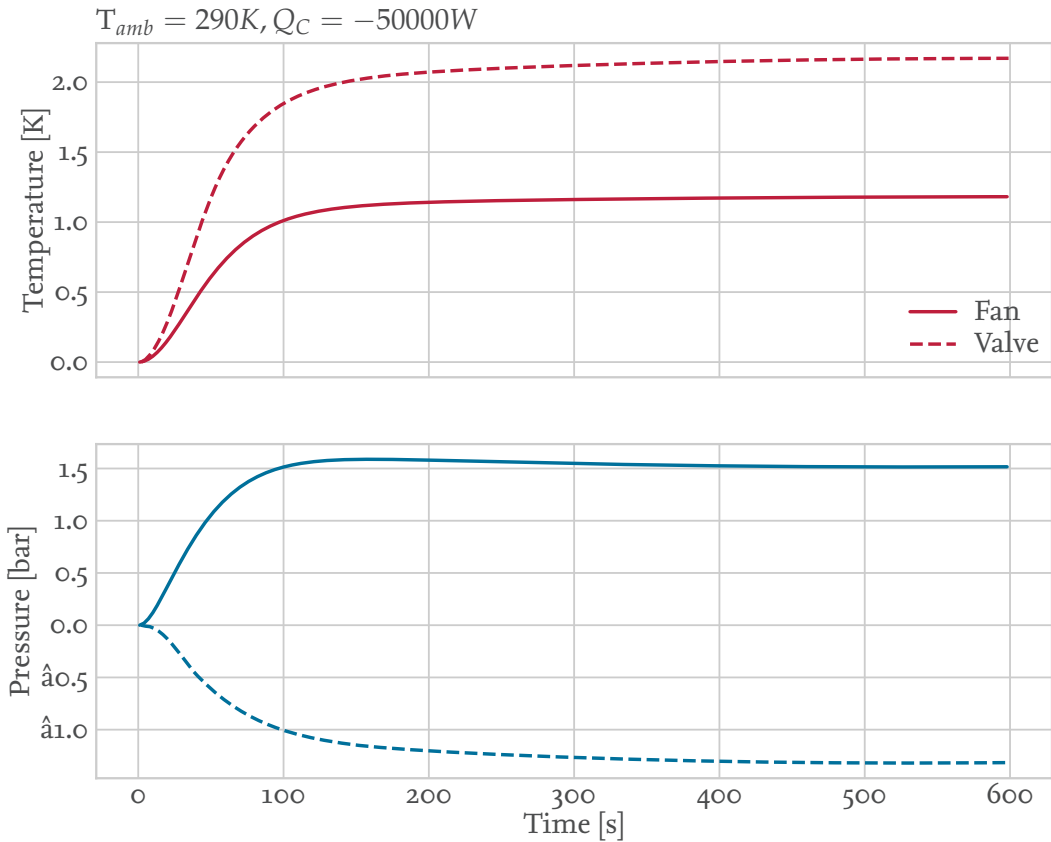


Figure 7.2: Example of the influence of scaled input steps within the simulation model

It can be seen that the system is monotonic increasing and shows a very similar behavior to a higher order system. The system is identified using the area approach described in Ch.3. The transfer function matrix consisting of FOTD models is given by :

$$\hat{\mathbf{G}} = \begin{bmatrix} \frac{-2.363}{45.943s+1} e^{-17.381s} & \frac{7.236}{49.723s+1} e^{-14.230s} \\ \frac{-3.177}{26.225s+1} e^{-15.645s} & \frac{-4.399}{72.381s+1} e^{-7.953s} \end{bmatrix}$$

However, these results can vary depending on the operating conditions, e.g. ambient temperature, the systems state, e.g. pressure and temperature at the outlet of the gascooler, and the parameter like piping length, compressor model etc.. Parameter studies have been performed to estimate the effect of dominant parameters of the system, e.g. the valve dynamics, fan dynamics and number of tubes of the heat exchanger. The evaluation of all results of this study would go beyond the scope

of this work, but for reasons of completeness the influence of the cooling capacity and the ambient temperature on the FOTD parameter is shown in Fig. 7.3.

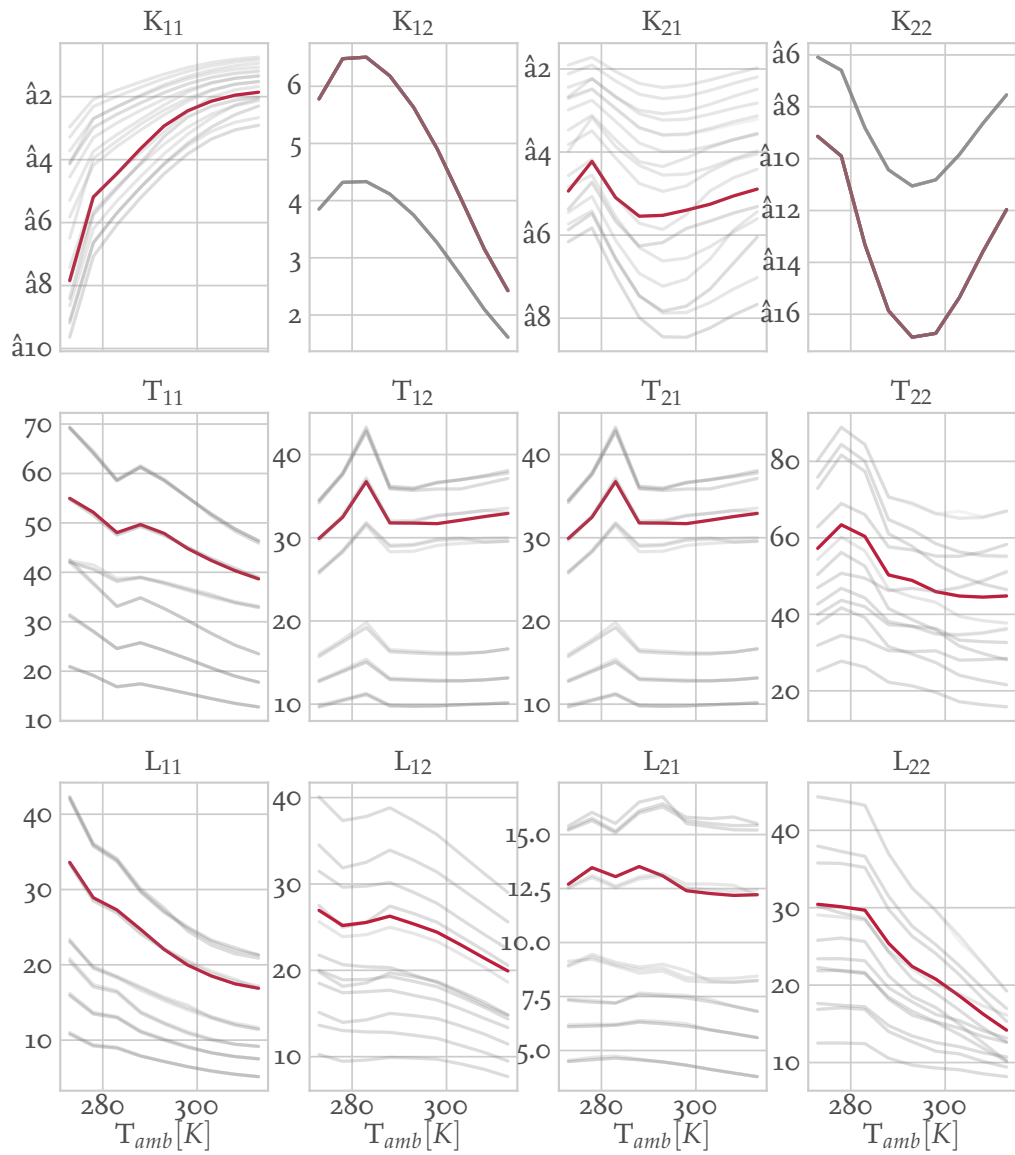


Figure 7.3: Variation of the FOTD model parameter due to simulation parameter and operating conditions

It can be noticed that while the gain of the transfer functions connected to the fan are sensitive to changes in the model parameter, the gain of transfer functions related to the valve are only different in an offset. K_{11} , the gain of the fan to the temperature, is decreasing over the ambient temperature.

If the temperature difference between point 2 and 3 is large, smaller changes will occur because most of the heat is already transported out of the system. If the difference is small, large variations of the rotational speed will significantly increase the heat transported out of the system. Therefore the gain is large at lower ambient temperatures which correspond to lower pressure levels, where the distance between isotherms is large. The same reasoning can be used to explain the decrease of the gain from fan to pressure K_{21} where an appropriate scaling with the nonlinear material values has to be taken into account.

Likewise the transfer function gain K_{22} is most likely depending on variations of the density and the mass flow through the valve, hence the nearly quadratic form and a variation given only by an offset. The same can be said for the gain K_{12} , also scaled with the nonlinear material values. An interesting property is given in form of the lags T_{12}, T_{21} which are identical for the marked example scenario. Hence, the time dependent behavior of the processes is most likely governed by its physical properties and not by the technical components. With the difference in delay, $L_{12} \geq L_{21}$, the assumption that the delay is strongly dependent on the mass flow and hence the fluid flow direction is obvious.

To estimate the error $\Delta_D \in \mathbb{C}$ of the simple decoupling, given in terms of Eq.4.40, the steady state of the system is evaluated for all parameter values and shown in Fig.7.4. It can be seen that the error is within a certain limits and does not exceed 0.68. Also, all variations of the system show a similar behavior, only scaled for ambient temperatures $T_{amb} \geq 283$ K. Hence, it is most likely that the error is strongly dominated by the transfer functions connected to the valve. The error can be also used to indicate the usefulness of deriving a model for the combined transfer functions $g_{ii}^* = g_{ii} + \sum_{j=1}^{n_y} \Sigma_{ji} g_{ij}$, which is obviously useful for higher ambient temperatures.

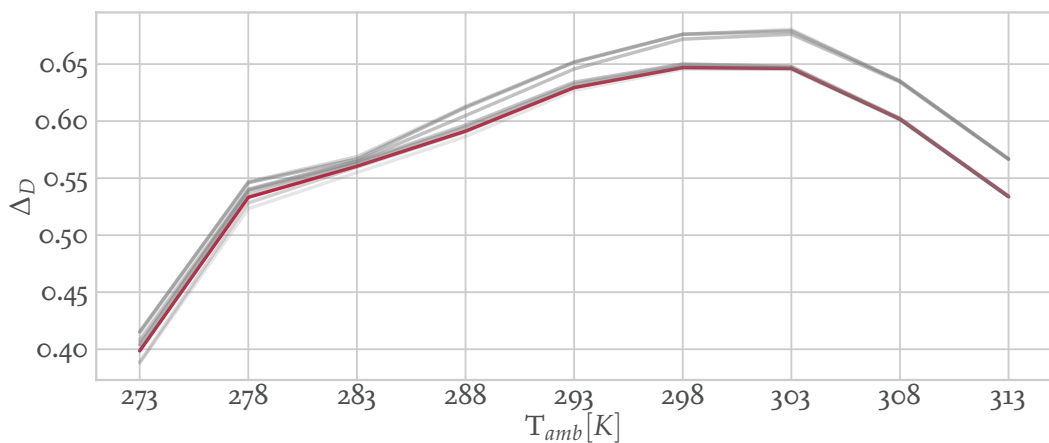


Figure 7.4: Error within the model use of the main diagonal within R2D2, steady state of the system

Likewise, the relative magnitude of the transfer functions, $E \in \mathbb{C}^{n_y \times n_y}$ as given in Eq.4.42, can be calculated. Fig.7.5 shows the determinant of the relative magnitudes for the decentralized controller and the added simple decoupler, which indicates the usefulness with respect to tracking behavior

even though an error is dynamics is given.

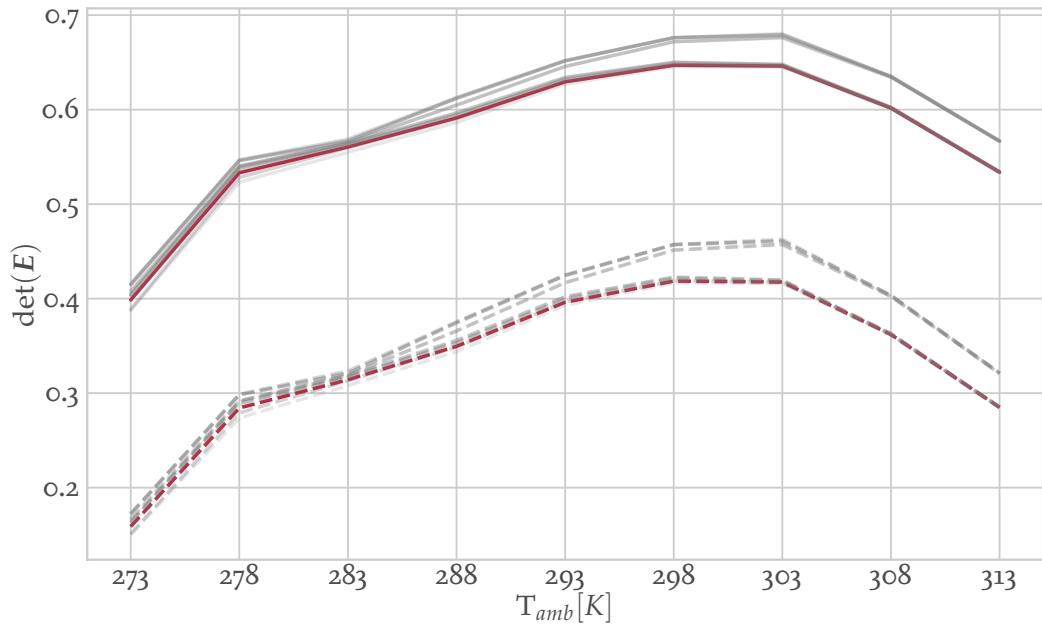


Figure 7.5: Relative magnitude within the model for decentralized control (full) and simple decoupling (dashed), steady state of the system

It is also important to notice that while in theory only the physical effects are measured, in practice effects of all other controllers will be measured and taken into account. Hence, not only the influence of the valve to the temperature of point 2 is measured but the effect of the valve on point 2 and all closed loops of the system, meaning the loops for controlling points (1, 3, 4, 5, 6, 7).

7.3 Closed Loop Results

In the following section, some results of the autotuning methods are shown. The simulation has used a very robust controller to derive a steady state, where the controller was switched off and the experiment for identification has been performed. Afterwards, the model with the calculated controller parameters has been started and evaluated with respect to disturbance rejection and tracking performance. A static decoupled system is not explicitly given, since the simulation was not been able to start in all cases with the controller at hand.

Three cases are presented and the closed loop behavior with respect to tracking performance and disturbance rejection is shown. At first, the identification example as shown in Fig.7.2 is examined. The process operates with $T_{amb} = 290K$, $Q_C = -50kW$. In Fig.7.6 an input disturbance is simulated with a scaled step function acting on the effective Area at 6000 s and likewise at 10000 s for the rotational speed.

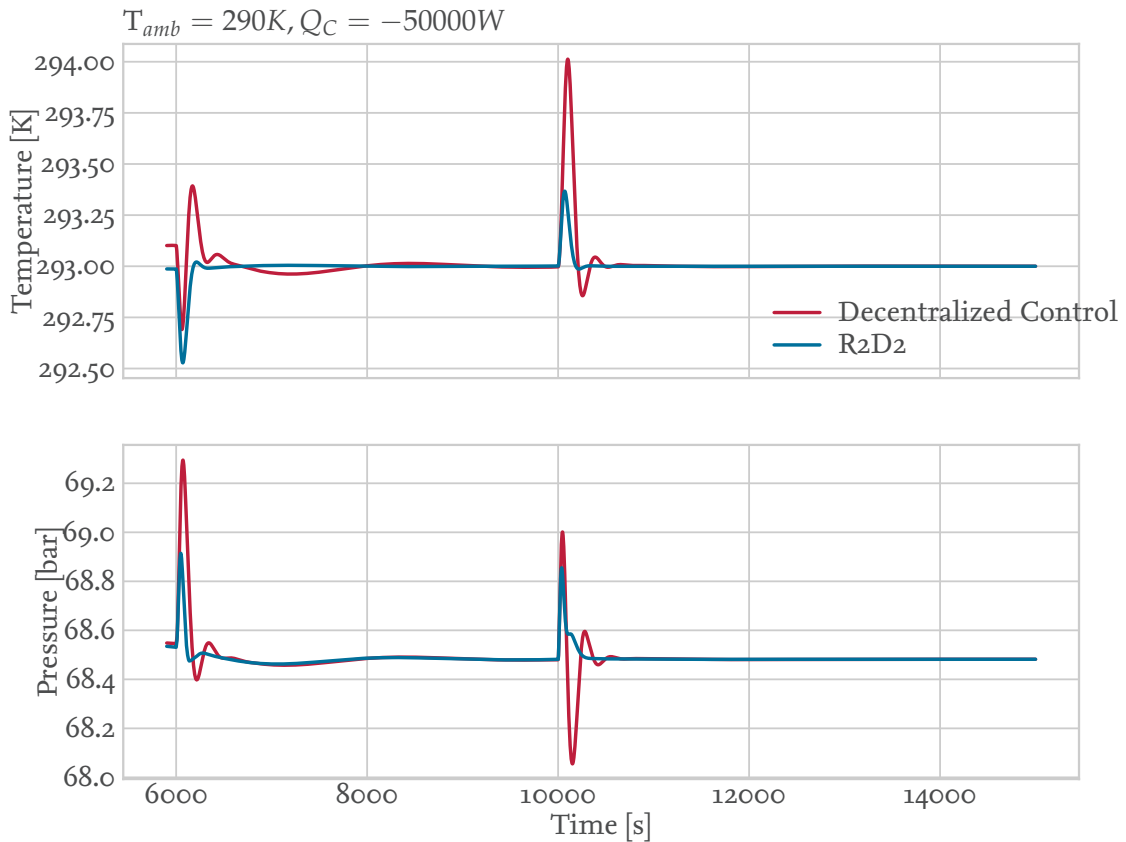


Figure 7.6: Disturbance rejection of the closed loop simulated by a step acting on the systems input, Example 1

It can be seen that both temperature and pressure act immediately on the disturbance. However,

the controller enhanced by a simple decoupling method is able to return to the set point much faster than its purely decentralized counterpart. This is an indicator for the effect of the interconnections in the system, since the disturbance signal is able to spread out over all loops and hence last longer in the control loop if no compensation in form of the splitter is given.

Additionally, the overshoot due to the rejections is decreased, which can be related to the interconnections as well, since any error acts on every output for a purely decentralized control.

In Fig.7.7 the set point of pressure has been changed at 6000 s by a unit step, so is the set point of the temperature at 10000 s. The effects due to interaction are visible immediately, since the temperature is influenced by the excitation of the valve. Due to the coupling of the loops, this resembles in an overshoot of the pressure. Likewise the set point change in temperature acts on the pressure, where the effects are also minimized due to the splitter.

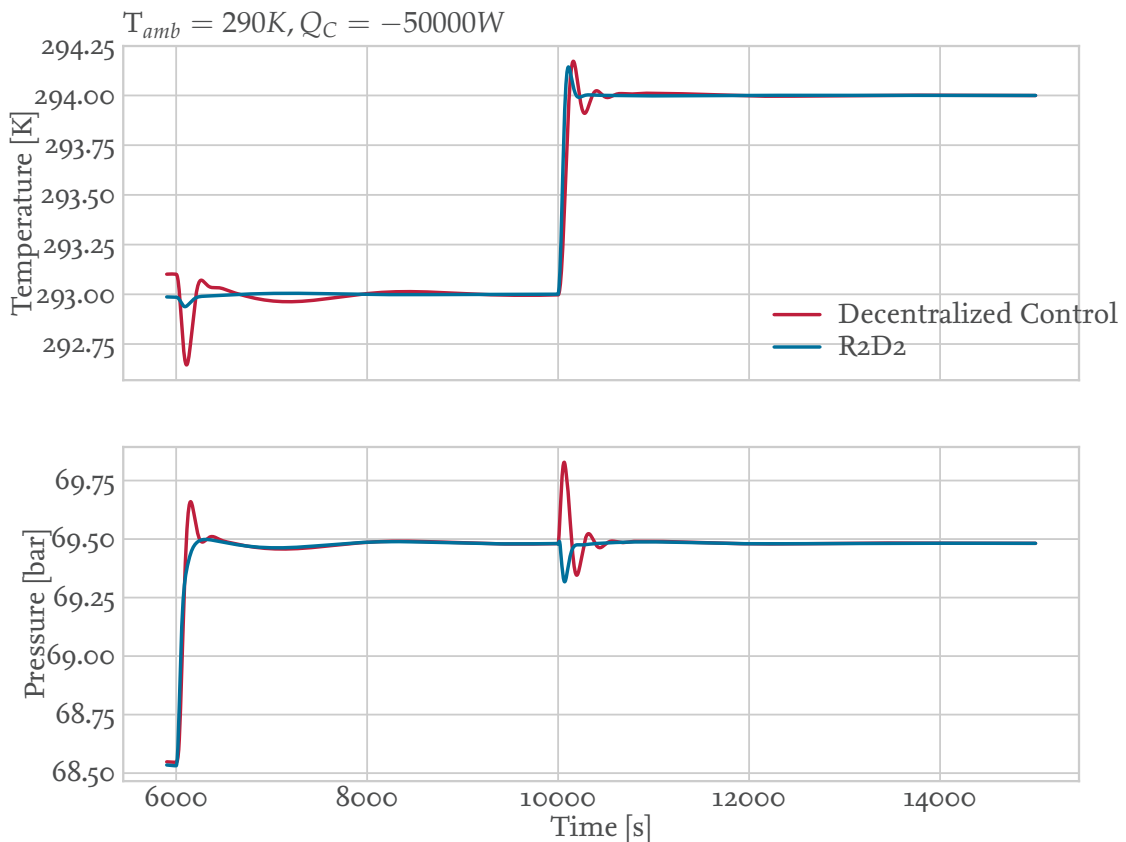


Figure 7.7: Tracking behavior of the closed loop simulated by a step acting on the systems set point, Example

1

Next, both ambient temperature and cooling capacity have been changed to $T_{amb} = 295K$, $Q_C = -60kW$. The disturbance rejection is shown in Fig.7.8, the tracking performance in Fig.7.9. Both

scenarios show similar behavior by reducing both settling time and magnitude of the interaction while performing better with respect to tracking behavior.

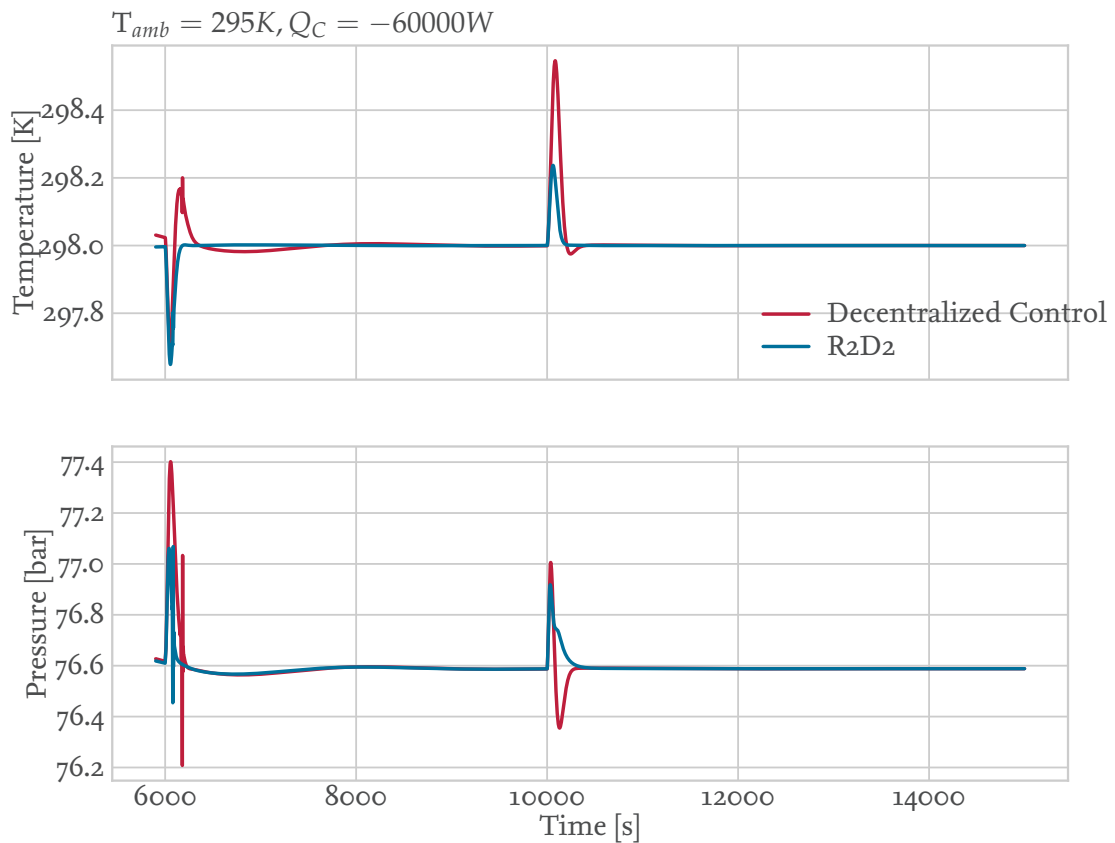


Figure 7.8: Disturbance rejection of the closed loop simulated by a step acting on the systems input, Example 2

It is worth noticing that the coupling between the valve and temperature has nearly canceled out, as can be seen in Fig.7.9. This indicates a strong similarity between both processes with respect to its dynamics. Likewise, the strong interconnection between the fan and the pressure is weakened by the use of a splitter.

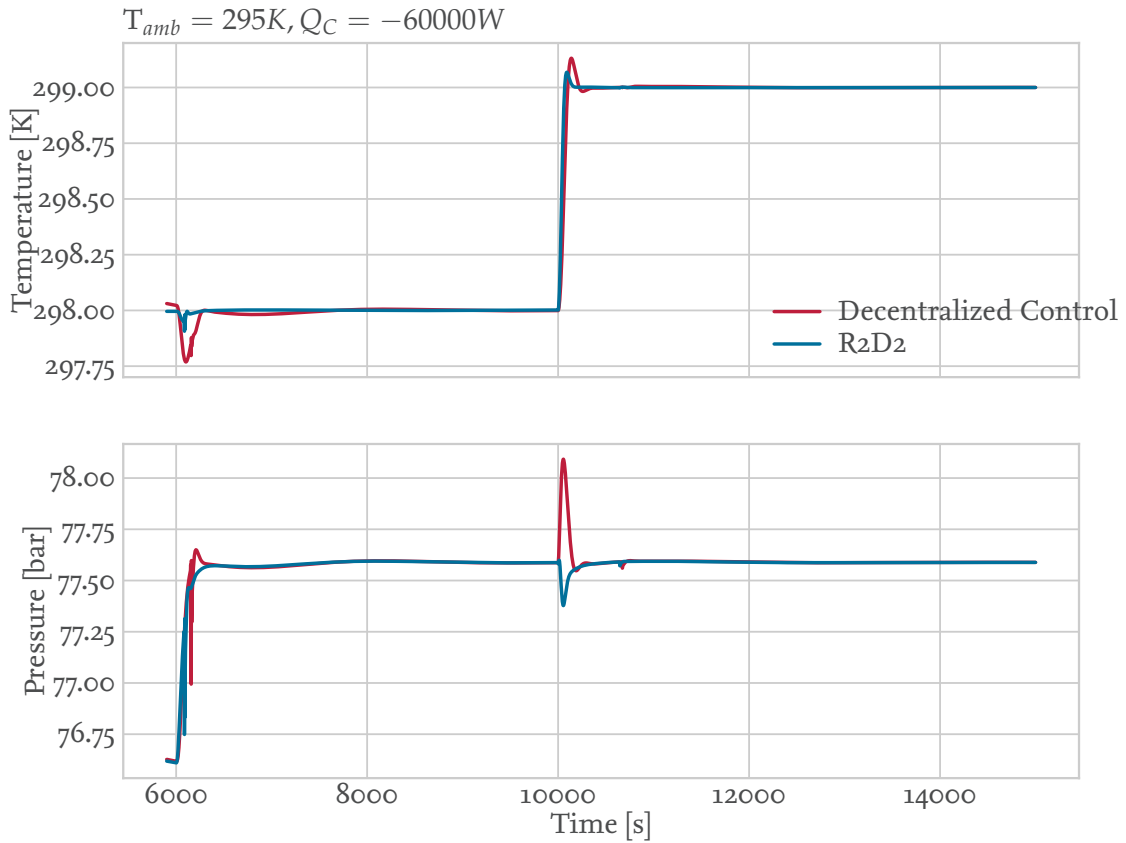


Figure 7.9: Tracking behavior of the closed loop simulated by a step acting on the systems set point, Example 2

The last example is operated at $T_{amb} = 272K$, $Q_C = -65kW$. Again, the use of a splitter minimizes the distribution of disturbances throughout the closed loop system, as can be seen in Fig.7.10. While the settling time is not enhanced significant, the overshoot due to a disturbance in the rotational speed is compensated quicker.

The tracking behavior of the process is shown in Fig.7.11. The benefits of the splitter with respect to set point change are clearly visible, since both disturbances due to interconnections can be minimized while keeping the performance of the decentralized control.

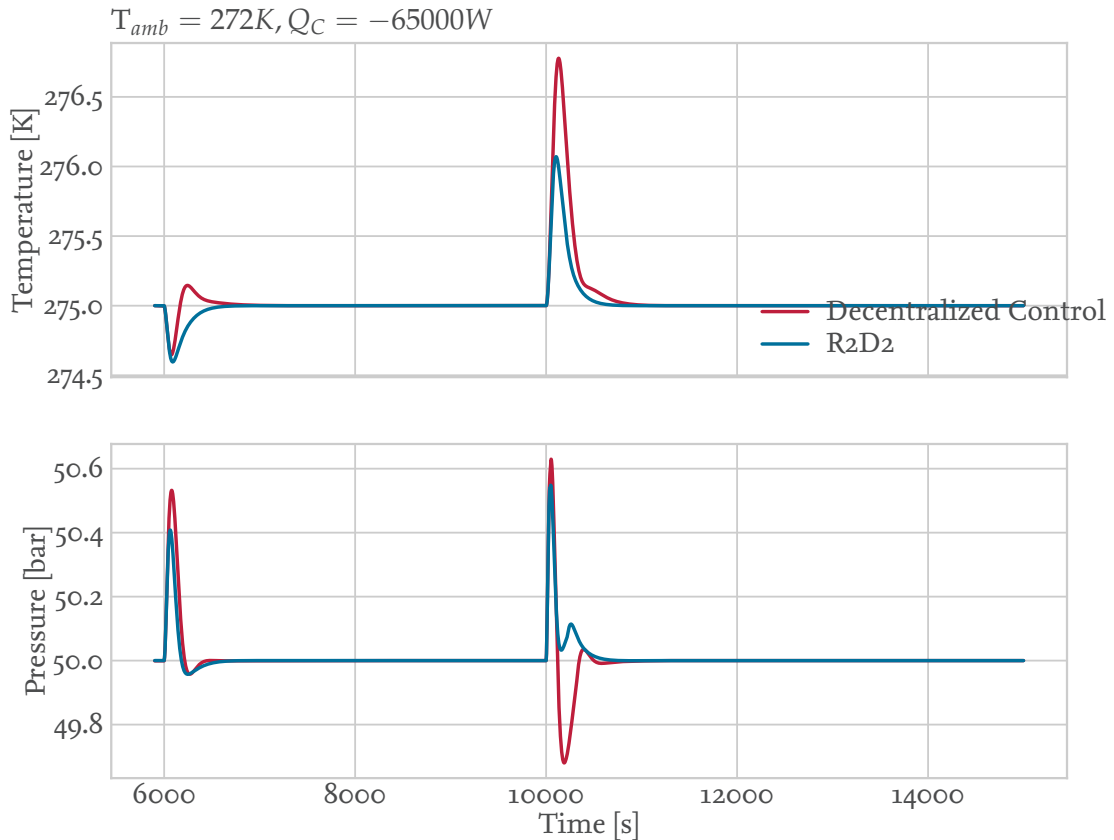


Figure 7.10: Disturbance rejection of the closed loop simulated by a step acting on the systems input, Example 3

From the examples given above, the nonlinearity of the system is clearly visible in the performance of the closed loop and the splitter. While not being always useful with respect to disturbance rejection, the compensation of the signals never amplifies the unwanted behavior. Instead in almost all cases the tracking performance is enhanced while the disturbance rejection is at least as good as given by the not compensated controller.

7.4 Review

This chapter has given some important insights to the system and the behavior of the applied identification process. The FOTD model of all transfer functions is shown to be sensitive to change in physical parameter and operational conditions.

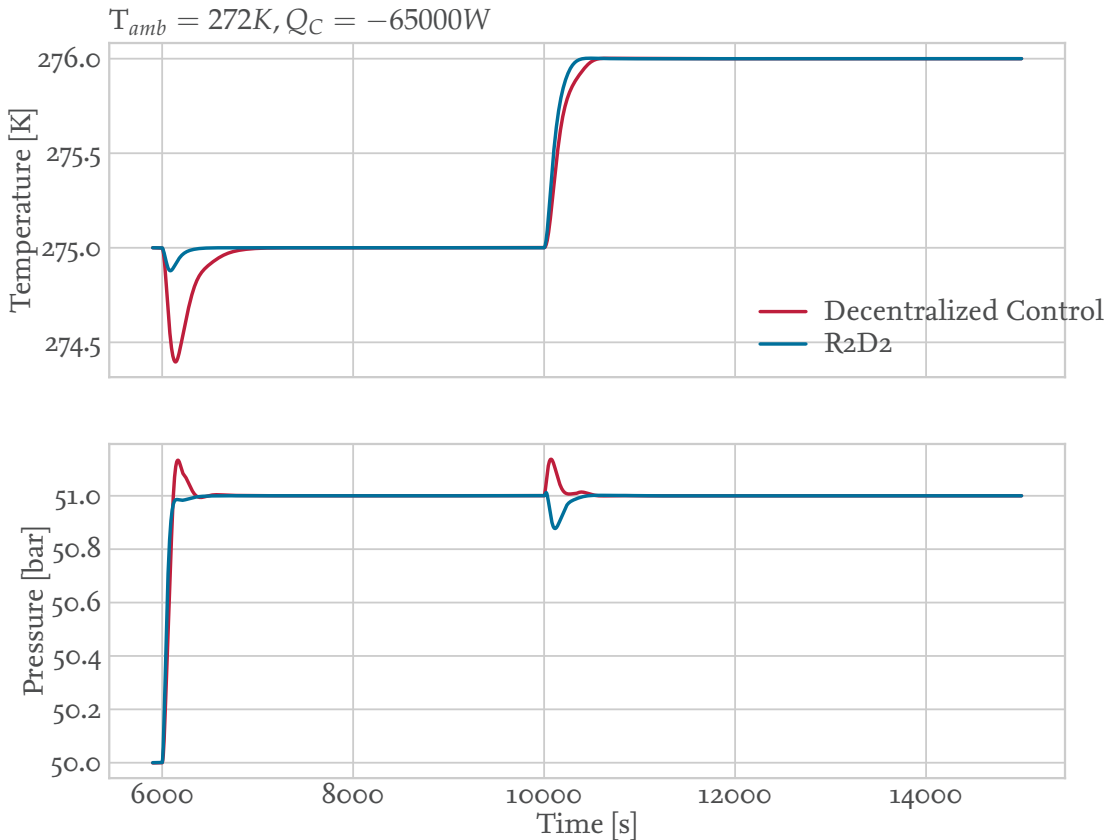


Figure 7.11: Tracking behavior of the closed loop simulated by a step acting on the systems set point, Example 3

However, over all changes a similar behavior with respect to the ambient temperature is visible. The two major remarks with respect to the change in behavior and interconnection are visible in the gain of valve related transfer functions and the time constants of the cross couplings. Both K_{12} and K_{22} show only two characteristic curves over the ambient temperature, which indicates a dominant parameter for both curves. Likewise, the lag of the interconnections is equal while the delay differs strongly. As mentioned, this can most likely be related to the fluids physical properties and its flow direction.

The examples given in Sec.7.3 show the benefits of the usage of a compensation of unwanted effects by applying the splitter. The behavior of all processes with respect to disturbance rejection have been at least as bad as the purely decentralized controller but mostly better. The tracking performance is enhanced in all cases, even though the error in the transfer function, shown in Fig.7.4, is quite large.

8 Conclusion and Outlook

Bibliography

- [1] ADAMY, J. : *Nichtlineare Systeme und Regelungen.* Springer Berlin Heidelberg. – 626 S. <http://dx.doi.org/10.1007/978-3-642-45013-6>. – ISBN 978-3-642-45012-9
- [2] AÌŠSTROÌM, K. J. K. J. ; HAÌGGlund, T. ; AÌŠSTROÌM, K. J. K. J.: *PID controllers.* International Society for Measurement and Control <https://www2.isa.org/store/products/product-detail/?productId=116103>. – ISBN 9781556175169
- [3] ASTRÖM, K. J. ; MURRAY, R. M.: Feedback Systems An Introduction for Scientists and Engineers. (2009). <http://press.princeton.edu/titles/8701.html>.
- [4] ÅSTRÖM, K. ; HÄGGLUND, T. ; AÌŠSTROÌM, K. J. K. J. ; HAÌGGlund, T. : *Advanced PID control.* ISA-The Instrumentation, Systems, and Automation Society. – 460 S. <http://lup.lub.lu.se/record/535630>. – ISBN 1556179421
- [5] ASTROM, K. ; JOHANSSON, K. : Design of decoupled PID controllers for MIMO systems. In: *Control Conf. 2001* ... (2001). <http://ieeexplore.ieee.org/abstract/document/946038/>
- [6] ÅSTRÖM, K. ; WITTENMARK, B. : On self tuning regulators. In: *Automatica* 9 (1973), mar, Nr. 2, 185–199. [http://dx.doi.org/10.1016/0005-1098\(73\)90073-3](http://dx.doi.org/10.1016/0005-1098(73)90073-3). – DOI 10.1016/0005-1098(73)90073-3. – ISSN 00051098
- [7] BERNER, J. : Automatic Tuning of PID Controllers based on Asymmetric Relay Feedback. (2015). <https://lup.lub.lu.se/search/publication/44d2f23c-f801-4fc1-9298-a74d1c252e3d>
- [8] BERNER, J. ; ÅSTRÖM, K. J. ; HÄGGLUND, T. : Towards a New Generation of Relay Autotuners. (2014). <https://lup.lub.lu.se/search/publication/1778b470-6724-4134-95e4-cb1005640c9b>
- [9] BERNER, J. ; HÄGGLUND, T. ; ÅSTRÖM, K. J.: Asymmetric relay autotuning – Practical features for industrial use. In: *Control Eng. Pract.* (2016). <http://dx.doi.org/10.1016/j.conengprac.2016.05.017>. – DOI 10.1016/j.conengprac.2016.05.017. – ISSN 09670661
- [10] BI, Q. ; CAI, W.-J. ; LEE, E.-L. ; WANG, Q.-G. ; HANG, C.-C. ; ZHANG, Y. : Robust identification of first-order plus dead-time model from step response. In: *Control Eng. Pract.* 7 (1999), jan, Nr. 1, 71–77. [http://dx.doi.org/10.1016/S0967-0661\(98\)00166-X](http://dx.doi.org/10.1016/S0967-0661(98)00166-X). – DOI 10.1016/S0967-0661(98)00166-X. – ISSN 09670661
- [11] BRISTOL, E. : On a new measure of interaction for multivariable process control. In: *IEEE Trans. Automat. Contr.* 11 (1966), jan, Nr. 1, 133–134. <http://dx.doi.org/10.1109/TAC.1966.1098266>. – DOI 10.1109/TAC.1966.1098266. – ISSN 0018-9286

- [12] DOYLE, J. ; FRANCIS, B. ; TANNENBAUM, A. : Feedback Control Theory. <http://www.control.utoronto.ca/people/profs/francis/dft.pdf>
- [13] FEDELE, G. : A new method to estimate a first-order plus time delay model from step response. In: *J. Franklin Inst.* (2009). http://s3.amazonaws.com/academia.edu.documents/41626596/A_{ }new_{ }method_{ }to_{ }estimate_{ }a_{ }first-order_{ }p20160127-1753-sogvnL.pdf?AWSAccessKeyId=AKIAIWOWYYGZ2Y53UL3A&Expires=1494916663&Signature=pAbvbvKu2oGpo2%252BSoKdGWZcjQL6E%253D&response-content-disposition=inline
- [14] GLAD, T. ; LJUNG, L. : *Control theory : multivariable and nonlinear methods*. Taylor & Francis, 2000. – 467 S. – ISBN 0748408789
- [15] ISERMANN, R. : *Identifikation dynamischer Systeme 1*. Springer Berlin Heidelberg (Springer-Lehrbuch). <http://dx.doi.org/10.1007/978-3-642-84679-3>. <http://dx.doi.org/10.1007/978-3-642-84679-3>. – ISBN 978-3-642-84680-9
- [16] ISERMANN, R. : *Identifikation dynamischer Systeme 2*. Springer Berlin Heidelberg (Springer-Lehrbuch). <http://dx.doi.org/10.1007/978-3-642-84769-1>. <http://dx.doi.org/10.1007/978-3-642-84769-1>. – ISBN 978-3-642-84770-7
- [17] KEESMAN, K. J.: *System identification : an introduction*. Springer. – 323 S. https://books.google.de/books/about/System_{ }Identification.html?id=gHssIP_{ }dDwUC&redir_{ }esc=y. – ISBN 0857295225
- [18] LJUNG, L. : Perspectives on system identification. In: *Annu. Rev. Control* (2010). <http://www.sciencedirect.com/science/article/pii/S1367578810000027>
- [19] LUNZE, J. : *Regelungstechnik 2*. Springer Berlin Heidelberg (Springer-Lehrbuch). <http://dx.doi.org/10.1007/978-3-642-53944-2>. <http://dx.doi.org/10.1007/978-3-642-53944-2>. – ISBN 978-3-642-53943-5
- [20] LUNZE, J. : *Regelungstechnik 1*. Springer Berlin Heidelberg. <http://dx.doi.org/10.1007/978-3-662-52678-1>. <http://dx.doi.org/10.1007/978-3-662-52678-1>. – ISBN 978-3-662-52677-4
- [21] SKOGESTAD, S. ; POSTLETHWAITE, I. : *Multivariable feedback control : analysis and design*. John Wiley, 2005. – 574 S. – ISBN 047001167X
- [22] STRUCHTRUP, H. : *Thermodynamics and Energy Conversion*. Springer Berlin Heidelberg. <http://dx.doi.org/10.1007/978-3-662-43715-5>. <http://dx.doi.org/10.1007/978-3-662-43715-5>. – ISBN 978-3-662-43714-8
- [23] WANG, Q.-G. : *Lecture Notes in Control and Information Sciences*. Bd. 285: *Decoupling Control*. Springer Berlin Heidelberg. <http://dx.doi.org/10.1007/3-540-46151-5>. <http://dx.doi.org/10.1007/3-540-46151-5>. – ISBN 978-3-540-44128-1
- [24] WEIGAND, B. ; KÖHLER, J. ; WOLFERSDORF, J. von: *Thermodynamik kompakt*. Springer Berlin Heidelberg (Springer-Lehrbuch). <http://dx.doi.org/10.1007/978-3-642-37233-9>. <http://dx.doi.org/10.1007/978-3-642-37233-9>. – ISBN 978-3-642-37232-2

- [25] ZEIDLER, E. (Hrsg.): *Springer-Handbuch der Mathematik III*. Springer Fachmedien Wiesbaden.
<http://dx.doi.org/10.1007/978-3-658-00275-6>. <http://dx.doi.org/10.1007/978-3-658-00275-6>. – ISBN 978-3-658-00274-9
- [26] ZHOU, K. ; DOYLE, J. C.: *Essentials of robust control*. Prentice Hall. – 411 S. <https://www.ece.lsu.edu/kemin/essentials.htm>. – ISBN 0135258332
- [27] ZHOU, K. ; DOYLE, J. C. ; GLOVER, K. K.: *Robust and optimal control*. Prentice-Hall https://books.google.de/books/about/Robust_and_Optimal_Control.html?id=RPS0QgAACAAJ&redir_esc=y. – ISBN 0134565673

Anhang

A.1 Erster Anhang

Ein Anhang.

A.2 Zweiter Anhang

Ein weiterer Anhang.



Technische Universität Braunschweig
Institut für Thermodynamik
Hans-Sommer-Strasse 5
38106 Braunschweig